CONF-9705121--

Proceedings of the

FIFTEENTH SYMPOSIUM ON ENERGY ENGINEERING SCIENCES

May 14-15, 1997

at

ARGONNE NATIONAL LABORATORY

Argonne, Illinois

Cosponsored by

Office of Basic Energy Sciences
U.S. DEPARTMENT OF ENERGY

and

Energy Technology Division
ARGONNE NATIONAL LABORATORY

Coordinated by

Argonne National Laboratory
9700 South Cass Avenue
Argonne, Illinois 60439

FIFTEENTH SYMPOSIUM ON ENERGY ENGINEERING SCIENCES

FOREWORD

This Proceedings Volume includes the technical papers that were presented during the Fifteenth Symposium on Energy Engineering Sciences on May 14-15, 1997, at Argonne National Laboratory, Argonne, Illinois. The Symposium was organized into eight technical sessions, which included 32 individual presentations followed by discussion and interaction with the audience. A list of participants is appended to this volume.

The DOE Office of Basic Energy Sciences, of which Engineering Research is a component program, is responsible for the long-term mission-oriented research in the Department. It has the prime responsibility for establishing the basic scientific foundation upon which the Nation's future energy options will have to be identified, developed, and built. It is committed to the generation of new knowledge necessary for the solution of present and future problems of energy exploration, production, conversion, and utilization, consistent with respect for the environment.

Consistent with the DOE/BES mission, The Engineering Research Program is charged with the identification, initiation, and management of fundamental research on broad, generic topics addressing energy-related engineering problems. Its stated goals are: 1) to improve and extend the body of knowledge underlying current engineering practice so as to create new options for enhancing energy savings and production, for prolonging useful life of energy-related structures and equipment, and for developing advanced manufacturing technologies and materials processing with emphasis on reducing costs with improved industrial production and performance quality; and 2) to expand the store of fundamental concepts for solving anticipated and unforeseen engineering problems in the energy technologies.

In achieving these goals, the Engineering Research Program supports approximately 130 research projects covering a broad spectrum of topics cutting across traditional engineering disciplines with a focus on three areas: 1) mechanical sciences, 2) control systems and instrumentation, and 3) engineering data and analysis. The Fifteenth Symposium involved approximately one-fourth of the research projects currently sponsored by the DOE/BES Engineering Research Program.

The Fifteenth Symposium was held under the joint sponsorship of the DOE Office of Basic Energy Sciences and Argonne National Laboratory. Local arrangements were handled by Ms. Joan Brunsvold and Ms. Marianne Adair of the ANL Conference Services. Ms. Gloria Griparis of the ANL Office of Technical Communication Services was responsible for assembling these proceedings and attending to their publication.

I am grateful to all who contributed to the success of the program, particularly to the participants for their uniformly excellent presentations, their active involvement in discussions, and their infectious enthusiasm. The resulting interactions made this Symposium a most stimulating and enjoyable experience.

Robert Goulard, ER-15
Division of Engineering and Geosciences
Office of Basic Energy Sciences

FIFTEENTH SYMPOSIUM ON ENERGY ENGINEERING SCIENCES

May 14-15, 1997

Argonne National Laboratory

Argonne, IL

TABLE OF CONTENTS

INTERFACIAL AREA TRANSPORT IN BUBBLY FLOW

M. Ishii, Q. Wu, S.T. Revankar, T. Hibiki, W.H. Leung, S. Hogsett, and A. Kashyap

Thermal Hydraulics and Reactor Safety Laboratory
Purdue University, West Lafayette, IN 47907 U.S.A.

ABSTRACT

In order to close the two-fluid model for two-phase flow analyses, the interfacial area concentration needs to be modeled as a constitutive relation. In this study, the focus was on the investigation of the interfacial area concentration transport phenomena, both theoretically and experimentally. The interfacial area concentration transport equation for air-water bubbly up-flow in a vertical pipe was developed, and the models for the source and sink terms were provided. The necessary parameters for the experimental studies were identified, including the local time-averaged void fraction, interfacial area concentration, bubble interfacial velocity, liquid velocity and turbulent intensity. Experiments were performed with air-water mixture at atmospheric pressure. Double-sensor conductivity probe and hot-film probe were employed to measure the identified parameters. With these experimental data, the preliminary model evaluation was carried out for the simplest form of the developed interfacial area transport equation, i.e., the one-dimensional transport equation.

I. INTRODUCTION

In multiphase flow modeling, the overwhelming difficulties encountered in a local instant formulation stem from the existence of deformable moving interfaces and the turbulent fluctuations of the field variables. Even for single phase flow without free interfaces, the exact solutions for the local instant fluctuations are beyond our present mathematical capability. Therefore, the common approaches to depict the macroscopic aspects of two-phase flow use averaging techniques (Vernier and Delhaye, 1965 [1]; M. Ishii, 1975 [2]; Boure, 1978 [3]) because the microscopic details of the interface behaviors and the fluid particle fluctuations are

rarely needed in engineering applications. In a certain sense the averaging techniques can be considered as a low-pass filtering process that excludes unwanted high frequency signals from local instant chaotic fluctuations. Subsequently, based on proper averaging operations, the well-known two-fluid model is established, which is widely accepted as the most sophisticated measure for two-phase flow analyses. In this model the averaged macroscopic properties of the flow field are considered separately in terms of two sets of conservation equations that govern the balance of mass, momentum and energy in each phase. However, the two averaged macroscopic fields are coupled to each other through certain phase interaction terms in the field equations to characterize the interfacial transfers. According to Ishii [2], the generalized interfacial interaction terms can be expressed in the following form:

$$\text{Interfacial Transfer Term} = a_i \times (\text{Driving Flux}), \tag{1}$$

where the Driving Flux depends on the transfer mechanisms and a_i is the interfacial area concentration, defined as the total interface area per unit mixture volume. In order to close the two-fluid model, these parameters need to be modeled individually. In this study, the focus is on the investigation of the interfacial area concentration transport phenomena, both theoretically and experimentally. The interfacial area concentration transport equation for air-water bubbly up-flow in a vertical pipe is developed, and the models for the source and sink terms are provided. The necessary parameters for the experimental studies are identified, including the local time-averaged void fraction, interfacial area concentration, bubble interfacial velocity, liquid velocity and turbulent intensity. Experiments are performed with an air-water mixture at atmospheric pressure. Double-sensor conductivity probe and hot-film probe are employed to measure the identified parameters. The experimental results provide a comprehensive data base for the model evaluation. At the present stage, the model evaluation is in progress with the detailed experimental data. The preliminary results are presented here for the simplest form of the developed interfacial area transport equation, i.e., the one-dimensional transport equation.

II. INTERFACIAL AREA TRANSPORT EQUATION

The interfacial area concentration is proportional to the fluid particle density, and thus its variation is primarily dominated by the fluid particle expansion, agglomeration and disintegration. Analogous to Boltzman's transport equation, Reyes (1989 [4]) proposed a Population Balance Approach (PBA) to develop a particle number density transport equation for chemically non-reacting, dispersed spherical fluid particles. For the interfacial area transport phenomena, Kocamustafaogullari and Ishii (1995 [5]) obtained the following form of the generalized particle number density transport equation:

$$\frac{\partial f(\mathbf{x}, \mathcal{V}, t)}{\partial t} + \nabla \cdot \left(f(\mathbf{x}, \mathcal{V}, t) \mathbf{v}_p \right) = \sum_j s_j(\mathbf{x}, \mathcal{V}, t) + s_{ph}(\mathbf{x}, \mathcal{V}, t), \tag{2}$$

where $f(\mathbf{x}, \mathcal{V}, t)$ is the local number density distribution function of the fluid particles with volumes between $\mathcal{V}$ and $\mathcal{V}+\mathrm{d}\mathcal{V}$, while $\mathbf{v}_p(\mathbf{x}, \mathcal{V}, t)$ refers to the local time-averaged particle

velocity. The fluid particle sink or source rate due to phase change is denoted by $s_{ph}(\mathbf{x}, \mathcal{V}, t)$. Detailed treatment of this term may follow the approach suggested by Kocamustafaogullari and Ishii (1983 [6]), whereas the wall nucleation rate must be specified as a boundary condition. The other terms on the right-hand-side of Eq. (2), $s_j(\mathbf{x}, \mathcal{V}, t)$, represent the net rate of change in the fluid particle number density distribution function resulting from particle breakage and coalescence. Some phenomenological models for these source and sink terms were summarized by Prince and Blanch (1990 [7]) and Lafi and Reyes (1991 [8]). These models depend on the fluid particle volume and present the detailed insight of the driving mechanisms. However, the particle volume dependent transport equation described by Eq. (2) is too detailed for the averaged two-fluid model, in which the primary interest is in the average fluid particle behaviors. It is then advantageous to develop a transport equation averaged over all fluid particles. From the integration of Eq. (2) over the fluid particle volume, the overall local particle number density is given by:

$$\frac{\partial n(\mathbf{x}, t)}{\partial t} + \nabla \cdot \left(\bar{\bar{\mathbf{v}}}_p(\mathbf{x}, t) n(\mathbf{x}, t) \right) = \sum_j S_j(\mathbf{x}, t) + S_{ph}(\mathbf{x}, t), \tag{3}$$

where $n(\mathbf{x}, t)$ is the local particle number per unit mixture volume, and $\bar{\bar{\mathbf{v}}}_p(\mathbf{x}, t)$ is the average local particle velocity weighted by the particle number, which is identical to the local time-averaged particle velocity weighted by the void fraction if the sample size is sufficiently large and the internal circulation in each fluid particle is neglected.

In the two-fluid model, the parameter of interest is the interfacial area concentration rather than the bubble number density. To replace the bubble number density in Eq. (3) with the interfacial area concentration, the following geometric relation is applied:

$$n = \frac{\alpha}{\mathcal{V}_b} = \psi \left(\frac{a_i^3}{\alpha^2} \right) \tag{4}$$

where ψ is a factor depending on the shape of the bubbles, and $\mathcal{V}_b$ denotes the average bubble volume. For spherical bubbles ψ equals $1/(36\pi)$. Substituting Eq. (4) into Eq. (3) leads to:

$$\frac{\partial a_i}{\partial t} + \nabla \cdot \left(a_i \bar{\bar{\mathbf{v}}}_g \right) = \frac{1}{3\psi} \left(\frac{\alpha}{a_i} \right)^2 \left[\sum_j S_j + S_{ph} \right] + \left(\frac{2a}{3\alpha} \right) \left[\frac{\partial \alpha}{\partial t} + \nabla \cdot \left(\bar{\bar{\mathbf{v}}}_g \alpha \right) \right]. \tag{5}$$

The second term on the right-hand-side represents the effects of the variation in the mean bubble volume. Without phase change, this term is related to the gas phase continuity equation in the following manner:

$$\frac{\partial \alpha}{\partial t} + \nabla \cdot \left(\bar{\bar{\mathbf{v}}}_g \alpha \right) = -\frac{1}{\rho_g} \left[\frac{\partial \rho_g}{\partial t} + \left(\bar{\bar{\mathbf{v}}}_g \cdot \nabla \right) \rho_g \right]. \tag{6}$$

This term is important when the system pressure is low and the change in gas density is significant along the flow path, which is quite common especially in air-water experiments conducted under atmospheric pressure conditions. For steady-state bubbly flow, if the gas density decreases along the flow path, the bubble size grows resulting in larger interfacial area

concentration. By introducing Eq. (6) into Eq. (5), the interfacial area transport equation without considering phase change effects is readily reduced to:

$$\frac{\partial a_i}{\partial t}+\nabla\cdot\left(a_i\vec{\mathbf{v}}_g\right)=\frac{1}{3\psi}\left(\frac{\alpha}{a_i}\right)^2\left(\sum_j S_j\right)-\left(\frac{2a_i}{3\alpha}\right)\frac{1}{\rho_g}\frac{D_g\rho_g}{Dt}. \tag{7}$$

The remaining unknowns in the above equation are the source and sink terms due to bubble coalescence and breakage. According to the preliminary studies of Wu et al. (1997 [9]), three major mechanisms are responsible for bubble coalescence and disintegration in dispersed bubbly flow. These are the coalescence due to random collisions driven by turbulence, the coalescence due to wake entrainment, and the breakage upon the impact of turbulent eddies.

For the turbulence induced bubble coalescence, the net rate of change in the bubble number per unit mixture volume is given by [9]:

$$S_{RC}=-C_{RC}\left[\frac{\psi u_t a_i^4}{\pi\alpha^2}\right]\left[\frac{1}{\alpha_{\max}^{1/3}\left(\alpha_{\max}^{1/3}-\alpha^{1/3}\right)}\right]\left[1-\exp\left(-C\frac{\alpha_{\max}^{1/3}\alpha^{1/3}}{\alpha_{\max}^{1/3}-\alpha^{1/3}}\right)\right], \tag{8}$$

where, the subscript "*RC*" stands for Random Collision, C_{RC} is proportional to the coalescence efficiency of each random collision, and u_t is the root-mean-square of the turbulent velocity fluctuation caused by the eddies with a characteristic length comparable to the mean bubble size. It is postulated that smaller eddies do not provide considerable bulk motion to a bubble, while larger eddies transport groups of bubble without leading to significant relative motion for coalescence. The term in the first bracket is similar to the collision rate proposed by Coulaloglou and Tavlarides [10] in 1976 for a liquid-liquid droplet flow system, analogous to the particle collision model in an ideal gas. The term in the second bracket is due to the finite size of bubbles that cannot be neglected when compared to the mean free path. The maximum void fraction, α_{max}, is chosen to be 0.8, a value at the transition point between annular flow and slug flow (Wallis, 1969 [11]). In the final bracket, a modification factor is introduced to consider the effect of the mean bubble distance compared to the bubble traveling range. For the sparsely distributed bubbles, the collision probability decreases because the turbulent eddies that drive the bubbles toward each other cannot sustain such long range interactions. It should be emphasized that the coalescence efficiency in this study is assumed to be constant. The most popular model for the coalescence efficiency is the film thinning model developed by Oolman and Blanch (1986 [12]). However, their model suggests that the coalescence rate decreases exponentially with respect to the turbulent fluctuating velocity, which is much stronger than the linear dependence of the collision rate, resulting in an overall decreasing trend of the coalescence rate as the turbulent fluctuation increases. This may cause serious trouble when the model is applied to experimental data, especially at high liquid flow rates. Nevertheless, constant coalescence efficiency is only an approximation, further efforts are needed to model the efficiency mechanistically.

The bubble coalescence due to the so-called wake-entrainment mechanism may occur when bubbles enter the wake region of a leading bubble and then accelerate toward the preceding one. By considering the relative motion as the driving mechanism, the corresponding rate of change in bubble number density satisfies the following simple formula [9]:

$$S_{WE} = -\frac{\psi}{\pi} C_{WE} u_r \left(\frac{a_i^2}{\alpha} \right)^2 , \tag{9}$$

where u_r is the relative velocity between the gas bubble and the ambient liquid, given by:

$$u_r = \left(\frac{Dg}{3C_D} \frac{\Delta\rho}{\rho_f} \right)^{1/2} \tag{10}$$

with $$C_D = 24 \frac{\left(1 + 0.1 \mathrm{Re}_D^{0.75}\right)}{\mathrm{Re}_D}, \text{ and } \mathrm{Re}_D \equiv \frac{\rho_f u_r D}{\mu_f} (1-\alpha). \tag{11}$$

Again, the coefficient C_{WE} is proportional to the coalescence efficiency and is assumed to be constant here.

The final mechanism is the bubble disintegration due the impact of the turbulent eddies. From simple force balance on a gas bubble, the net rate of change in bubble number density is given by [9]:

$$S_{TI} = \frac{1}{18} C_{TI} u_t \left(\frac{a_i^2}{\alpha} \right) \left(1 - \frac{\mathrm{We}_{cr}}{\mathrm{We}} \right)^{1/2} \exp\left(-\frac{\mathrm{We}_{cr}}{\mathrm{We}} \right), \quad \mathrm{We} > \mathrm{We}_{cr}, \tag{12}$$

where, $$\mathrm{We} = \frac{6\rho_f u_t^2 \alpha}{\sigma a_i}. \tag{13}$$

The subscript "*TI*" refers to Turbulent Impact. The unique feature of this expression is that the breakup rate equals zero when the Weber number is less than a critical value, We_{cr}. At low liquid flow rates, the turbulent fluctuation is small and thus no breakup would be counted, which enables the fine-tuning of the adjustable parameters in the coalescence terms, independent of the bubble breakage at low liquid flow rate with small void fraction.

Eqs. (7), (8), (9) and (12) constitute the closure relations of the interfacial area concentration in two-phase vertical dispersed bubbly flow. The variables in these equations are coupled with the field equations in the two-fluid model. For the information of the local interfacial area concentration, the field equations should be solved together with the closure relations. On the other hand, these models also provide the detailed requirements to the experimental investigation for the interfacial area transport phenomena. In addition to the measurements of local time-averaged void fraction and interfacial area concentration, information about the bubble velocity, liquid turbulent intensity and bubble relative velocity should be obtained for the evaluation of the proposed models.

III. EXPERIMENTAL INVESTIGATION

For the purpose of studying the interfacial area transport process, a vertical cocurrent two-phase flow test facility was designed and constructed with three measurement ports at different axial positions. In order to obtain the parameters identified in the previous section for the characteristics of the interfacial area transport phenomena, double-sensor conductivity probe and hot-film probe were employed in the experimental investigations. Comprehensive measurements were carried out mainly in the bubbly flow regime. For every flow condition, the radial distributions of each parameter were obtained at three axial positions. These parameters include the local time-averaged liquid velocity, liquid turbulent intensity, gas velocity, void fraction, interfacial area concentration, and bubble Sauter mean diameter.

3.1. Test Facility and Instrumentation

The schematic of the test loop is depicted in Fig. 1. The test section is a 3.6 m long acrylic pipe (5.08 cm ID). Air and deionized water are used in the experiments. With a 1.5 hp water pump (SP15-150, Price Pump Company), the liquid superficial velocity in the test section can reach about 2.0 m/s, whereas the lab's stable 0.7 MPa dry air supply is sufficient for the experiment up to the churn-turbulent flow regime. The uniform two-phase mixture enters the test section from an air-water mixing chamber with a conical section connected to the bottom end of the test pipe. Inside the air-water mixer, an air-injector consists of 400 hypodermic needles held together by a resin base as shown in Fig. 1, providing bubbles with diameters of 3 mm to 5 mm. In the upper plenum, water is separated from air and flows back to the water tank, where a heat exchanger is installed to maintain a constant liquid temperature for the hot-film probe measurement. Along the flow path in the test section, three instrument ports are equipped at the axial positions of L/D equal to 2, 32 and 62, and a traversing mechanism is installed at each probe port. The traversing mechanism utilizes a micrometer that is accurate to 0.025 of a millimeter. Since the existence of the probe support can induce bubble breakage and coalescence and therefore affect the downstream measurements, the measurement at the four probe locations have to be performed individually. For the measurements of the time-averaged local void fraction, interfacial area concentration and bubble velocity, a double-sensor conductivity probe is developed, whereas the water velocity and turbulent intensity measurements are made using a hot-film anemometer system (FLOWPOINT, TSI Inc.). The local instantaneous data are acquired with a 486 PC, and the time-averaged variables are obtained through software developed in the TRSL of Purdue University.

The double-sensor probe is made of two thin electrodes as shown schematically in Fig. 2a. The tip of each electrode is exposed to the two-phase mixture and measures the impedance between the probe tip and the common ground. Due to the significant difference in the conductivities of the liquid phase and the gas phase, the impedance signal rises sharply when a bubble passes through the probe (Fig. 2b). From the front tip signal, the bubble residual time fraction is the local time-averaged void fraction. On the other hand, the time delay, Δt, of the two impedance signals can thus be utilized to characterize the time interval for the bubble surface

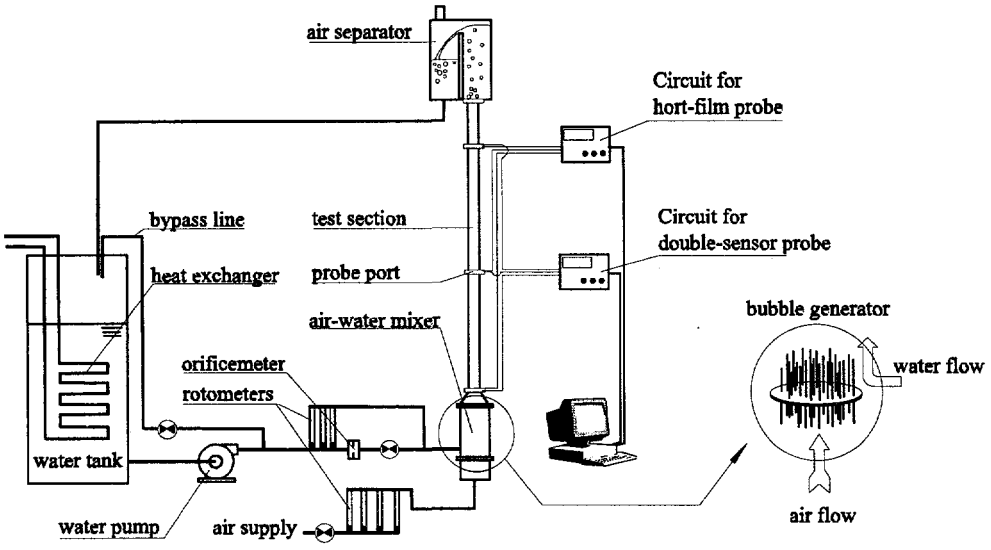

Fig. 1 Schematic diagram of the experimental loop

traveling from the front probe tip to the back tip. Since the separation of the two probe tips is known, defined as Δs, a measurable bubble axial velocity, Δs/Δt, is obtained. For the measurement of the local time-averaged interfacial area concentration, according to Wu and Ishii (1997 [13]), the following formula is suggested in considering the effects of the bubble lateral motion and the probe spacing:

$$a_i = \left(\frac{2N_b}{\Delta T\left(N_b - N_{miss}\right)}\right)\left[2+\left(\frac{V_b'}{\overline{V}_b}\right)^{2.25}\right]\sum_j\left(\Delta t_j/\Delta s\right), \qquad D = 1.2\Delta s \sim 3\Delta s, \tag{14}$$

where the subscript j denotes the j-th measured bubble, N_b stands for the number of the bubbles that pass the first probe tip in the ΔT time interval for time-averaging, D refers to the Sauter mean diameter of the bubbles, and N_{miss} is the number of the missed bubbles. A bubble is defined as missed when the second probe tip either cannot touch the bubble or enters the bubble before the first tip. These cases may occur if the bubble has lateral velocity components [13]. If the Sauter mean diameter of the measured bubbles is in the range of 1.2 to 3 times the probe spacing and the sample size is sufficiently large, the error of this expression is within ±1.5%. The term $\left(V_b'/\overline{V}_b\right)$ in Eq. (14) represents the relative bubble velocity fluctuation, given by [13]:

$$\left(\frac{V_b'}{\overline{V}_b}\right) = 1.2\frac{\sigma_{\Delta t_j}}{\left(\Delta t_j\right)}, \qquad D = 1.2\Delta s \sim 3\Delta s, \tag{15}$$

where $\sigma_{\Delta tj}$ is the standard deviation of Δt_j. Moreover, in order to control the statistic fluctuations within ±5%, the sample for time-averaging should contain no less than 1000 bubbles [13]. With the measured local time-averaged void fraction and interfacial area concentration, if the bubbles are assumed to be spherical, the bubble Sauter mean diameter is given by the following relation:

$$D = \frac{6\alpha}{a_i}. \tag{16}$$

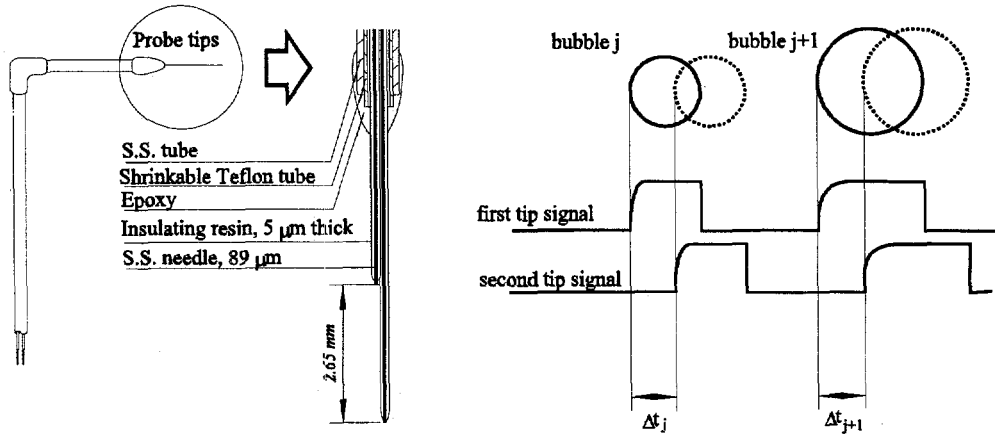

(a) Schematic of double-sensor probe (b) Signals form the probe

Fig. 2 Double-sensor conductivity probe

The hot-film probe used in the experiment for the measurements of the water velocity and turbulent intensity is a constant temperature probe with a conical tip (Model 1231W, TSI Inc.), which measures the one-dimensional liquid velocity with a maximum frequency response of 5 kHz. The calibration of the hot-film probe was performed with either an orifice flowmeter or a Pitot-static probe positioned at the test section centerline. In order to maintain constant liquid temperature, a cooling coil was installed in the water tank as shown in Fig. 1, which controls the temperature fluctuation within ±1°C. Typically, the loop is allowed to run for an hour or so until a steady-state temperature is reached. For small temperature fluctuations, a thermocouple is placed in the test section and the FLOWPOINT software adjusts the hot-film output signal accordingly.

The hot-film probe is designed for single phase water flow at an operating temperature of 66.7°C. When applied to air-water two-phase bubbly flow, however, the operation temperature should be reduced in order to achieve consistent probe sensitivity (Hogsett, 1996 [14]; Hibiki, 1997 [15]). Otherwise a frequent output voltage drift may occur due to the dramatic change in local convection heat transfer coefficients between the liquid phase and the gas phase. In the experiment, the operating temperature was chosen at 45°C and the probe calibration was carried out using the orifice flow meter installed in the liquid supply line as shown in Fig. 1. Even at low temperature conditions, significant drift of the calibration curve is observed. Hence, frequent recalibrations are conducted. In Fig. 3, the typical time history of a hot-film probe signal for a two-phase bubbly flow is presented. Besides the chaotic fluctuations caused by the turbulence in the liquid phase, some voltage spikes exist due to the bubbles passing through the probe tip. In order to obtain a liquid velocity representative of the flow, it is necessary to filter out these spikes. This has been done using a threshold scheme developed by Hogsett [14] and the filtered signal is also shown in Fig. 3. From the signal of the hot-film probe, average liquid velocity as well as the root-mean-square velocity fluctuations are obtained. Moreover, the filtered signal gives the local bubble residual time and provides an alternative measure to calibrate the void fraction measurement from the double-sensor conductivity probe.

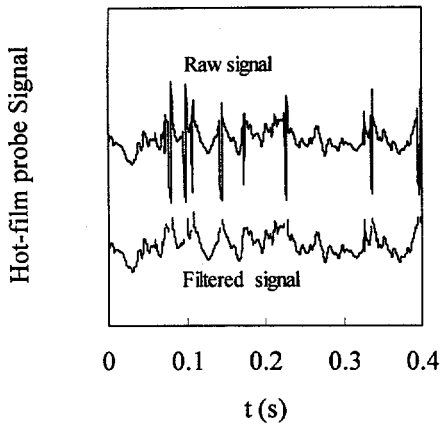

Fig. 3 Raw and filtered hot-film signals

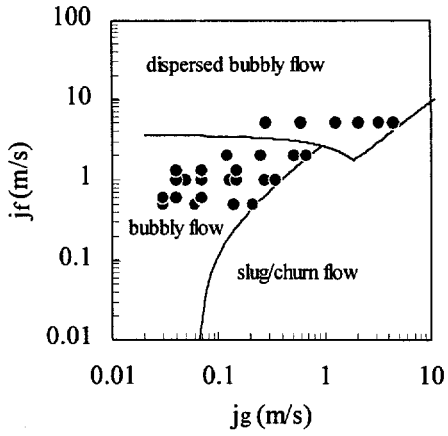

Fig. 4 Flow conditions for the tests

3.2 Typical Test Results

Comprehensive measurements were carried out mainly in the bubbly flow regime as shown in Fig. 4. For every flow condition, the radial distributions of each parameter were obtained at three axial positions. These parameters include the local time-averaged liquid velocity, liquid turbulent intensity, gas velocity, void fraction, interfacial area concentration, and the bubble Sauter mean diameter. The liquid velocity and turbulent intensity were measured with a hot-film anemometer, whereas the bubble velocity, void fraction, interfacial area concentration, and bubble Sauter mean diameter were acquired using a double-sensor conductivity probe.

Typical liquid velocity profiles at different axial locations are shown in Fig. 5. Generally, the liquid velocity profiles are flat, presenting a typical turbulent flow characteristics. Under the specific flow condition, a subtle wall peak is observed at the pipe entrance region with L/D equal to 2, which corresponds to a void fraction wall peak in Fig. 7. On the other hand, the turbulent intensity profile appears to depend on the relative difference between the bubble-induced turbulence and the turbulence generated by wall shear. Based on the data obtained by Hogsett [14] at low liquid flow rates, the turbulent intensity peaks in the core of the flow where bubbles tend to cluster, even for the lowest void fraction case with $\langle\alpha\rangle=0.018$. This evidence implies that the bubble-induced turbulence seems to be the dominant mechanism at low liquid flow rates. As the liquid flow rate increases, however, wall shear effects gradually overtake the bubble-induced turbulence, and the turbulent intensity profiles at different axial positions shown in Fig. 6 tend to collapse to a fixed line that resembles the behavior of a single phase turbulent flow.

All the void fraction profiles at different flow conditions exhibit similar trends, as shown in Fig. 7. The radial void fraction profile peaks near the wall. Along the flow path, the peak moves away from the wall and decreases considerably. The variation of the peak depends on the flow conditions. At low liquid flow rates the peak may decrease by 40% to 50%, while at high liquid flow rates the decrease is about 10%. In Fig. 8, the radial interfacial area concentration profile

exhibits the same trends as the void fraction profile. Hence, the bubble Sauter mean diameter, which is proportional to the ratio of the void fraction to the interfacial area concentration, remains approximately constant within the pipe cross-sectional area (Fig. 9). However, as the bubbles move upward, their average size becomes larger because of expansion and agglomeration. Moreover, the bubble velocity profiles measured by the double-sensor probe are presented in Fig. 10. Near the entrance, at L/D equal to 2, the bubble velocity is slightly higher in the wall region. Downstream, at L/D equal to 32 and 62, the bubble velocity reaches its terminal velocity and the velocity profiles resemble the liquid velocity profile.

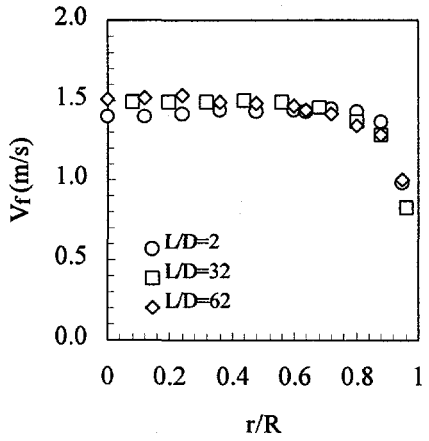

Fig. 5 Liquid velocity profile
(jg=0.039m/s jf=1.3m/s)

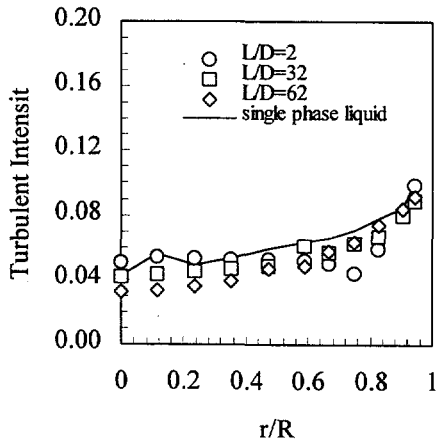

Fig. 6 Turbulent intensity profile
(jg=0.039m/s jf=1.3m/s)

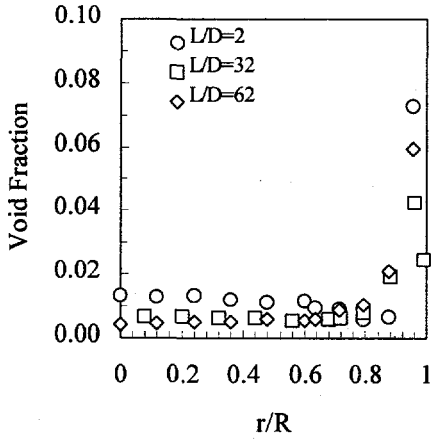

Fig. 7 Void fraction profile
(jg=0.039m/s jf=1.3m/s)

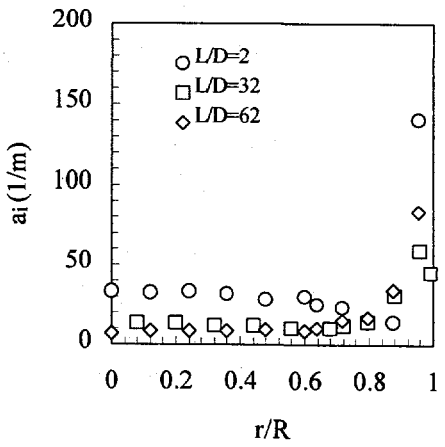

Fig. 8 Interfacial area concentration profile
(jg=0.039m/s jf=1.3m/s)

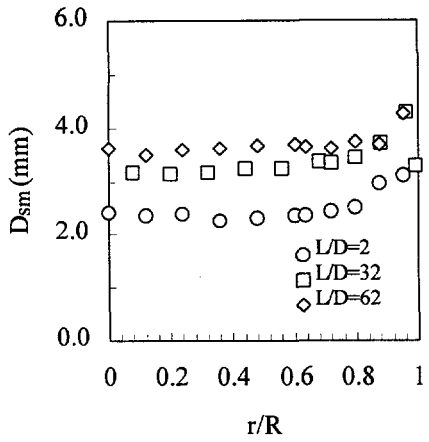

Fig. 9 Bubble Sauter mean diameter profile (jg=0.039m/s jf=1.3m/s)

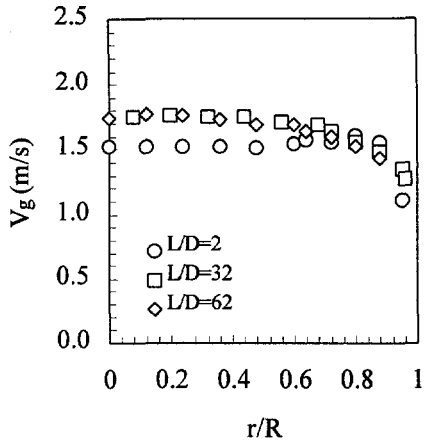

Fig. 10 Bubble velocity profile (jg=0.039m/s jf=1.3m/s)

IV. PRELIMINARY MODEL EVALUATIONS

At the present stage, the modeling evaluation is in progress with the detailed experimental data presented in the previous section. Here, the preliminary results are presented for the simplest form of the developed interfacial area transport equation, i.e., the steady-state, one-dimensional transport equation obtained by applying cross-sectional area averaging over Eq. (7):

$$\frac{\partial}{\partial z}\left(\langle a_i \rangle \langle\langle v_{gz} \rangle\rangle\right) = \langle S_{a,RC} \rangle + \langle S_{a,WE} \rangle + \langle S_{a,TI} \rangle, \tag{17}$$

where the bubble expansion effects are neglected and the gas phase is assumed to be incompressible. Due to the uniform bubble size assumption, the area-averaged bubble interface velocity weighted by interfacial area concentration is the same as the conventional area-averaged gas velocity weighted by the void fraction, if the internal circulation in bubbles is neglected. The exact mathematical expressions for the area-averaged source and sink terms would involve many covariances, which may further complicate the one-dimensional problem. However, since these local terms were originally obtained from a finite mixture element, the functional dependence of the area-averaged source and sink terms on the averaged parameters may be approximately the same if the hydraulic diameter of the flow path is considered as the length scale of the finite element. Therefore, Eqs. (8), (9), and (12) with the parameters averaged within the cross-sectional area are applicable for the area-averaged source and sink terms Eq. (17)

Following the procedure suggested by Wu et al. [9], seven cases of tests (Kashyap, 1994 [16]) with identical initial bubble injection mechanisms are employed for the preliminary model evaluation. With the measured interfacial area concentration at L/D=2 as the initial condition, Eq. (17) is integrated numerically to predict the axial distribution, and the adjustable parameters C_{RC}, C, C_{WE}, C_{TI} and We_{cr} are determined once the predictions at the other two locations match

the experimental data. The final results of these parameters are listed in Table 1. It should be mentioned that the coalescence efficiency is assumed to be constant in this evaluation. For very small bubbles, the chance for bubble coalescence upon each collision may be smaller, and thus the coalescence efficiency should be investigated.

Table 2 Adjustable parameters

C_{RC}	C	C_{WE}	C_{TI}	We_{cr}
0.0565	3	0.151	0.18	2.0

Compared to the experimental data, all 7 cases are shown in Fig. 11a and 11b. The model predicting interfacial area concentration is generally in good agreement with the measurements. The maximum relative difference is about 8% at very small void fraction with high liquid flow rate. Nevertheless, the conclusions are based on the simplified one-dimensional model with constant coalescence efficiency. Fine-tuning of these models and the adjustable parameters is needed.

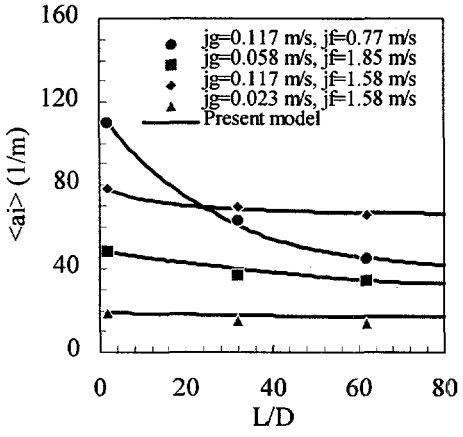

Fig. 11a a_i versus L/D

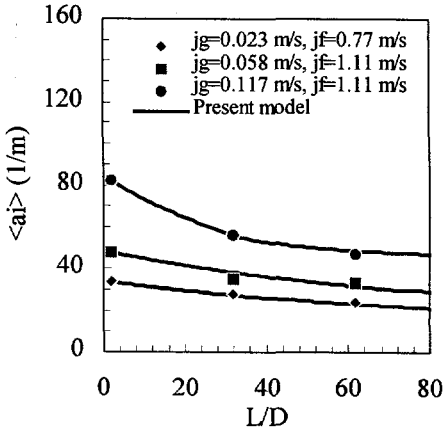

Fig. 11b a_i versus L/D

V. CONCLUSIONS

In this study, the efforts focused on the investigation of the interfacial area concentration transport phenomena, both theoretically and experimentally. Starting from the bubble number transport equation, the interfacial area concentration transport equation for the air-water bubbly up-flow in a vertical pipe was developed. The models for the source and sink terms due to bubble agglomeration and disintegration were provided. For bubble coalescence, two mechanisms are considered to be important in bubbly flow, i.e., the random collisions caused by turbulence and the wake-entrainment process. For bubble disintegration, the impact of turbulent eddies is included. From these mechanistic models, the necessary parameters for the experimental studies were identified, including the local time-averaged void fraction, interfacial

area concentration, bubble interfacial velocity, liquid velocity and turbulent intensity. Experiments were performed with an air-water mixture at atmospheric pressure. Double-sensor conductivity probe and hot-film probe were employed to measure the identified parameters. Detailed local time-averaged measurements were obtained at three axial positions and the experimental results provided a comprehensive data base for the model evaluation. At the present stage, the model evaluation is in progress with the detailed experimental data. Only the preliminary results were presented for the simplest form of the developed interfacial area transport equation, i.e., the one-dimensional transport equation. For application to three-dimensional problems, however, the adjustable parameters need to be evaluated. It should be emphasized again that the coalescence efficiency in the models was assumed to be constant. In reality, the liquid surface tension and bubble size have strong influences on the coalescence probability, and thus this assumption may not be universal. Further studies need to be performed to understand the bubble coalescence mechanism upon each collision. Moreover, the present transport equation is applicable only to bubbly flow. When cap/slug bubbles appear, another group transport equation should be constructed to depict the cap/slug bubble behaviors. In such a situation, some inter-group interactions would play important roles in the interfacial area transport process.

ACKNOWLEDGMENTS

This study was performed under the auspices of the U.S. Department of Energy. The authors would like to express their sincere appreciation to Dr. O.P. Manley of DOE/BES for his support of this project.

REFERENCES

1. P. Vernier and J.M. Delhaye, "General Two-Phase Flow Equations Applied to the Thermohydrodynamics of Boiling Nuclear Reactor," Engr. Primaire, Vol. No. 1, 5 (1968).
2. M. Ishii, *Thermo-Fluid Dynamic Theory of Two-Phase Flow*, Collection de la Direction des Etudes et Reserches d'Electricité de France, Eyrolles, Paris (1975).
3. J.A. Boure, "Mathematical Modeling of Two-Phase Flows," Proc. of CSNI Specialist Meeting, S. Banerjee and K.R. Weaver, Eds. A.E.C.L., Vol. 1, 85, Aug. 3-4, Toronto (1978).
4. J.N. Reyes, "Statistically Derived Conservation Equations for Fluid Particle Flows," 5th Proc. ANS-THD, P. 12, 1989 ANS Winter Meeting, San Francisco, CA, Nov. (1989).
5. G. Kocamustafaogullari and M. Ishii, "Foundation of the Interfacial Area Transport Equation and its Closure Relation," *Int. J. Heat and Mass Transfer*, Vol. 38, No. 3, 481 (1995).
6. G. Kocamustafaogullari and M. Ishii, "Interfacial Area and Nucleation Site Density in Boiling Systems," *Int. J. Heat and Mass Transfer*, Vol. 26, 1377 (1983).
7. M.J. Prince and H.W. Blanch, "Bubble Coalescence and Break-Up in Air-Sparged Bubble Columns," *AIChE Journal*, Vol. 36, No. 10, 1485 (1990).

8. A.Y. Lafi and J.N. Reyes, Jr., "Phenomenological Models for Fluid Particle Coalescence and Breakage," OSU-NE-9120, Report of the Department of Nuclear Engineering, Oregon State University, Corvallis, Oregon 97331, USA (1991).

9. Q. Wu, S. Kim, M. Ishii, and S.G. Beus, "One-Group Interfacial Area Transport in Vertical Air-Water Bubbly Flow," Accepted by the 1997 National Heat Transfer Conference to be held in Baltimore, Maryland, Aug. 10-12 (1997).

10. C.A. Coulaloglu and L.L. Tavlarrides, "Drop Size Distributions and Coalescence Frequencies of Liquid-Liquid Dispersion in Flow Vessels," *AIChE J.*, Vol. 22, 289 (1976).

11. G.B. Wallis, *One-dimensional Two-phase Flow*, McGraw-Hill Book Company, NY. 350 (1969).

12. T. Oolman and H.W. Blanch, "Bubble Coalescence in Stagnant Liquids," *Chem. Eng. Commun.*, Vol. 43, 237 (1986).

13. Q. Wu and M. Ishii, "Sensitivity Studies on Double-Sensor Conductivity Probe for the Measurement of Interfacial Area Concentration in Bubbly Flow," submitted to the *Int. J. Multiphase Flow*, (1997).

14. S. Hogsett, "The Axial Development of Liquid Turbulence and Interfacial Area in Bubbly Two-Phase Flow," M.S. Thesis, Department of Nuclear Engineering, Purdue University, (1996).

15. T. Hibiki, S. Hogsett, and M. Ishii, "Local Measurement of Interfacial Area, Interfacial Velocity and Liquid Turbulence in Two-Phase Flow," OECD/CSNI Specialist Meeting on Advanced Instrumentation and Measurement Techniques, Santa Barbara, March 17-20 (1997).

16. A. Kashyap, M. Ishii and S.T. Revankar, "An Experimental and Numerical Analysis of Structural Development of Two-Phase Flow," PU-NE-94/2, Report of the Nuclear Engineering Department, Purdue University, West Lafayette, IN 47907, USA (1994).

ASPECTS OF SUBCOOLED BOILING

S. G. Bankoff

Chemical Engineering Department
Northwestern University
Evanston, IL 60208

ABSTRACT

Subcooled boiling boiling refers to boiling from a solid surface where the bulk liquid temperature is below the saturation temperature (subcooled). Two classes are considered: 1) nucleate boiling, where, for large subcoolings, individual bubbles grow and collapse while remaining attached to the solid wall, and 2) film boiling, where a continuous vapor film separates the solid from the bulk liquid. One mechanism by which subcooled nucleate boiling results in very large surface heat transfer coefficient is thought to be latent heat transport within the bubble, resulting from simultaneous evaporation from a thin residual liquid layer at the bubble base, and condensation at the polar bubble cap. Another is the increased liquid microconvection around the oscillating bubble. Two related problems have been attacked. One is the rupture of a thin liquid film subject to attractive and repulsive dispersion forces, leading to the formation of mesoscopic drops, which then coalesce and evaporate. Another is the liquid motion in the vicinity of an oscillating contact line, where the bubble wall is idealized as a wedge of constant angle sliding on the solid wall. The subcooled film boiling problem has been attacked by deriving a general long-range nonlinear evolution equation for the local thickness of the vapor layer. Linear and weakly-nonlinear stability results have been obtained. A number of other related problems have been attacked.

INTRODUCTION

Subcooled boiling refers to boiling from a hot solid surface in the presence of subcooled bulk liquid. Two major regimes can be distinguished: a) subcooled nucleate boiling, in which myriads of small bubbles grow and collapse while remaining attached to the heating surface, and b) subcooled film boiling, in which a continuous film (except possibly for transient and limited contacts) separates the hot wall from the subcooled bulk liquid. The transition from nucleate boiling to film boiling occurs at some critical value of

the surface heat flux, and may lead to disastrous overheating of the solid wall. On the other hand, subcooled nucleate boiling is a highly efficient mode of heat transfer, with reported heat fluxes in the neighborhood of 3×10^3 w/cm^2, or more in some cases. On the other hand, film boiling is much less efficient, although with sufficient liquid subcooling the quasi-steady film thickness may be quite small. At a critical surface temperature, known as the minimum film boiling temperature, the vapor film collapses, and the transition to nucleate boiling occurs at constant heat flux.

The mechanism whereby such large heat fluxes are attained in subcooled nucleate boiling is naturally of great interest. Two major theories have been proposed: 1) increased turbulent mixing and transient liquid-wall contact owing to the presence of the growing and collapsing bubbles, 2) latent heat transport within the bubbles, in which evaporation occurs from a thin liquid residual layer left behind by the bubble growth, and simultaneous condensation at the colder polar region of the bubble in contact with the bulk liquid. Arguments have been advanced for and against these theories [1]. Better understanding of the basic mechanisms is needed. Some specialized problems have therefore been attacked in order to make progress on understanding the overall mechanism of subcooled nucleate boiling. The first examines the rupture of the residual microlayer at the base of the bubble while it is attached to the wall [2]. The formation of an array of isolated microdrops connected by extremely thin liquid film is predicted. These drops evaporate while coalescing, and eventually disappear. A second problem addresses the liquid motion in the vicinity of the oscillating contact line as the bubble grows and collapses periodically. The bubble wall is idealized as a wedge of constant contact angle moving with respect to the solid wall [3]. Approximate solutions are obtained, using double (Laplace and Mellin) transforms, showing attainable regions of parameter space, and flow reversals even at very small Strouhal numbers (dimensionless frequencies).

At the other end of the spectrum, the mechanism of destabilization of subcooled film boiling is poorly understood. There is a steady base-state thickness at which condensation exactly balances evaporation for a vapor film separating a plane heating surface from the bulk subcooled liquid [4]. To make progress on this problem, one can assume an average heat transfer coefficient at the vapor-liquid surface. Small perturbations from the base state can be studied by linear theory, but contact with the solid wall involves wave amplitudes which are of the same order as the base vapor film thickness. Lubrication theory, as in the treatment of the stability of thin liquid films, can then be employed prior to contact, since long-wave theory is appropriate. An interesting difference between the present problem and the instability of an evaporating liquid film is that vapor recoil effects, owing to the spatial variations of the reactive pressure on the evaporating liquid surface, are stabilizing for the vapor film, but destabilizing for the liquid film. A weakly nonlinear analysis reveals a supercritical branch of new equilibrium solutions corresponding to wave-like modulations of the uniform film. These disturbances satisfy the Newell-Whitehead-Segel (NWS) equation on an unbounded heating surface. Work on this problem is continuing.

SUBCOOLED NUCLEATE BOILING

Unsteady Stokes flow near an oscillating contact line [3].

Consider the flow in a wedge of incompressible fluid bounded by a solid surface and

a passive gas, as shown in Figure 1. We assume that the no-slip boundary condition is relaxed near the contact line, so that the stress singularity is removed by posing a slip velocity. The origin of the polar-coordinate system is placed at the contact line. The flow within the wedge is governed by the Navier-Stokes equations with continuity.

$$\nabla \cdot \mathbf{u} = 0 , \tag{1}$$

$$\rho(\mathbf{u}_t + \mathbf{u} \cdot \nabla\mathbf{u}) = -\nabla p + \upsilon\nabla^2\mathbf{u} , \tag{2}$$

with interfacial conditions of continuity of shear stress, the jump in normal stress balanced by surface tension σ times the curvature κ, and the kinematic boundary condition at $\theta = \alpha(r,t)$

$$[\mathbf{n} \cdot \mathbf{T} \cdot \mathbf{T} = 0 , \tag{3}$$

$$[\mathbf{n} \cdot \mathbf{T} \cdot \mathbf{t}] = \sigma\kappa , \tag{4}$$

$$\left[1 + (r\frac{\partial\alpha}{\partial r})^2\right]^{1/2} \alpha_t + u \cdot n = 0 , \tag{5}$$

where [f] is the jump in the quantity f across the interface. A tangential velocity profile on the solid boundary at $\theta = 0$ is prescribed

$$u(r,t) = U_o(r) \cos \omega t , \tag{6}$$

$$v(r,t) = 0 , \tag{7}$$

where (u,v) are the radial and azimuthal velocities respectively. The prescribed velocity profile $U_o(r)$ is assumed to be zero at $r = 0$, and approaches a general constant velocity amplitude U as $r \rightarrow \infty$. The transition scale between these velocities occurs on a prescribed slip length-scale L_s. This prescribed condition is an assumption on the plate velocity.

Lengths are scaled on this slip length scale L_s, velocities on the amplitude of the oscillating boundary U, time on the period of the oscillation $1/\omega$, along with a Stokes pressure scale $\mu U/L_s$ to arrive at the scaled system

$$\nabla \cdot \mathbf{u} = 0 , \tag{8}$$

$$S\ \mathbf{u}_t + Re\ \mathbf{u} \cdot \nabla\mathbf{u} = -\nabla p + \nabla^2\mathbf{u} , \tag{9}$$

where $S = L^2\omega/\upsilon$ is the Strouhal number, and $Re = UL/\upsilon$ is the Reynolds number. The interfacial conditions at $\theta = \alpha(r,t)$ become

$$[\mathbf{n} \cdot \mathbf{T} \cdot \mathbf{t}] = 0 \tag{10}$$

$$Ca[\mathbf{n} \cdot \mathbf{T} \cdot \mathbf{t}] = \sigma \tag{11}$$

$$\left[1 + (r\frac{\partial\alpha}{\partial r})^2\right]^{-1/2} \alpha_T + u \cdot n = 0 \tag{12}$$

where $Ca = \mu U/\sigma$ is the capillary number and

$$\kappa = \frac{1}{r}\frac{d}{dr}\left[r^2\frac{d\alpha}{dr}\right] + r^2\left[\frac{d\alpha}{dr}\right]^3\left\{1 + r\left[\frac{d\alpha}{dr}\right]\right\}^{-3/2} \tag{13}$$

The prescribed tangential velocity profile on the solid boundary at $\theta = 0$ becomes

$$u(r,t) = u_o(r) \cos t \tag{14}$$

$$v(r,t) = 0 , \tag{15}$$

with the prescribed velocity $u_o(r) \rightarrow 1$ as $r \rightarrow \infty$.

In studying local effects near a contact line that is strongly unsteady, it is assumed that inertial effects are small ($Re = 0$) but time variations are significant ($S = O(1)$). Capillary effects are also neglected ($Ca = 0$) and hence also the dynamics of the interface ($\alpha(r,t) = \alpha_0$). With these assumptions, a stream function formulation is used to consider the following problem:

$$S(\nabla^2\psi)_t = \nabla^4\psi \tag{16}$$

with, at $\theta = 0$,

$$\psi = 0 \tag{17}$$

$$\psi_{\theta\theta} = 0 . \tag{18}$$

By using Mellin and Laplace transforms in r and t, one obtains a stream function solution, whose poles provide the eigenvalues for each of the characteristic modes. One finds that nonuniformities are always present when there is both a steady forcing component and an arbitrarily small amplitude of an oscillatory component. One further finds that the drag force on the plate increases as the frequency of the oscillation increases.

NONLINEAR DYNAMICS OF ULTRA-THIN LIQUID FILMS

The breakdown and evaporation of the thin residual film left on the solid wall as the bubble grows is modeled as the spatio-temporal evolution of a two-dimensional thin volatile liquid layer, subjected to long-range molecular attractive forces and short-range repulsive forces. The evaporating film is described in dimensionless form by the nonlinear evolution equation

$$h_t + \frac{E}{h + K} + [(Ah^{-1} - BH^{-2})h_x]_x + S(h^3 h_{xxx})_x = 0, \tag{19}$$

provided that the disjoining/conjoining pressure is represented by the dimensionless potential

$$\Pi = \frac{A}{3}h^{-3} - \frac{B}{4}h^{-4}, \tag{20}$$

where t is time and x is the spatial coordinate along the solid substrate supporting the film. Here A,B are, respectively, dimensionless Hamaker constants for attractive long-range and repulsive short-range molecular forces, E is the dimensionless evaporation number and K is a thermal resistance at the interface owing to evaporation.

Linearizing the rescaled equations for a non-volatile liquid (E=0) yields

$$\omega = (\frac{1}{h_o} - \frac{\beta}{h_0^2})k^2 - h_0^3 k^4, \tag{21}$$

where k and ω are the wave number and growth rate of the interfacial disturbance, which is proportional to $\exp(\omega t + ik_x x + ik_y y)$, $k = \sqrt{k_x^2 + k_y^2}$. It follows from Eq. (21) that destabilization of the interface is due to attractive molecular forces, while its stabilization stems from both repulsive molecular and capillary forces.

Figure (2a,b,c,d) display the evolution of a volatile liquid film subject to a relatively slow evaporation rate, E = 0.5, and a finite interfacial resistance K = 1. The nucleation of the "dry spot" begins at t = 1.835 and the process of dewetting is accompanied by receding of the liquid, which is due to the squeeze effect of attractive molecular forces, Fig. (2a), formation of the rims and their disintegration into drops separated by new dry spots, Fig. (2b). Later, evaporation of the liquid and widening of the dry spots lead to the disappearance of smaller drops and growth of the larger ones, Fig (2c). Further, the larger drops coalesce due to evaporation and recession of the rims walls, Fig. (2d). Once a single large drop is formed, the dominant effect is evaporation and flattening of the interface. The last stage of the evolution begins with the last curve shown in Fig. (2d) which represents an almost flat interface. The film then disappears uniformly in space.

ACKNOWLEDGMENTS

This work was supported by Grant DE-FG02-86ER 13641, S.G. Bankoff and S.H. Davis, Co-Principal Investigators. Contributors were A. Oron, Visiting Scholar, B.S. Tilley, Applied Mathematics, New Jersey Institute of Technology, and C.A. Panzarella, graduate student.

REFERENCES

1. G. TSUNG-CHANG, and S.G. BANKOFF, "On the Mechanism of Forced-Convection Subcooled Nucleate Boiling," *J. Heat Transfer*, 112, 213-217 (1990).

*2. A. ORON and S.G. BANKOFF, "Nonlinear Dynamics of Ultra-Thin Liquid Films," manuscript in preparation (1997).

*3. B.S. TILLEY, S.H. DAVIS and S.G. BANKOFF, "Unsteady Stokes Flow Near an Oscillating Contact Line, submitted to *J. Fluid Mech.* (1997).

*4. C.H. PANZARELLA, S.G. BANKOFF and S.H. DAVIS, "A Long-Wave Analysis of Film Boiling," manuscript in preparation (1997).

*Work supported by grant in report period.

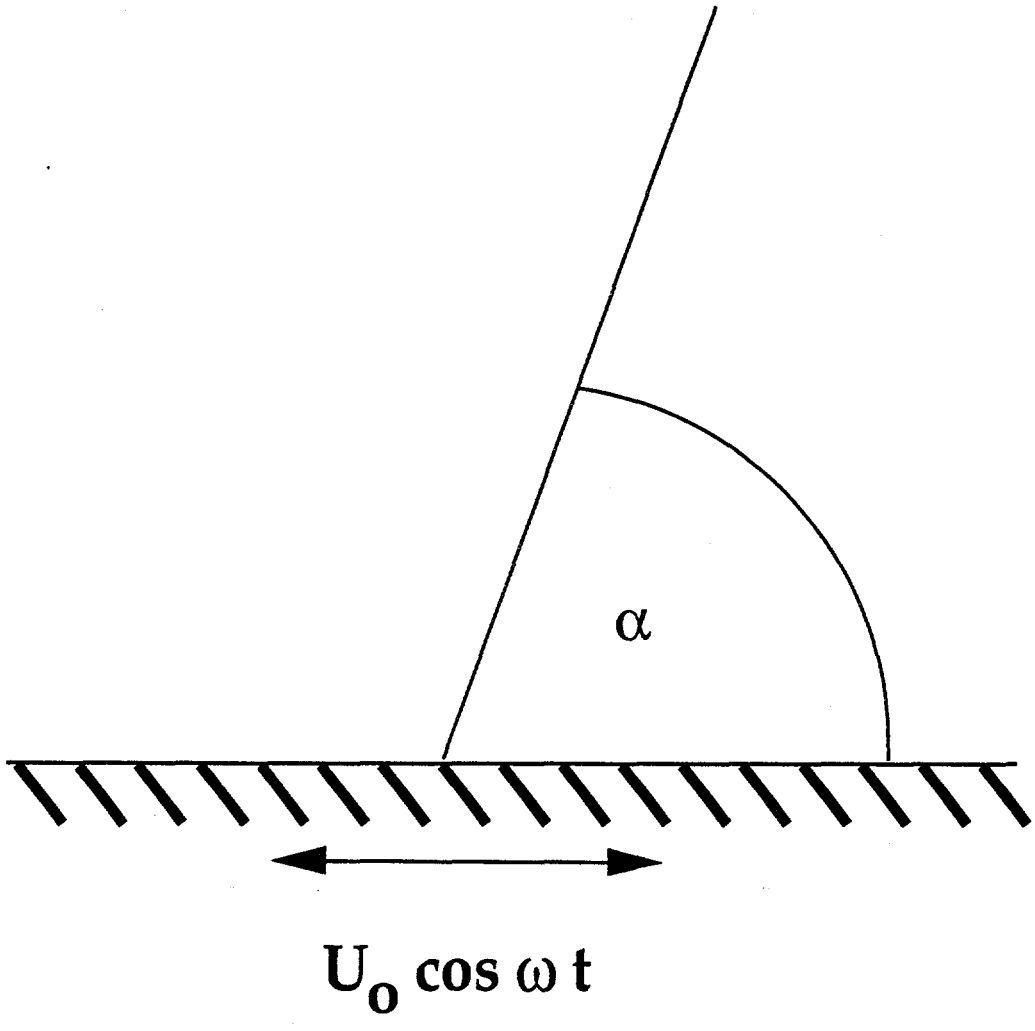

Fig. 1 Oscillating Wedge

Fig. 2a

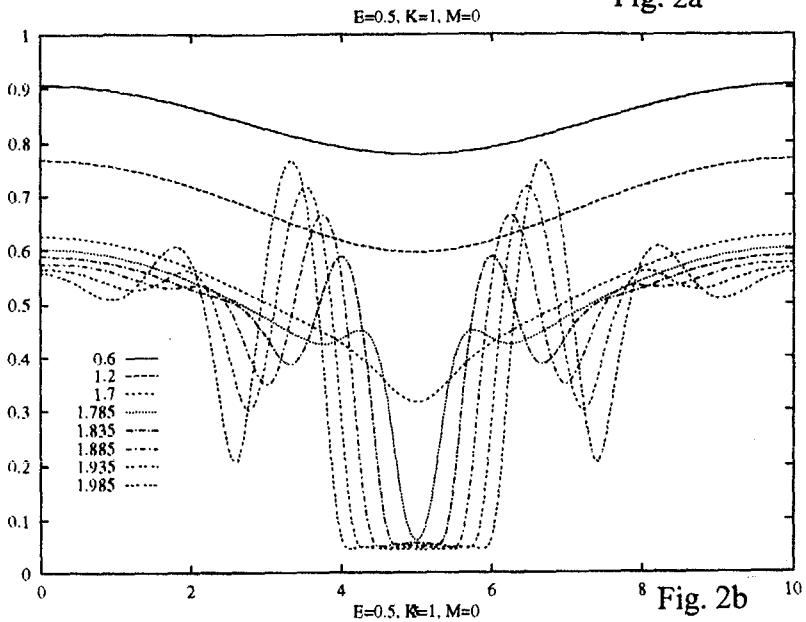

Fig. 2b

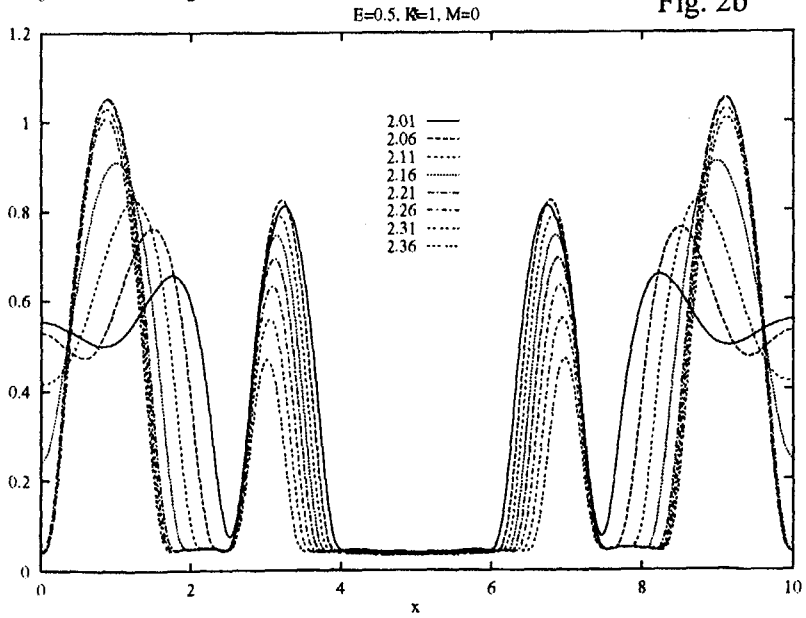

Fig. 2c

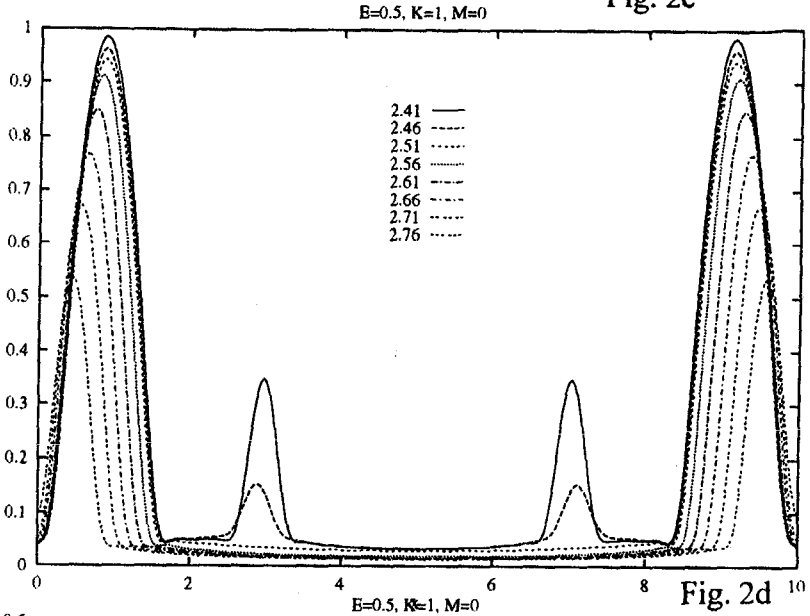

Fig. 2d

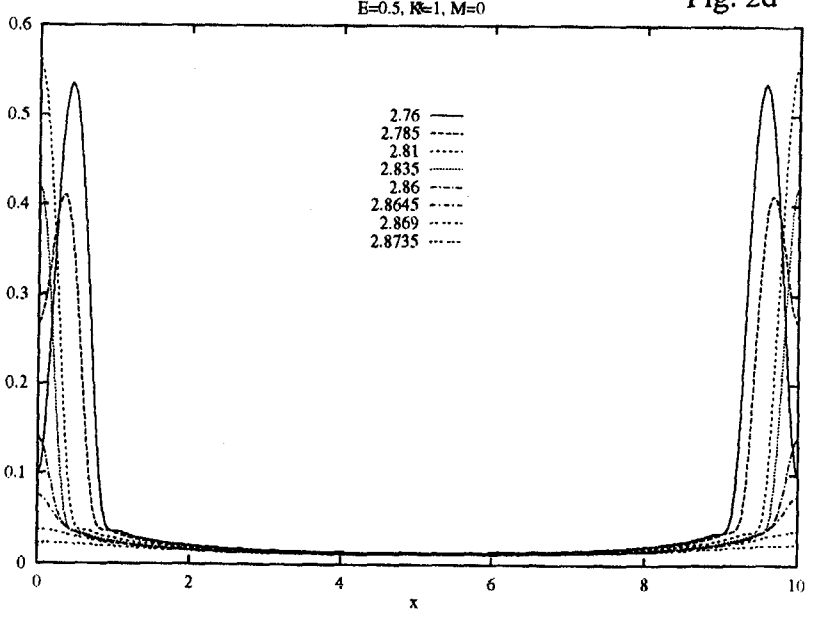

DESIGN OF A VAPOR-LIQUID-EQUILIBRIUM, SURFACE TENSION, AND DENSITY APPARATUS[1]

C.D. Holcomb and S.L. Outcalt

National Institute of Standards and Technology
Physical and Chemical Properties Division
325 Broadway
Boulder, Colorado 80303

ABSTRACT

The design and performance of a unique vapor-liquid equilibrium (VLE) apparatus with density and surface tension capabilities is presented. The apparatus operates at temperatures ranging from 218 to 423 K, at pressures to 17 MPa, at densities to 1100 kg/m^3, and at surface tensions ranging from 0.1 to 75 mN/m. Temperatures are measured with a precision of ±0.02 K, pressures with a precision of ±0.1% of full scale, densities with a precision of ±0.5 kg/m^3, surface tensions with a precision of ±0.2 mN/m, and compositions with a precision of ±0.005 mole fraction.

The apparatus is designed to be both accurate and versatile. Capabilities include: 1) the ability to operate the apparatus as a bubble point pressure or an isothermal pressure-volume-temperature (PVT) apparatus, 2) the ability to measure densities and surface tensions of the coexisting phases, and 3) the ability for either trapped or capillary sampling. We can validate our VLE and density data by measuring PVT or bubble point pressures in the apparatus. The use of the apparatus for measurements of VLE, densities, and surface tensions over wide ranges of temperature and pressure is important in equation of state and transport property model development. The use of different sampling procedures allows measurement of a wider variety of fluid mixtures. VLE measurements on the alternative refrigerant system R32/134a are presented and compared to literature results to verify the performance of the apparatus.

INTRODUCTION

Experimental properties of fluids in the two-phase region are very valuable in the characterization of the thermodynamic surface of fluids. The search for alternative refrigerants is

[1] Contribution of the National Institute of Standards and Technology, not subject to copyright in the U. S.

one of many research areas where high quality data on the vapor-liquid equilibria and densities of the coexisting phases are needed. These properties are essential in the design and optimization of many industrial processes including air-conditioning and refrigeration systems. Vapor-liquid equilibrium and coexisting density measurements are essential for developing models for the saturation boundaries of fluids. Surface tension measurements are important in calculating heat transfer coefficients for boiling and condensation. In an effort to increase our capabilities for making accurate vapor-liquid-equilibrium measurements over a large temperature range and to include the ability to measure coexisting densities and surface tensions, a new apparatus has been designed and constructed which covers the temperature range of 218 to 423 K at pressures up to 17 MPa.

APPARATUS DESIGN

Physical Description

The apparatus is designed for density and surface tension measurements in addition to the vapor-liquid-equilibrium measurements. The primary components of the apparatus are an equilibrium cell, two recirculation pumps, three platinum resistance thermometers (PRTs), two quartz crystal pressure transducers, two differential pressure transducers, a gas chromatograph (GC), two vibrating tube densimeters, a recirculating refrigerator, two heating systems, a temperature controlled enclosure, and a data acquisition system. Figure 1 shows a schematic of the apparatus. In order to obtain accurate measurements, the equilibrium cell, densimeters, and recirculating pumps must be maintained at the desired temperature and the gradients must be minimized between these components. A well-stirred liquid bath is used to achieve temperature control and minimize temperature gradients. A large glass Dewar is used to contain the silicone-oil bath and insulate it from the room. The five components are immersed in the oil. Other items located in the Dewar include the heating/cooling coils, a stirrer with three impellers, and three PRTs. The PRT located closest to the equilibrium cell is a standard-reference-quality four-wire PRT while the other two (located near the densimeters) are industrial quality four-wire PRTs. These three PRTs allow us to monitor the temperature gradients within the bath and adjust the stirrer speed to minimize the gradients.

A length of stainless steel tubing connects the system to a temperature controlled enclosure which houses the differential pressure transducers and valving for filling and evacuating the system. Located outside of the enclosure are the filling system (a liquid piston pump and a manual screw pump) and the pressure transducers. The enclosure is maintained at a temperature 10 K above the main apparatus temperature to ensure that only vapor is present in the enclosure. Liquid condensation in this part of the apparatus would adversely affect the pressure and surface tension measurements.

The vapor and liquid samples needed to determine the compositions are obtained using capillary sampling. Capillary lines are connected to the top and bottom of the main cell. The samples are withdrawn from the system and flow through two gas chromatograph injection valves. The valves inject small amounts of the samples into a helium carrier gas stream. This carrier stream flows directly into a gas chromatograph where the samples are analyzed.

Temperature Control

The uncertainties of the properties measured in this apparatus are close to state-of-the-art, especially considering the wide range of properties simultaneously measured on the same sample and the wide ranges of temperatures and pressures covered. The pressures are measured with a

precision of ±0.1% of full scale, the temperatures with a precision of ±0.02 K, the compositions with a precision of ±0.005 mole fraction, the densities with a precision of ±0.5 kg/m^3, and the surface tensions with a precision of ±0.2 mN/m. Accurate measurements are attainable because possible sources of systematic errors like large temperature gradients or a low degree of temperature stability are eliminated.

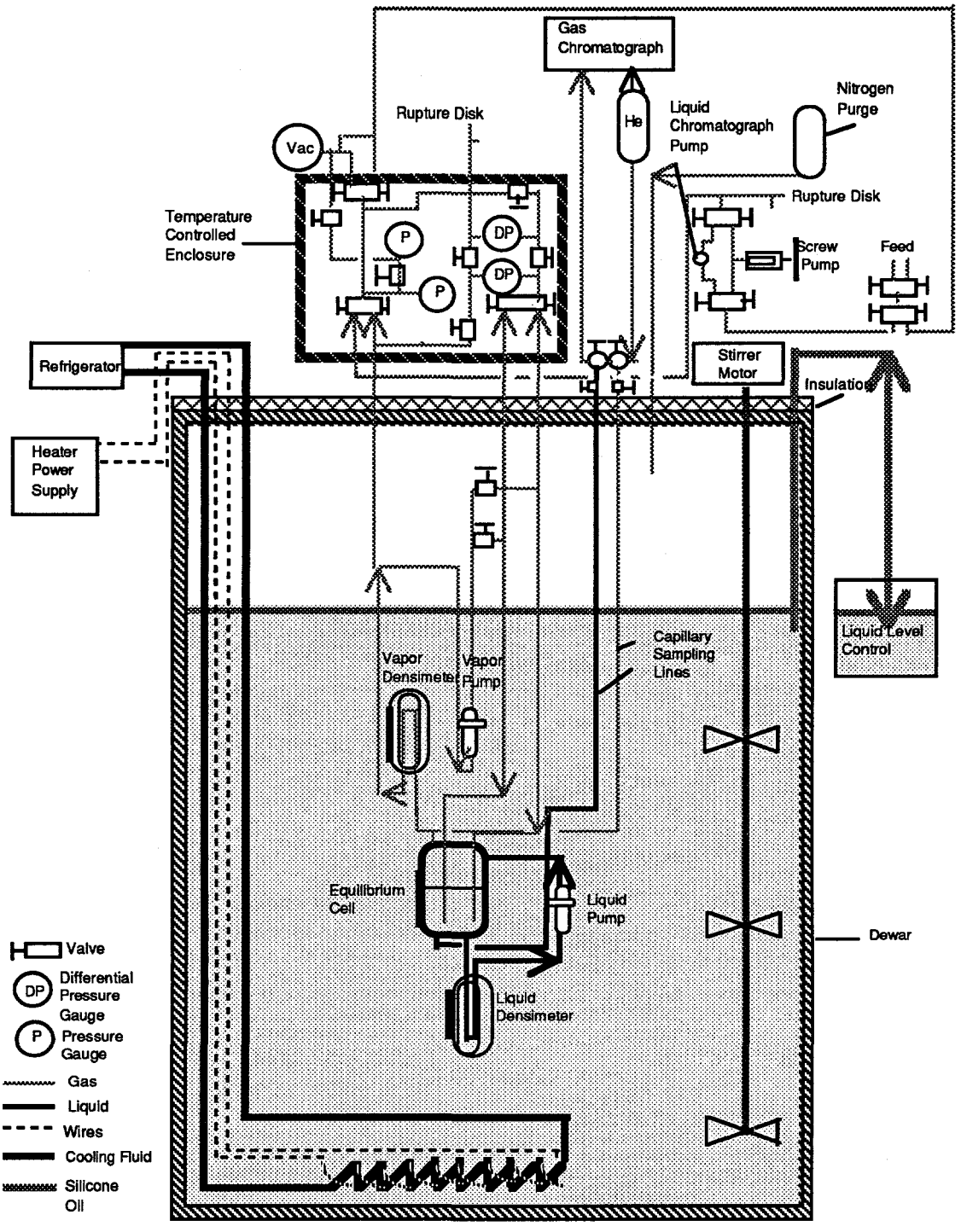

Figure 1. Schematic Diagram of the Coexisting Density and Vapor-Liquid-Equilibrium Apparatus with Surface Tension Measurement Capabilities

In designing this liquid-bath apparatus, particular care was taken to minimize thermal gradients within the Dewar. Silicone oil was selected as the bath fluid because of its excellent heat transfer properties and because it is one of the few commercially available heat transfer fluids that has a low viscosity and low vapor pressure over the entire temperature range of the apparatus. It is also non-flammable, non-toxic and relatively inexpensive.

Temperature control of the silicone oil bath is achieved with two heating systems and a recirculating refrigerator. The fine heating system is a low-power, computer-controlled system used for fine temperature control. It is capable of maintaining the bath temperature within ± 0.02 K of the set-point temperature for several hours. The coarse heating system consists of a high-power system with a programmable controller. It is the major source of heat when increasing the temperature of the system.

A large recirculating refrigerator cools the silicone oil bath. The set-point temperature of the recirculating fluid exiting the refrigerator is ten degrees colder than the set-point temperature of the apparatus. This temperature difference allows the refrigerator to remove heat from the system without introducing a cold spot. A metering valve is used to adjust the flow rate through the cooling coils. The valve is fully open when cooling the bath to a new set-point temperature and almost closed when providing the necessary cooling to maintain a given set-point temperature.

Vapor-Liquid Equilibrium Measurements

The apparatus is evacuated before initiating measurements on a new mixture. After the system reaches the desired temperature, the fluids of interest are loaded into the system. The components are added to the system using either the screw pump or the piston pump. Then, the recirculation pumps are turned on and the liquid and vapor phases are recirculated to ensure thorough mixing. The vapor is returned to the bottom of the cell and the liquid to the top. Next, the pumps are turned off and the pressure and temperature of the system are monitored. Once equilibrium is achieved, the pressure and temperature are recorded and the compositions of the two phases are determined. To advance to the next point on the isotherm, an additional amount of one component is added to change the composition. The phases are mixed and equilibrium is attained before the next set of measurements is obtained.

Sampling Systems

The compositions of the coexisting phases are determined by withdrawing vapor and liquid samples and analyzing them with a GC. The two basic methods for withdrawing the samples are known as capillary sampling and trapped sampling. A review and comparison of these two methods is reported by Noles[1]. The apparatus can be configured to use either type of sampling system, but is currently arranged for capillary sampling. Capillary sampling is used with systems that are sensitive to temperature gradients. These samples must be withdrawn directly from the equilibrium cell. This method relies on plug flow in the capillary lines to allow the mixture to flash to an all-vapor phase without stratification. A small quantity of the flashed vapor is injected into a helium carrier stream using a rotary GC valve. The sample is carried to the GC for analysis.

Trapped sampling is used when studying mixtures that are toxic, are available only in small quantities, or have a bubble-point pressure less than 0.3 MPa. Trapped sampling for this system involves mounting high pressure GC valves inside the lid of the dewar. The valves are piped into the recirculation loops, and the quantity of material is trapped in the rotor and then injected into a helium carrier stream. The sample is carried to the GC for analysis.

Density and Surface Tension Measurements

Coexisting densities and surface tension measurements can also be made with this apparatus. Two commercially available vibrating tube densimeters are used to measure the liquid and vapor densities. The densimeters are mounted so that they are self-draining, one densimeter is located above and one below the equilibrium cell. They are located in the recirculation lines to ensure that they are entirely filled with the equilibrium liquid or vapor. The temperature differences for the densimeters, pumps, and the equilibrium cell are within ±0.05 K. This ensures that the densities measured are representative of the bulk liquid and vapor.

The surface tension is measured using the differential bubble pressure method[2]. The vapor recirculation pump is used to supply vapor to two dip tubes mounted in the equilibrium cell. The equilibrium vapor is bubbled into the liquid through one dip tube at a time, and the maximum pressure that the bubble reaches during the bubble growth is measured with a differential pressure transducer. The surface tension is a function of the difference in the two maximum pressures, the radii of the two dip tubes, and the density difference between the vapor and liquid phases.

Apparatus Versatility

The system can be operated as an isothermal single-phase PVT or a two-phase bubble-point pressure apparatus as well as a vapor-liquid-equilibrium apparatus. The system can be filled completely with a gravimetrically prepared standard mixture and the densimeters used to measure the density as a function of pressure at a given temperature for that composition. This provides isothermal PVT measurements which can be used to supplement or validate existing PVT data.

The system can be nearly filled with a standard mixture and the bubble-point pressure can be measured as a function of temperature. The bubble-point pressure measurements eliminate the uncertainty introduced by sampling and analysis to determine the liquid composition. These measurements represent an independent verification of the bubble-point measurements from the vapor-liquid equilibrium measurements, and can be used to check the validity of the GC calibration.

PERFORMANCE VERIFICATION

Alternative refrigerant mixtures are excellent candidates for testing the performance of a vapor-liquid-equilibrium apparatus. These systems have small heats of vaporization and are especially sensitive to temperature gradients. Comparisons of the data measured for the alternative refrigerant mixture R32/134a with independent measurements demonstrate the ability of the apparatus for accurate vapor-liquid-equilibrium measurements.

The data for the R32/134a system cover 5 isotherms from 279 to 340 K. A total of 48 vapor-liquid equilibrium measurements are presented in Table 1. The data are compared to four other data sets available in the literature. We compare the data sets with the predictions of the Lemmon-Jacobsen model [3] in REFPROP 6.0 [4]. The deviations between the data and the values predicted from the Lemmon-Jacobsen model are presented in Figures 2 and 3. In Figure 2 the deviations between the measured bubble-point pressures and the predicted values are shown.

The scatter in the data might appear large compared to the experimental uncertainties quoted for the apparatus. However, a distinction must be made between the experimental uncertainty of a specific parameter measurement (such as temperature, pressure, or composition)

and the state-point uncertainty. The state point is system dependent and is defined as the equilibrium bubble-point pressure and vapor composition at a given liquid composition and temperature. Each of the parameters (P,T,x,y) has an experimental uncertainty associated with the measurement of that parameter. However, the state-point uncertainty is a function of the uncertainties of each of these four parameters as well as the dependencies between them. The state-point uncertainties are different for each system and vary with temperature and composition. The bubble-point state point uncertainty is calculated by multiplying the uncertainty in the composition measurement by dP/dx at that state point, adding the uncertainty of the pressure measurement, and adding the temperature measurement uncertainty multiplied by dP/dT at that state point. The bubble-point pressure state-point uncertainty for the R32/134a system at temperatures from 280 to 340 K ranges from ±0.22 to ±0.30% (±2σ)

Table 1

Vapor-Liquid Equilibrium Data for R32/134a Mixtures from 280 to 340 K [5].

x(R32) Liquid Mole Fraction	Temperature K	Pressure MPa	y(R32) Vapor Mole Fraction	x(R32) Liquid Mole Fraction	Temperature K	Pressure MPa	y(R32) Vapor Mole Fraction
0.000	280.39	0.379	0.000	0.619	299.96	1.357	0.761
0.299	279.98	0.555	0.489	0.262	303.87	1.076	0.403
0.478	280.05	0.674	0.676	0.609	303.07	1.453	0.756
0.604	279.98	0.739	0.757	0.000	309.31	0.913	0.000
0.642	279.98	0.772	0.797	0.181	309.98	1.167	0.292
0.642	280.09	0.774	0.793	0.225	310.00	1.225	0.370
0.650	279.99	0.778	0.805	0.228	309.97	1.215	0.363
0.650	280.19	0.778	0.796	0.360	309.98	1.392	0.515
0.737	280.13	0.852	0.869	0.681	309.99	1.826	0.793
1.000	280.00	1.006	1.000	1.000	309.99	2.294	1.000
0.302	283.02	0.609	0.483	0.000	324.50	1.367	0.000
0.632	283.06	0.840	0.782	0.162	325.00	1.643	0.256
0.640	283.01	0.846	0.795	0.294	324.99	1.889	0.422
0.640	283.08	0.847	0.795	0.595	325.00	2.423	0.710
0.283	289.91	0.746	0.466	0.733	324.99	2.698	0.809
0.637	289.79	1.030	0.782	0.783	324.99	2.805	0.860
0.282	292.93	0.811	0.457	1.000	324.99	3.279	1.000
0.634	292.92	1.124	0.773	0.000	340.16	1.986	0.000
0.000	294.69	0.596	0.000	0.466	339.87	3.036	0.569
0.275	294.95	0.856	0.448	0.577	339.93	3.315	0.669
0.452	294.99	1.018	0.626	0.763	339.99	3.807	0.820
0.529	295.13	1.091	0.696	1.000	339.98	4.561	1.000
0.584	294.94	1.149	0.748				
0.632	294.96	1.187	0.773				
0.720	294.94	1.271	0.838				
1.000	295.48	1.575	1.000				

The deviations in figure 2 compare the data to the predictions of the model. There is a slight composition dependent systematic deviation between the model and the data that appears as a spread in the deviations at a given temperature. The data taken with this apparatus agree with

Nagel and Bier [5] within ±1.0 %, and most of the data of Higashi [6] and of Widiatmo et al. [7] within ±2 % except for a few points. The data of Fujiwara et al. [8] at 273 K are consistently lower than any of the other data sets.

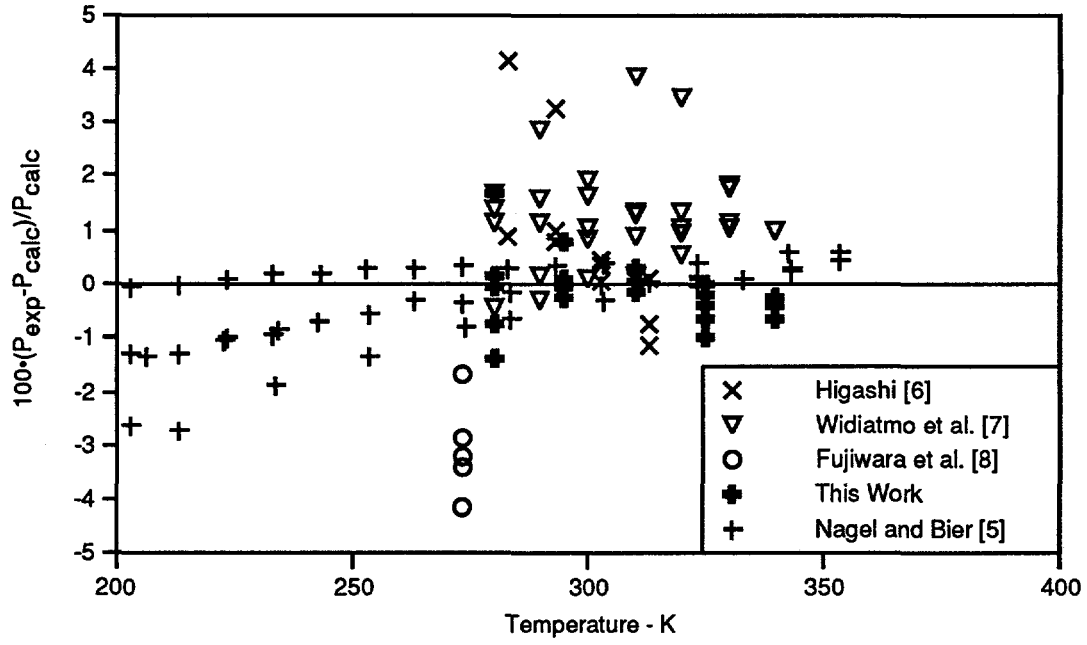

Figure 2. Comparison of Bubble-Point Pressures for the R32/134a System; the baseline is from the Lemmon-Jacobsen Model in REFPROP 6.0.

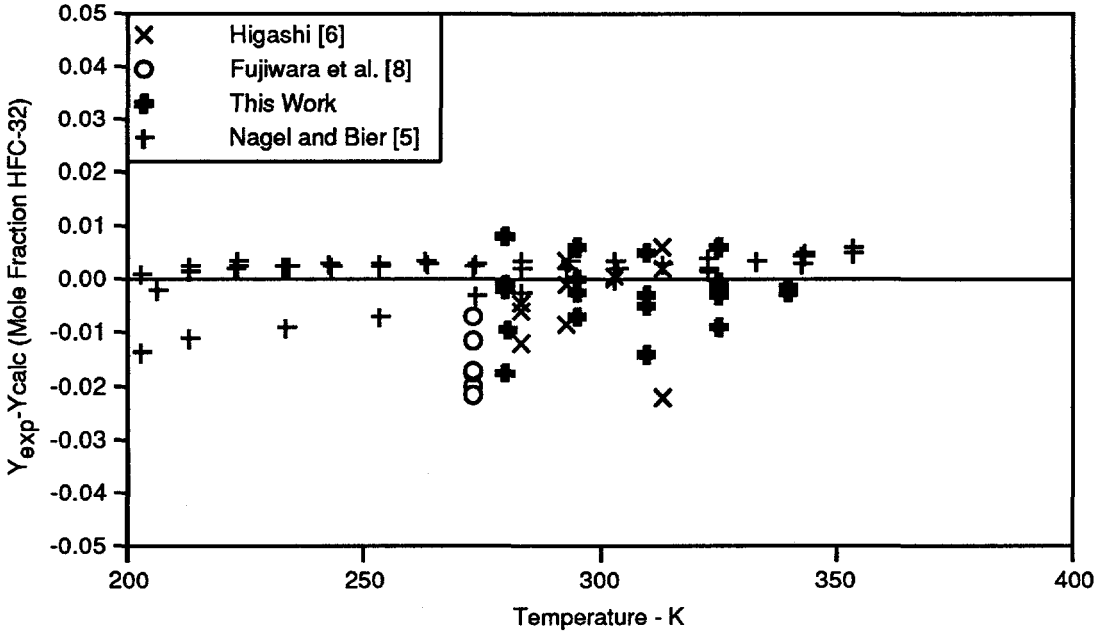

Figure 3. Comparison of Vapor Compositions for the R32/134a System; the baseline is from the Lemmon-Jacobsen Model in REFPROP 6.0.

In Figure 3 the vapor compositions of the data sets are compared. In general, the four data sets agree within ±0.015 mole or mass fraction HFC-32. The data of Fujiwara et al. [8] at 273 K are systematically 0.015 mole fraction HFC-32 lower than the data of Nagel and Bier [5].

The vapor-composition state-point uncertainty ranges from ±0.006 to ±0.013 mole fraction HFC-32 for the R32/134a system at temperatures from 280 to 340 K.

R32/134a is one of the many refrigerant mixtures that have been studied with this apparatus. Some of the systems included in the study were R32/125, R125/134a, R32/125/134a, R32/143a, R143a/125, R143a/134a, R32/290, R125/290, R134a/290, and R41/744 [9]. The apparatus is currently being used to study mixtures containing CF_3I and hydrocarbon mixtures.

ACKNOWLEDGEMENT

The financial assistance of the United States Department of Energy is gratefully acknowledged. The apparatus was constructed under a grant from the Division of Engineering and Geosciences in the Office of Basic Energy Sciences and the measurements on R32/134a mixtures were funded under a grant from the Building Equipment Division in the Office of Building Technologies.

REFERENCES

1. J. R. NOLES, "Vapor-Liquid Equilibria of Solvating Binary Mixtures," Ph. D. Thesis, Department of Chemical Engineering, Cornell University, Ithaca, NY. (1991).

2. C. D. HOLCOMB and J. A. ZOLLWEG, "An Improved Differential Bubble Pressure Surface Tensiometer," *Journal of Colloid and Interface Science* 154, 51 (1992).

3. E. W. LEMMON, "A Generalized Model for the Prediction of the Thermodynamic Properties of Mixtures Including Vapor-Liquid Equilibrium," Ph. D. Thesis, Department of Mechanical Engineering, University of Idaho, Moscow, ID. (1996).

4. M. O. MCLINDEN and S. A. KLEIN, "A Next Generation of Refrigerant properties Database," Proceedings of the 6th International Refrigeration Conference at Purdue, West Lafayette, IN, July 23-26, 409 (1996).

5. M. NAGEL and K. BIER, "Vapour-Liquid Equilibrium of Ternary Mixtures of the Refrigerants R32, R125 and R134a," *International Journal of Refrigeration* 18, 534 (1995).

6. Y. HIGASHI,"Vapor-Liquid Equilibrium, Coexistence Curve, and Critical Locus for Binary HFC-32/HFC-134a Mixture," *International Journal of Thermophysics* 16 ,1175 (1995).

7. J. V. WIDIATMO, H. SATO, and K. WATANABE, "Measurements of the Liquid Densities of the Binary HFC-32 + HFC-134a System," *Fluid Phase Equilibria* 99, 199 (1994).

8. K. FUJIWARA, H. MOMOTA, and M. NOGUCHI, "Vapor-Liquid Equilibria of HFC-32 Mixtures," 13th Japanese Symposium Thermophysical Properties A116, 61 (1992).

9. W. M. HAYNES, "Thermophysical Properties of HCFC Alternatives", Final Report, Air-Conditioning and Refrigeration Technology Institute", November 1996.

INTERFACIAL WAVE BEHAVIOR IN OIL-WATER CHANNEL FLOWS: PROSPECTS FOR A GENERAL UNDERSTANDING

M. J. McCready, D. D. Uphold, K. A. Gifford
Department of Chemical Engineering
University of Notre Dame
Notre Dame, Indiana 46556 USA

ABSTRACT

Oil-water pressure driven channel flow is examined as a model for general two-layer flows where interfacial disturbances are important. The goal is to develop sufficient understanding of this system so that the utility and limitations of linear and nonlinear theories can be known *a priori*. Experiments show that sometimes linear stabilty is useful at predicting the steady or dominant evolving waves. However in other situations there is no agreement between the linearly fastest growing wave and the spectral peak. An interesting preliminary result is that the bifurcation to interfacial waves is supercritical for all conditions that were studied for an oil-water channel flow, gas-liquid channel flow and two-liquid Couette flow. However, three different mechanisms are dominant for each of these three situations.

INTRODUCTION

All facets of energy production and distribution involve processes that contain multi-fluid flows. Hydrocarbon production and transportation, energy exchange devices such as condensers are common examples. Further, there is extensive use of multiphase reactors for chemical production in which hydrodynamic instabilities can alter the chemical product distribution.

Unfortunately, even for the simplest class of two-fluid flows, stratified, it is not possible to predict the nature of the instabilities that occur and the eventual downstream behavior. While it is in principle possible to perform a linear stability analysis of the base flow (the complication being the possible presence of turbulence), linear theory tells information only about the initial instability. This is sufficient to predict if any disturbances will grow and their initial nature. If the waves grow and then saturate at small amplitude without changing wavelength, then only the saturation process involves nonlinear effects. However, often, the initial waves form subharmonics[1,2], overtones [1] or even interact with wavelengths much longer than the fundamental [1].

Because of this (for general flows), the next level of theory, nonlinear analysis, cannot be done without looking at what happens in the experimental system. For example, nonlinear analysis is often based on the long wave assumptions [3,4]. For falling films the waves often evolve to long wavelengths, (even if the initial instability is short) so that this approach works. However, for two-layer systems where gravity is stabilizing, the positive linear growth rate region is often bounded away from 0 wavenumber [5,6]. Further, waves may remain of moderate wavenumber even though the linear growth rate is positive down to 0 wavenumber[7]. Thus long wave theory is not of general applicability for two-layer systems.

Blennerhassett [8] Renardy and Renardy [9] have formulated the interfacial problem as a weakly nonlinear expansion and derived equations for the amplitude of the one or two dominant modes. Sangalli et al. [5] showed that for a two-layer Couette flow that experiments agree quite well with theory. Thus the eigenfunction expansion and center manifold projection approach

works for this system. However, a single Stuart Landau equation [8,9] will be valid only for situations when a single short-wave mode is dominant. Formation of subharmonic or other modes cannot be predicted and this single equation does not tell when a different one is required. (At least when the bifurcation is supercritical which it is for all interfacial systems that we have done calculations for.) Thus at the present time the weakly nonlinear problem is not well understood.

A serious need exists for a well defined system to study to sort out as many of this issues as possible. The gas-liquid channel flow does not conveniently exhibit a useful range of behavior for two-layer laminar flows. We have found that an oil-water system has several features that make it appropriate for study. First is a significant range of laminar flow. Second is that there are two distinct modes that lead to interfacial waves and which travel at different speed. Third, these two modes can be simultaneously neutrally stable. Further there is another condition where the long wave region and the short wave region of the same mode can be simultaneously neutrally stable. Thus we can study conditions where two distinct wave modes can be generated and then interact and other conditions where the same mode, but at different wavelengths, interact. Therefor we have an experimental system that allows a broad range of different nonlinear interactions.

In this paper, preliminary results from this study are given. We have found the linear stability theory predicts the onset well. Further, both waves lead to observable interfacial disturbances. (which is not the case for gas-liquid flows). Nonlinear theory suggests that even though the bifurcation seems to always be supercritical, the mechanism responsible for stabilization is different in different ranges.

EXPERIMENTAL SYSTEM

Figure 1 shows a schematic of the oil-water channel that is used for the experiments. Data are obtained from visual and video observations and from conductance probes. We are currently working on an optical technique for measuring the interface tracings to replace the conductance probes. The fluids are water, with Sodium Silicate added to improve its ability to wet the Plexiglas® channel and a light hydrocarbon oil with a density of 0.88 g/cm^3 and a viscosity of 17.8 cP. More details about the flow system and its construction are included in a thesis by McKee[10].

THEORY

Theoretical analysis for this system includes (temporal) linear stability analysis for a two-layer laminar flow that has been completely formulated in papers by Yih[11]or Blennerhassett [8]. The problem is solved numerically with Chebyshev-Tau spectral technique [12] using a scheme devised by Gardner et al.[13]. It is difficult to get accurate results in the long wave region so the results are compared to the analytical long wave solution of Blennerhassett [8]. Strictly speaking, the channel flow geometry is a convective situation and should require a spatial stability formulation. However, this is much more complicated to program and lengthy to compute and we have found that satisfactory results can be obtained from the temporal stability problem with a Gaster transformation if necessary.

Nonlinear analysis for the two-layer problem has been formulated with a multiple scales technique by Blennerhassett [8] and an eigenfunction, center manifold approach by Renardy and Renardy [9]. We use the basic approach of Renardy and Renardy [9] except that the individual contributions to the coefficient β, in the Stuart-Landau equation

$$\frac{\partial A}{\partial t} = L(\lambda)\, A + \beta\, |A|^2 A \qquad [1]$$

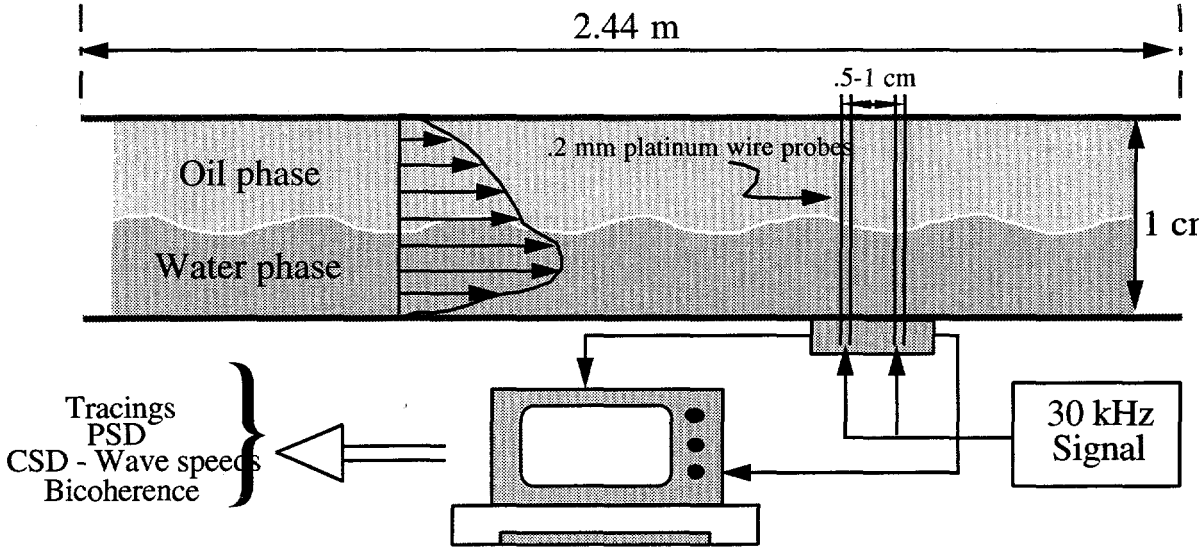

FIGURE 1. OIL-WATER CHANNEL FOR STUDYING INTERFACIAL WAVES

are separated into a quadratic contribution, a cubic self interaction and a cubic interaction with the mean flow (see [6]) for details. This equation tells the nature (i.e., super or subcritical) of the initial bifurcation from a steady base state if the neutral wave number occurs away from 0 wavenumber. If the flow is unstable to long waves, then the neutral wavenumber is 0 and this analysis is not valid. A further difficulty is that even when the initial bifurcation is supercritical, at sufficient forcing, the region of unstable modes and the growth rates get large enough for other modes to occur -- even though the amplitude/wavelength ratio of any mode remains small.

RESULTS

The linear stability diagram should predict the initial transition behavior. Figure 2 shows a plot in Re_{oil} versus Re_{water} of the long wave and short wave stability boundaries. At two points, the different wave types are simultaneously neutrally stable. Thus there are regions where two distinct modes are simultaneously linearly unstable and (by change of the inclination angle of the flow) can have a variable growth rate ratio. It is important to examine the nature of these modes. Figure 3 shows the growth and speed plots for conditions close to the crossing point at low Re_o. The three most unstable modes are plotted. Because an individual mode would be expected to vary smoothly with wavenumber (particularly on the speed plot) it is clear that the same mode is not most unstable always. The mode that is unstable at long wavenumber is distinct from the mode that is unstable at intermediate wavenumbers.

The disturbance eigen function is plotted in figure 4 as a contour plot (for one complete wave) to show what the different modes look like. It is seen that the low k disturbance has its water part centered in the water (lower) phase. However, there is a second unconnected (weaker) part that starts in the oil but is centered at the interface. The high k disturbance has the oil part of the

disturbance centered at the interface connected with a skewed part in the water phase. As the water phase travels much faster than the oil, this could be the reason that the high k disturbance has a

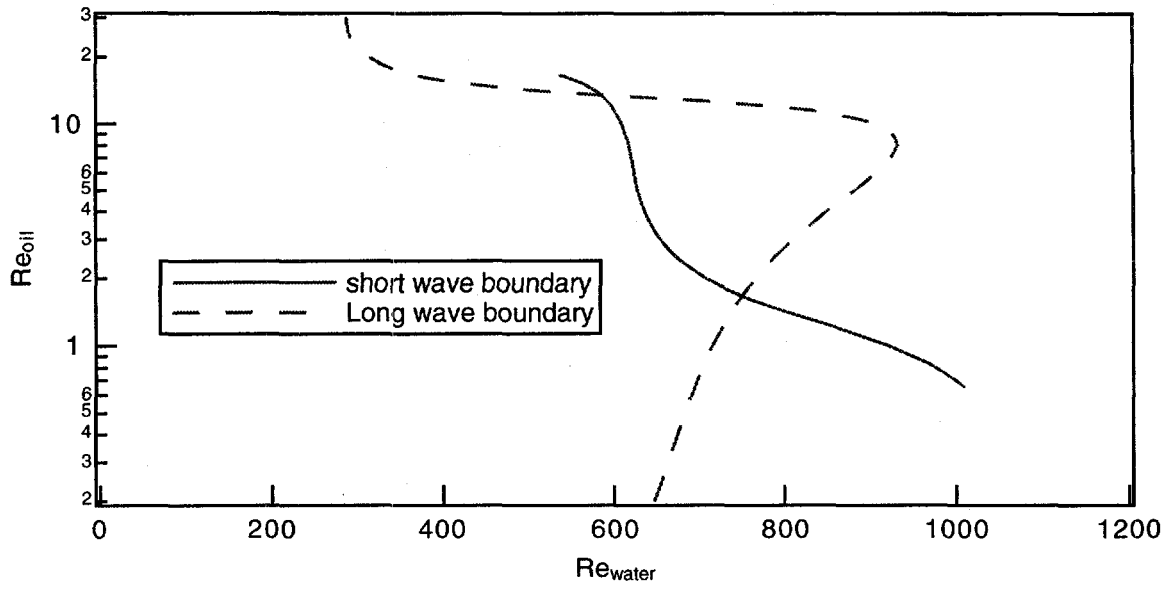

Figure 2. Plot of neutral stability boundaries for long and short waves.

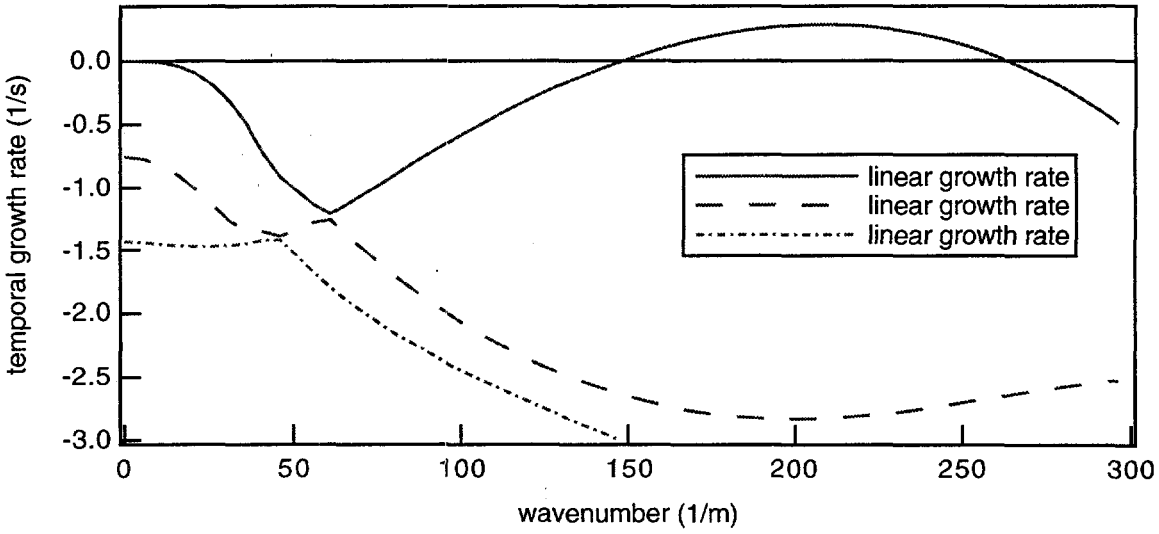

Figure 3a. Plot of growth curves for first three modes, $Re_o = 1.8$, $Re_w = 770$

much higher phase velocity. It should be noted that neither of these disturbances has the "pure" form of interfacial and internal modes as described by Yiantsios and Higgins[14]. Experiments show that both of them lead to interfacial waves. This is in contrast to situations for say, gas-liquid flows where a gas phase internal mode can be unstable, and perhaps be associated with turbulence, but not cause interface waves.

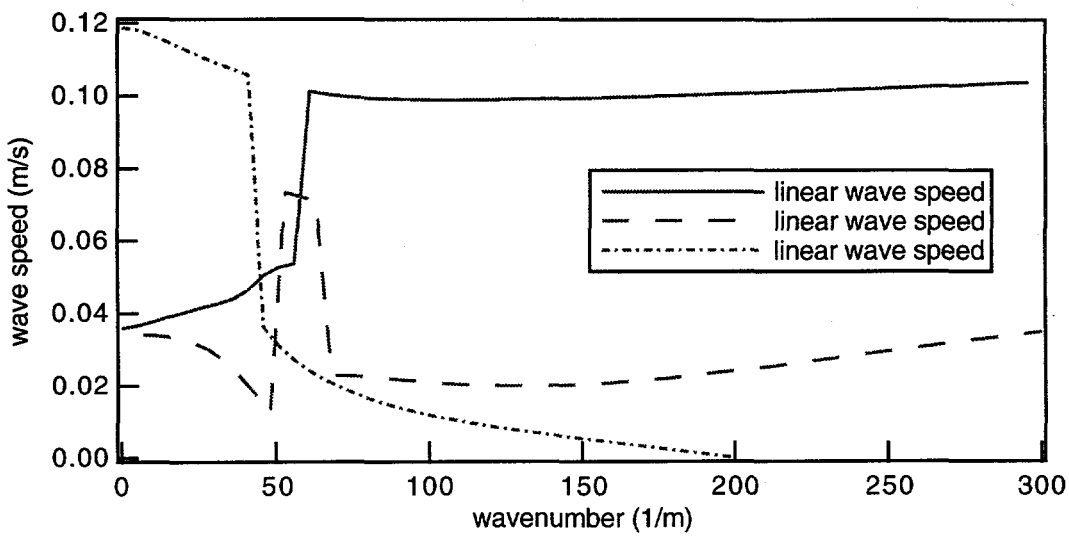

Figure 3b. Plot of wave speeds for first three modes, $Re_o = 1.8$, $Re_w = 770$

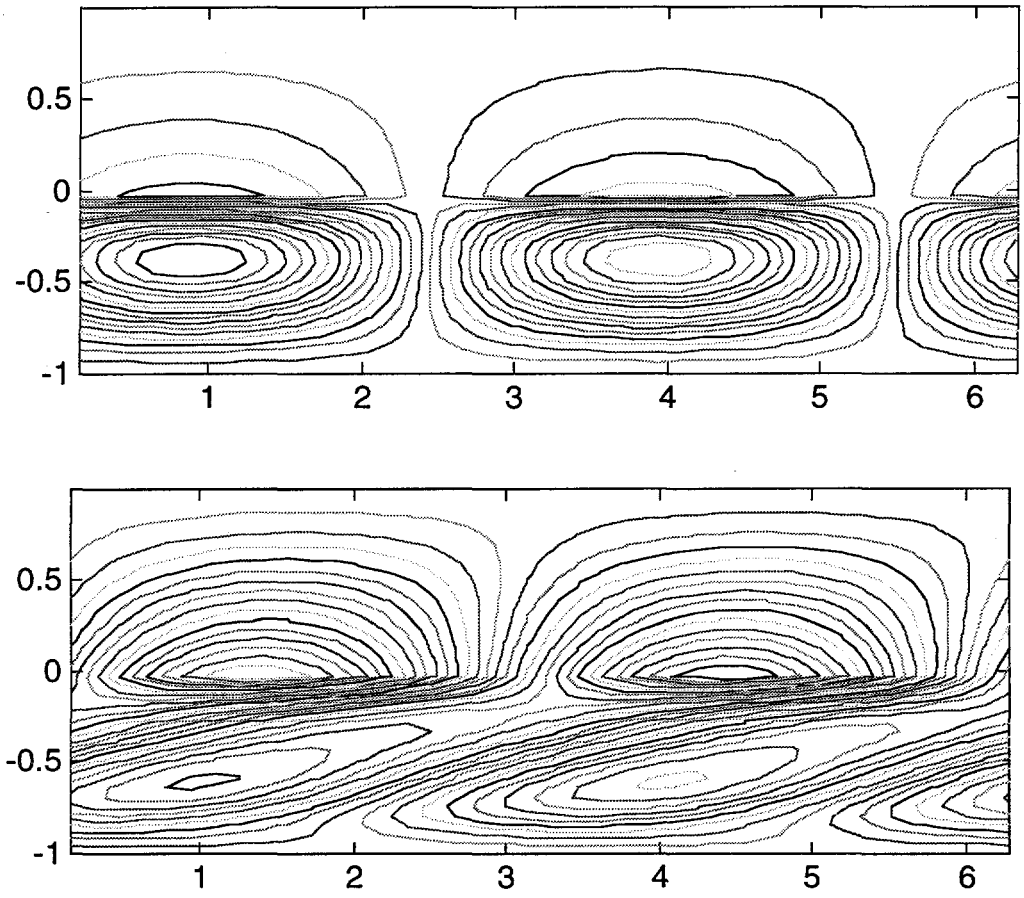

Figure 4. Disturbance eigen function at $Re_o = 1.8$, $Re_w = 770$. a. top: k=1/m
b. bottom: k=211/m.

The situation is different at the long-short crossing point at higher Re_o. Plots of the disturbance function would show that both the long and short waves are the same qualitative shape, (similar to figure 3b) and that the speeds of the long and short waves are comparable.

The importance of developing an better understanding of the nonlinear processes that affect wave behavior is shown by reference to figure 5. In figure 5a, the linear growth curve has a peak close to 3 Hz and the wave data have a corresponding spectral peak. Thus the wavelength and speed of steady waves are close to the linear stability values. However, if the water Reynolds number is increased the situation is very different. Now the spectrum of figure 5b has no relation to the peak in the linear growth region but occurs at much smaller frequency. While the low frequency region is linearly unstable, there is no indication that the low mode will dominate completely with almost no evidence of short waves. Further, video images of this condition show no evidence that the short wave instability is reforming even though the growth rate is large enough that short waves would be expected to reform between the large waves.

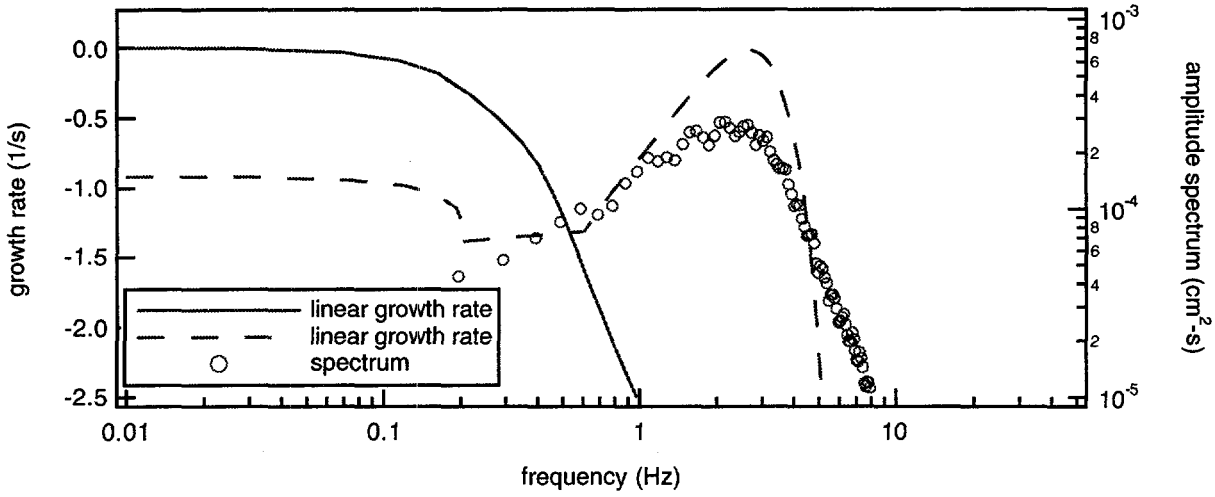

Figure 5a. Growth rate of two modes and measured spectrum at Re_o=3, Re_w = 700

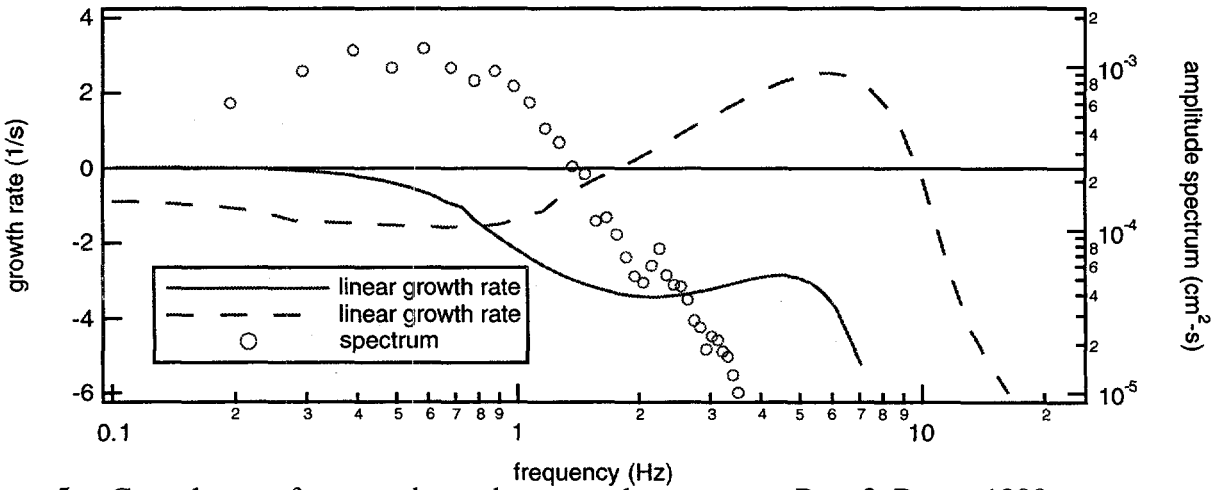

Figure 5a. Growth rate of two modes and measured spectrum at Re_o=3, Re_w = 1200

DISCUSSION

While this project is just beginning, there are several issues that have emerged which were not expected based on numerous previous studies of gas-liquid flows.

First the relative interaction rates of different wavelength modes with different speeds should be successfully determined by experiments in the vicinity of the two-mode crossing points. Preliminary indications are that close to the low mode crossing point there is no interaction between the modes. We are not yet sure about the region around the other crossing point. In either case, the two-mode weakly nonlinear theory is expected to be adequate to describe the process close to the neutral point.

An interesting issue emerges when the oil-water channel is compared to two other two-layer systems that we have studied. Sangalli et al.[6]studied a gas-liquid cocurrent flow close to neutral stability and found that weakly-nonlinear theory predicted the qualitative behavior of the system quite well. The results of most interest here are that the bifurcation of the short wave mode was always supercritical (for all cases calculated) and that the origin of the nonlinear stabilization was the cubic terms that originate in the boundary conditions except when the speeds of the fundamental and overtone were close to the same. In this case the system was nearly-resonant and efficient transfer of energy from the unstable fundamental to the stable overtone stabilized the system at amplitudes smaller than expected for cubic stabilization. A third mechanism [6] cubic interaction between the fundamental and the base flow was found to be unimportant. In contrast, for a two-layer Couette flow [7], we have calculated results for quite a few cases and found that the bifurcation is again supercritical and the overtone interaction is dominant even if the fundamental and overtone are not close to resonant. (In most cases the cubic interaction is destabilizing and the base state interaction is not significant.) Thus it is quite interesting that the oil-water channel flow should again exhibit a supercritical bifurcation for all tested conditions but, the dominant interaction is usually the cubic interaction between the fundamental and the mean flow. For the three different experiments available to us, there are three different mechanisms of stabilization. However, in all cases, cubic order stabilization is observed and the bifurcation is supercritical.

In light of these calculations a check of the calculation procedure as applied to two-layer flows is warranted (note that we had already reproduced the single phase subcritical behavior). For a gas - liquid flow it is possible to get a gas-phase internal mode to be neutrally stable before any interfacial modes occur by raising the gas Reynolds number above 6000-7000, while keeping the liquid one low. For $Re_G = 8000$, $Re_L = 2$, $\mu_L = 5$ cP, it was found that the gas mode appeared and was, as expected, subcritical. Thus the observed supercritical nature for two-layer flows is for the interfacial mode when the instability is bounded away from 0 wavenumber.

Of course it is not known if the bifurcation is supercritical of *all* conditions. It would be interesting to determine if this is the case. A proof seems impossible given the complexity of the system although perhaps worth looking for some restricted parameter ranges. Certainly we will continue to look for subcritical regions. If can find any, experiments will be done in this range to see what differences in behavior exist. Because this issue is so fascinating and we have not been able to find a subcritical region for the fundamental, calculations have been done to find how wavenumbers other than the peak would bifurcate if they were present. Interestingly, for the gas-liquid systems, most modes at wavenumbers less than the fundamental are subcritical. A way to simulate the behavior of these modes is to excite waves artificially with a paddle. For one set of flow conditions, paddling was done over the range of 1-10 Hz. In all cases no amplification of the paddled modes were observed and sufficiently far downstream the spectrum was identical to cases where no paddling was done. This result can not be considered conclusive, however the experiments do not seem consistent with the calculations and further work is needed.

One last issue that will require more study and probably a new formulation is how to deal with conditions far above criticality. For the conditions of figure 5b, the initial bifurcation was supercritical and the wave amplitude are never real large. However, once the growth curve has a sufficiently wide region of instability, it is clear that one or two amplitude equations will not be sufficient. Perhaps the weakly-nonlinear formulation of the Navier-Stokes equations can be solved by integration in time and space to produce results that predict the experiments.

ACKNOWLEDGMENT

This work has been supported by the U. S. Department of Energy, Office of Basic Energy Sciences

REFERENCES

1. L. A. Jurman, S. E. Deutsch, S. E. and M. J. McCready, "Interfacial mode interactions in horizontal gas-liquid flows," *J. Fluid Mech.* **238**, 187-219 (1992).
2. Z. Fan, F. Lusseyran, F. and T. J. Hanratty, "Initiation of slugs in horizontal gas-liquid flows, "*AIChE J.* **39** 1741-53 (1993).
3. B. S. Tilley, S. H. Davis and S. G. Bankoff, "Long-wave nonlinear stability of superposed fluids in an inclined channel," Phys. Fluids **6**, 3906 (1994).
4. F. Charru and J. Fabre, *Phys. Fluids* , **6** , 1223 (1994).
5. M. Sangalli, C. T. Gallagher, D. T. Leighton, H. -C. Chang and M.J. McCready,"Finite amplitude wave evolution at the interface between two viscous fluids", *Phys. Rev. Let.* **75**, pp 77-80, (1995).
6. M. Sangalli, M. J. McCready and H. -C. Chang, "Stabilization mechanisms of short waves in gas-liquid flow", *Phys. Fluids*, **9,** pp 919-939, (1997).
7. C. T. Gallagher, M. J. McCready and D. T. Leighton, "Experimental investigation of a two-layer shearing instability in a cylindrical Couette cell", *Phys. Fluids*, **8**, pp 2385-2392, (1996).
8. P. J. Blennerhassett, "On the Generation of waves by wind," *Proc. R. Soc. Lond.* A **298**, 451-494 (1980).
9. M. Renardy and Y. Renardy, "Derivation of amplitude equations and analysis of sideband instabilities in two-layer flows", *Phys. Fluids*, **A 5**, 2738-2762 (1993).
10. William McKee, "An experimental study of interfacial waves in cocurrent oil-water flows" -- M.S. Thesis, University of Notre Dame, (1995).
11. C. S. Yih, "Instability due to viscosity stratification", *J. Fluid Mech.* **27**, 337-352 (1967).
12. Y. Y. Su and B. Khomami, B., "Numerical Solution of Eigenvalue Problems Using Spectral Techniques", *Journal of Computational Physics* **100**, 297-305, (1992) .
13. D. R. Gardner, S.A. Trogdon, and R.W. Douglass, "A modified tau spectral method that eliminates spurious eigenvalues", *J. Comp. Phys.* **80**, 137 (1989).
14. S. G. Yiantsios and B. G. Higgins, "Linear stability of plane Poiseuille flow of two superposed fluids", *Phys. Fluids* **31**, 3225-3238 (1988).

SELF LUBRICATION OF BITUMEN FROTH IN PIPELINES

Daniel D. Joseph

University of Minnesota
Minneapolis, MN 55455
May, 1997

ABSTRACT

In this paper I will review the main properties of water lubricated pipelines and explain some new features which have emerged from studies of self-lubrication of Syncrudes' bitumen froth. When heavy oils are lubricated with water, the water and oil are continuously injected into a pipeline and the water is stable when in a lubricating sheath around the oil core. In the case of bitumen froth obtained from the Alberta tar sands, the water is dispersed in the bitumen and it is liberated at the wall under shear; water injection is not necessary because the froth is self-lubricating.

INTRODUCTION

There is a strong tendency for two immiscible fluids to arrange themselves so that the low-viscosity constituent is in the region of high shear. We can imagine that it may be possible to introduce a beneficial effect in any flow of a very viscous liquid by introducing small amounts of a lubricating fluid. Nature's gift is evidently such that the lubricating fluid will migrate to the right places so as to do the desired job. This gives rise to a kind of gift of nature in which the lubricated flows are stable, and it opens up very interesting possibilities for technological applications in which one fluid is used to lubricate another.

Water-lubricated transport of heavy viscous oils is a technology based on a gift of nature in which the water migrates into the region of high shear at the wall of the pipe where it lubricates the flow. Since the pumping pressures are balanced by wall shear stresses in the water, the lubricated flows require pressures comparable to pumping water alone at the same throughput, independent of the viscosity of the oil (if it is large enough). Hence savings of the order of the oil to water viscosity ratio can be achieved in lubricated flows. Lubricated flow in an oil core is called core annular fow, CAF for short.

Typically, waves appear on the surface of the oil core and they appear to be necessary for levitation of the core off the wall when the densities are different and for centering the core when the densities are matched. We call these flows wavy core annular flow (WCAF). Perfectly centered

core flows (PCAF) of density matched fluids in horizontal pipes and, generally in veritcal pipes, are possible but are rarely stable.

The science behind the technology of CAF has given rise to a large literature which has been reviewed by Oliemans & Ooms [1], by Joseph & Renardy [2], and by Joseph, Bai, Chen and Renardy [3], hereafter called [JBCR]. The story of self-lubrication appears in the open literature first here; apart from the internal Syncrude study of Neiman [4], there is no prior literature.

INDUSTRIAL EXPERIENCE

It is best to start this review with industrial experience since the potential of lubricated lines for energy efficient transport of heavy oil gives this interesting subject an even greater urgency. Heavy crudes are very viscous and usually are somewhat lighter than water, though crudes heavier than water are not unusual. Typical crudes might have a viscosity of 1000 poise and a density of 0.99 g/cm^3 at 25°C. Light oils with viscosities less than 5 poise do not give rise to stable lubricated flows unless they are processed into water/oil emulsions and stiffened.

Oil companies have had an intermittent interest in the technology of water-lubricated transport of heavy oil since 1904. Isaacs & Speed [5] in U.S. Patent #759374 were the first to discuss water lubrication of lighter oils which they proposed to stabilize by centripetal acceleration created by rifling the pipe. For stratified flow, Looman [6] patented a method of conveying oils by passing them over an array of water traps at the bottom of the pipe. An extended history of patents is presented in Joseph & Renardy [2]. The patent history of the subject as it is presently understood starts with the application of Clark & Shapiro [7] of Socony Vacuum Oil company who used additives to reduce the density differences between the oil and water and anionic surfactants to reduce emulsification of water into oil. Clifton & Handley [8] of Shell development proposed to prevent the emulsification of oil at pumps by removing the water before and inserting the oil after the pumps. In fact, water-in-oil emulsions an be pumped in a sheath of water despite the fact that the viscosity of the emulsion can be orders of magnitude larger than the oil alone. In general, lubricated flows are more effective when the oil is more viscous; the water/oil emulsion is an "effective" thickened oil whose density is closer to water. Kiel [9] of Exxon patented a CAF process for pumping heavy oils and water in oil emulsions, surrounded by water, for fracturing subterranean formations to increase oil and gas production. Ho & Li [10] of Exxon produced a *concentrated* water in oil emulsion with 7 to 11 times more water than oil, which they successfully transported in CAF.

Lubricated transport of concentrated oil-in-water emulsions is also an issue. The viscosity of such emulsions can be much smaller than the viscosity of the oil and may be independent of the oil viscosity for large viscosities. This has motivated the consideration of pumping heavy crudes through pipelines as concentrated oil-in-water emulsions. Lamb & Simpson [11] reports a commercial line in Indonsia which carries 40,000 barrels/day of 70% oil/water emulsion in a 20-inch diameter line, 238 kilometers long. Another commerical lubricated transport of Orimulsion®, a coal substitute fuel of 70% oil-in-water produced in Venezuela and marketed by Bitor, can be accomplished naturally since the water for lubrication is already there and will stick to the wall if the surfactant used to stabilize the emulsion and the material of wall construction is suitable (Núñez et al [12]).

Probably the most important industrial pipeline to date was the 6-inch (15.2 cm) diameter, 24-mile (38.6 km) long Shell line from the North Midway Sunset Reservoir near Bakersfield, California, to the central facilities at Ten Section. The line was run under the supervision of Veet Kruka for 12 years from 1970 until the Ten Section facility was closed. When lubricated by water at a volume

flow rate of 30% of the total, the pressure drop varied between 900 psi and 1,100 psi at a flow rate of 24,000 barrels per day with the larger pressure at a threshold of unacceptability which called for pigging. In the sixth year of operation the fresh water was replaced with water produced at the well site which contained various natural chemicals leached from the reservoir, including sodium metasilicate in minute 0.6 wt.% amounts. After that the pressure drop never varied much from the acceptable 900 psi value; the CAF was stable as long as the flow velocity was at least 3 ft/s. Industrial experience suggests that inertia is necessary for successful CAF.

Syncrude Canada Ltd. has undertaken studies of lubricated transport of a bitumen froth which is obtained from processing of oilsands of Alberta for upgrading to synthetic crude. The oil (bitumen) is extracted from mined oilsands rather than pumped directly from the reservoir. A hot-water extraction process is used to separate bitumen as froth from sand and the average composition of the froth is 60, 30 and 10 weight % bitumen, water and solids, respectively. Internal studies led by Neiman et al [4] and recent studies at the University of Minnesota showed that the produced bitumen froth will self lubricate in a pipe flow. The Minnesota studies showed also that once established, lubricating flows were stable and ran continuously for 4 days and nights without any pressure drop buildup or loss of mass flow. Further testing of self-lubrication in 24″ by 1 km pilot pipeline near Fort McMurray confirmed the Minnesota results at a commercial scale. Encouraged by these results, Syncrudes' management has decided to build a 35km line from the new Aurora mine to the upgrading plant at Mildred Lake. Further research impacting on the design of this self-lubricated pipeline of bitumen froth is being done by Syncrude and the University of Minnesota.

LUBRICATED PIPELINES (WITH WATER INJECTION)

Even though lubricated flows are hydrodynamically stable, oil can foul the wall. This is an adhesion rather than a hydrodynamic effect and is not taken into account in the equations used to study stability. The hydrodynamic stability of lubricated flow is very robust even when oil wets the wall. A water annulus can lubricate an oil core even in a pipe whose walls are spotted with oil. Sometimes, however, the fouling builds up, leading to rapidly increasing pressure drops even blocking the flow. Oil fouls some places more than others, near pumping stations where the pressure is highest and the holdup and core wave structure are developing and around line irregularities such as unions, bends, flanges and curves. Another major problem is an unexpected shut-down in the line; the oil and water stratify, causing the oil to stick to the pipe wall, making it harder to restart the line.

It is desirable to lubricate the oil core with as little water as possible because a small water input alleviates the problem of dewatering. On the other hand, oil is more likely to foul the pipe wall when a small amount of water is used, so it is desirable to suppress fouling for this as well as other reasons.

Remedial strategies to prevent fouling naturally alter the adhesive properties of the wall which depend on the solid surface and the oil used. The different strategies that have been employed are discussed in [JBCR]. Clean-up procedures for fouled pipes are important for a viable lubricated pipelines technology.

Obviously, the restart of a fouled pipe will be easier if the oil does not strongly stick to the pipe wall. The restart is also easier if there is an open channel through which water may flow. Such a channel can be opened by stratification under gravity in a large diameter horizontal line. The flowing water will produce a propagating solitary wave near the pump, which tends to partially block the flow of water in such a way that the high local pressure fingers water bewteen the oil and

pipe wall in an unzipping motion which restores core flow as the wave moves forward. The open channel may be closed at places where the pipe goes over a hill since the lighter oil will fill the pipe at high places and make restart more difficult. In small pipes, in which capillarity may dominate gravity, the oil will stratify in slugs separted by water lenses in which water is trapped.

Two-phase flows, liquid-liquid, gas-liquid and liquid-solid flows, can be arranged by dynamics into different configurations called flow types. Various properties of the solutions, like the pressure gradient needed to drive the flow, the area averaged velocity of each phase and the holdup ratio depend on the flow type. The holdup ratio of oil to water is the ratio:

$$h = \frac{Q_0}{A_0} \Big/ \frac{Q_w}{A_w} = \frac{\overline{U}_0}{\overline{U}_w}$$

of the area averaged oil velocity $\overline{U}_0 = Q_0/A_0$ and water velocity $\overline{U}_w = Q_w/A_w$ where Q is a volume flow rate. In the case of an emulsion of small water droplets uniformly dispersed in oil, we could assume that the water moves with the oil so that $\overline{U}_w = \overline{U}_0$, hence $h = 1$. This does not mean that the flow rates or superficial velocities are equal because, say, only a relatively small amount of water could disperse into small drops. In the case of PCAF, with only a very small water input so that the layer of water outside is thin and a uniform velocity for very viscous oil inside, we get

$$\overline{U}_w = \frac{1}{2}\overline{U}_0, \tag{1}$$

hence $h = 2$. In vertical flow with a pressure gradient producing flow of water down against a stationary bouyant slug of oil held in place by gravity, we have $h = 0$ because $Q_0 = 0$ even though the oil fills nearly all of the pipe.

Bai et al [19] found some remarkable holdup results for vertical core flows. For bamboo waves in up-flow, $h \approx 1.39$ independent of the flow rates. Though h varies between 0.8 and 1.4 with flow rates of oil and water, $h \to 1.4$ for fast flows $U_0/U_w > 5$. Thus, $h = 1.4$ is a good value for up-flow and fast down-flows in which buoyancy is not important. In the absence of better knowledge, reasers may assume $h \approx 1.4$.

The lubricated arrangements of oil in water flow are PCAF, WCAF, slugs of oil in water and drops of oil in water. Well-dispersed drops of oil in water are sometimes called oil-in-water (o/w) emulsions. Very concentrated o/w emulsions can be stabilized by surfactants.

Water-in-oil (w/o) emulsions are an oil continuous phase of an "effective" oil which can be lubricated with water. Effective oils of high viscosity can be formed from water in low viscosity oil emulsions (see Ho & Li [10]). When the water content of such w/o emulsions is high, the density of the effective oil will be close to water. It is desirable to transport as much oil as possible at a fixed pressure gradient or to minimize the pressure gradients for fixed oil flow. Minimum pressure gradients are found for flow types near to PCAF; wavy flows are energy efficient and the input ratio can be controlled to give maximum efficiency [JBCR].

Arney et al [14] plotted the friction factor λ vs. Reynolds number $\mathbb{R}$ data for core flows from 12 authors using special definitions which depend on the holup ratio [JBCR]. Most of the data points are in the region of turbulent flow where the Blasius formula $\lambda = 0.316/\mathbb{R}^{1/4}$ applies. There is a considerable scatter of the data which may be due to fouling. Huang et al [15] did turbulence modeling using a K-E model assuming that there were no waves on the core and the core moves forward as a rigid body. The agreement between model predictions, which have not adjustable parameters, and experimental and field data from all sources, was excellent. This result suggests that the major source of drag is turbulence in the water.

Lubrication may fail to fouling, to stratification under gravity when the density difference is large (and core speeds too low to levitate the core off the wall) and to inversion to w/o emulsions

(which can be relubricated as "effective" oils). Failure to stratification at low speeds is characteristic in large diameter pipes in which capillarity is not important. In small pipes, slugs of oil separated by water will stratify in the pipe.

STEEP WAVES & LEVITATION OF CORE FLOWS

A surprising property of core flow is that the flow in a horizontal line will lubricate with the core levitated off the wall even if the core is lighter or heavier than the lubricating water. This levitation could not take place without a hydrodynamic lifting action due to waves sculpted on the core surface. In the case of very viscous liquids, the waves are basically standing waves which are convected with the core as it moves downstream. This picture suggests a lubrication mechanism for the levitation of the core analogous to mechanisms which levitate loaded slider bearings at low Reynolds numbers. Ooms et al [16] and Oliemans and Ooms [1] gave a semi-empirical model of this type and showed that it generated buoyant forces proportional to the first power of the velocity to balance gravity. In this theory, the shape of the wave must be given as empirical input.

Consider water-lubricated pipelining of crude oil. The oil rises up against the pipe wall because it is lighter than the water. It continues to flow because it it lubricated by waves. However, the conventional mechanisms of lubrication cannot work. The saw tooth waves shown in Figure 1 are like an array of slipper bearings and the stationary oil core is pushed off the top wall by lubrication forces. If c were reversed, the core would be sucked into the wall, so the slipper bearing picture is obligatory if you want levitation.

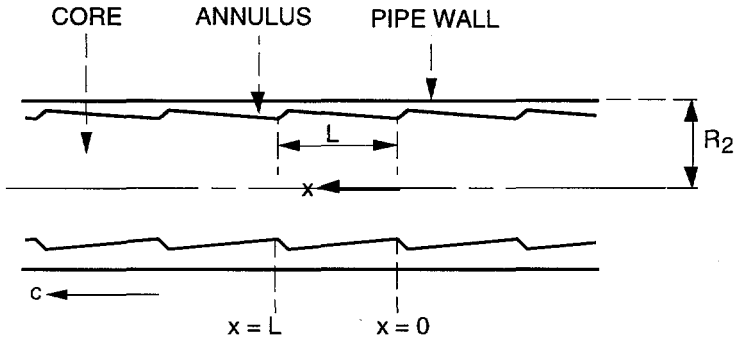

Figure 1: The core is at rest and the pipe wall moves to the left.

Obviously the saw tooth waves are unstable since the pressure is highest just where the gap is smallest, so the wave must steepen where it was gentle, and smooth where it was sharp. This leads us to the cartoon in Figure 2. To get a lift from this kind of wave it appears that we need inertia, as in flying. Liu's [17] formula for capsule lift-off in a pipeline in which the critical lift-off velocity is proportional to the square root of gravity times the density difference is an inertial criterion. Industrial experience also suggests an inertial criterion, since CAF in the Shell line could be maintained only when the velocity was greater than 3 ft/s; at lower velocities the drag was much greater.

Bai et al [19] did a direct simulation of steady axissymetric, axially periodic CAF, assuming that the core viscosity was so large that secondary motions could be neglected in the core. They found

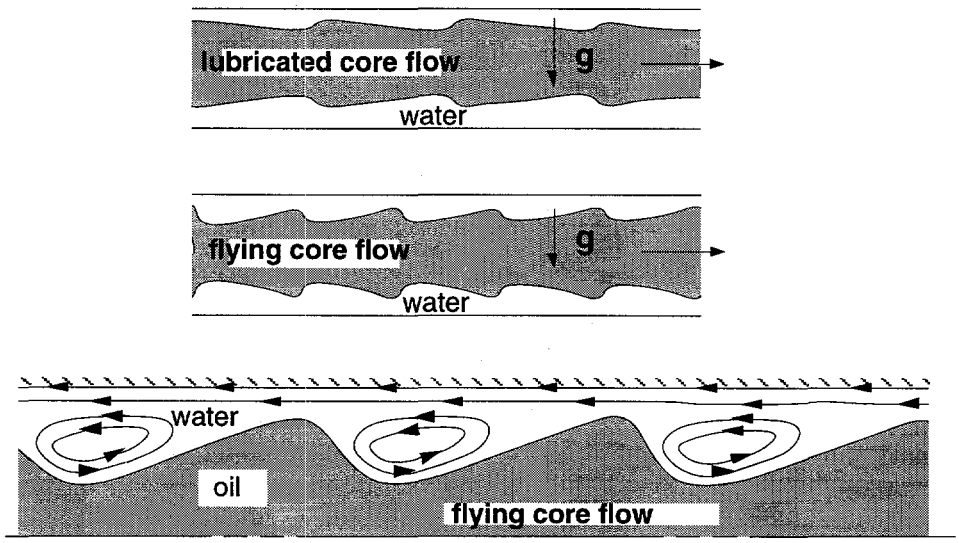

Figure 2: (After Feng et al 1995) (*top*) The interface resembles a slipper bearing with the gentle slope propagating into the water; the shape of these waves is unstable. (*middle*) The high pressure at the front of the wave crest steepens the interface and the low pressure at the back makes the interface less steep. (*bottom*) The pressure distribution in the trough drives one eddy in each trough.

that wave shapes with steep fronts like those shown in Figure 2 always rise from the simulation. The wave front steepens as the speed increases.

A new and important feature revealed by the simulation is that long waves do not arise when the gap size tends to zero as is usually assumed in long wave theories. As the gap size decreases, $\eta \to 1$, the wavelength $\overline{L}(\eta)$ decreases linearly with η. This means that the wave shape hardly changes and a steep wave will stay steep in this limit. The aforementioned properties of waves are in excellent agreement with the observed shape of waves in experiments [JBCR].

SELF LUBRICATION OF BITUMEN FROTH

The first studies of self-lubrication of bitumen froth were carried out in 1985 in unpublished studies by O. Neiman [4] for Syncrude Canada. Tests were conducted on the pipelining characteristics of froth using a research 50mm hydraulic test facility with froth produced on the External Extraction Circuit. They found that

> "The pipeline flow of froth was found to be governed by a special type of multi-phase behavior involving separated water. A concentration of water was observed to occur near the pipe wall, which effectively formed a lubricating water layer around the central plug of froth... Pipelining of froth in the syncrude expansion case may be considered technically and economically feasible."

Syncrude's business is to upgrade the bitumen found in the tar sands into high quality synthetic crude for which there is an active world market. After 25 years of operation, they ran into the

problem that untapped oilsands are located at increasing distances from the upgrading facilities at Mildred Lake. The next ore body they want to mine is at the Aurora mine, 35km north of the upgrading facility, hence the requirements for a bitumen froth pipeline.

The froth is very viscous; to pipeline froth you would have to heat and dilute it, or to use a core flow technology. Neiman's study, industrial experience and the literature on core flow favor the core flow approach but froth is a special material; Neiman did not do tests of long duration, the effects of water addition, pipeline fouling and restart after stopping were not considered. Syncrude identified the DOE supported lubricated pipeline research at the University of Minnesota as most relevant to their needs and they gave us a contract to look at the pipelining of bitumen froth. Our objective was to investigate restart and fouling and to establish an operating envelope and the mechanism for core flow to derive scaling parameters.

The Minnesota studies, in results to be published, established that

- Froth could be pumped in a core flow mode for up to 100 hours.
- External water addition was not required.
- There was no indication of a pressure drop increase even after four days of continuous running.
- An operating envelope from 0.7 m/sec to 2.5 m/sec was established. Core flow was lost below 0.7 m/sec but 2.5 m/sec was an equipment limited value. Possibly unlimited velocities in core flow are possible.
- Shutdowns less than three minutes were re-started without water injection at peak pressure less than 3 times operating pressure.
- Longer shutdown required water addition equivalent 20 wt% lubricating water.

Core annular flow has always referred to a pipelining process requiring a dedicated water addition to form the annulus. One of the insights gained in Minnesota is that froth is self-lubricating, shear liberates some of the water tied up in the froth emulsion. Free water migrates to the point of highest shear– at the pipe wall. Therefore, self-lubricating flow or natural froth lubricity, is probably a better description of the technology.

Second, fouling appears to be inhibited by the liberated water. Bench scale tests show that even carbon steel fouled by the Venezuelans' Zuata crude can be cleaned by liberated water from Syncrude froth.

Third a minimum velocity of 0.7 m/s is required. Below this velocity, the froth core would begin to separate into slugs of lubricated froth between sections of water. This core separation would continue slowly over time until enough water left the annulus that a plug of froth would become unlubricated. At this point pipeline pressures would increase dramatically.

PROPOSED MECHANISM OF SELF-LUBRICATION OF BITUMEN FROTH

We know that froth is highly viscous and offers resistance to *low rates* of shearing. Our proposed mechanism for self lubrication depends on the fact that froth is unstable to *higher shearing rates*, resulting in the coalescence of water droplets to form a lubricating layer of free water. The unique property of bitumen froth that promotes the coalescence of water droplets arises from the dispersion of clay particles in the water.

The clay present in the water inhibits the coalescence of bitumen droplets and promotes the coalescence of the water droplets through a mechanism we refer to as "powdering the dough". Anyone who has baked bread will appreciate this analogy.

Bread dough is sticky, but when a layer of flour is sprinkled on top, the dough will no longer stick to itself or other surfaces. The fine solids surrounding a droplet tend to act as a barrier protecting the oil droplets from coalescing with one another.

Given the encouraging results at Minnesota, Syncrude decided to continue with self lubricating flow as a base case for further development.

The intent for the commercial test was to run the equivalent of 110 000 BPD of bitumen as froth through a 24″ by 1 km pipeline to duplicate the commercial conditions at full scale with respect to line diameter. They were less concerned about line length.

Their first objective for the commercial program was to understand whether or not they could establish self lubricating flow given the shear regime that would exist in a large diameter pipe. It wasn't obvious how to scale-up the re-start results from a 1 inch line diameter to a 24″ line diameter. They also wanted to gain some confidence that the technology would work by seeing it at full scale.

A hurdle to overcome for commercial tests was to understand whether or not they could use a centrifugal pump. Centrifugal pumps are inexpensive and have high capacity but will not operate with fluid viscosity's higher than about 3000 cP. (The viscosity of froth at 50 C is closer to 10000 cP). Positive displacement pumps can operate at much higher viscosities, but require three pumps operating in parallel for the commercial tests, and each pump would have to be among the largest in the world.

However, if our insights about self lubrication were correct then a centrifugal pump could also work in this service. Some quick tests at Minnesota with a centrifugal pump verified that it could indeed work.

Results from the 24″ × 1km pilot pipeline showed that

- Lubricated froth can be established in large diameter pipelines and a centrifugal can be used to drive the flow
- Pipeline shutdowns from 1 minute to 6 hours were tested and restarted without high pressure water injection.

The present decision of management at Syncrude is to build a 35 km lubricated froth pipeline. This pipeline would possibly cost 200 million dollars. The design if this pipeline is presently being worked out.

The scientific details of the lubricated froth studies of Joseph, Bai, Sury, Grant & Mata will be reported in an Archival journal in a future publication.

REFERENCES

1. R.V.A. OLIEMANS and G. OOMS, "Core-annular flow of oil and water through a pipeline. Multiphase Science and Technology," ed G.F. Hewitt, J.M. Delhay, N. Zuber, Vol. 2, Hemisphere Publishing Corporation (1986).
2. D.D. JOSEPH and Y.Y. RENARDY, *Fundamentals of Two-Fluid Dynamics,* Springer-Verlag, New York (1993).

3. D.D. JOSEPH, R. BAI, K.P. CHEN and Y.Y. RENARDY, "Core-Annular Flows," *Annual Review of Fluid Mechanics* 13, 739 (1997).

4. O. NEIMAN, "Froth pipelining tests," *Syncrude Canada Research and Development Progress Report*, 15(1):373-407 (1986).

5. J.D. ISAACS, J.B. SPEED, U.S. Patent No. 759,374.

6. M.D. LOOMAN, U.S. Patent No. 1,192,43, (1916).

7. A.F. CLARK and A. SHAPIRO, U.S. Patent No. 2,533,878 (1949).

8. E.G. CLIFTON, L.R. HANDLEY, U.S. Patent No. 2,821,205 (1958).

9. O.M. KIEL, U.S. Patent 3,378,047, (1968).

10. W.S. HO AND N.N. LI, "Core-annular flow of liquid membrane emulsion," *AIChE Journal* 40, (12): 1961-68 (1994).

11. M.J. LAMB and W.C. SIMPSON, *Proc. World Petroleum Cong., 6th, Frankfurt,* 23-33 (1973).

12. G.A. NÚÑEZ, M. BRICEÑO, C. MATA, H. RIVAS, D.D. JOSEPH, "Flow characteristics of concentrated emulsions of very viscous oil in water," *J. Rheol.*, In press.

13. R. BAI, K. CHEN and D.D. JOSEPH, "Lubricated pipelining: Stability of core-annular flow. Part 5: Experiments and comparison with theory," *J. Fluid Mech.* 240, 97-142. (1992)

14. M.S. ARNEY, R. BAI, E. GUEVARA, D.D. JOSEPH, K. LIU, Friction factor and holdup studies for lubricated pipelining. *Int. J. Mult. Flow*, 19(6): 1061- 1076.

15. A. HUANG, C. CHRISTODOULOU, "Friction factor and holdup studies for lubricated pipelining. Part II: Laminar and $k-\varepsilon$ models of eccentric core flow." *Intl. J. of Mult. Flow.* 20(3): 481-91.

16. G. OOMS, A. SEGAL, A.J. VAN DER WEES, R. MEERHOFF, R.V.A. OLIEMANS, "A theoretical model for core-annular flow of a very viscous oil core and a water annulus through a horizontal pipe," *Int. J. Mult. Flow.* 10: 41-60 (1984).

17. H. LIU. "A theory of capsule lift-off in pipeline," *J. Pipelines*, 2:23–33 (1982).

18. J. FENG, P.Y. HUANG, D.D. JOSEPH, "Dynamic simulation of the motion of capsules in pipelines," *J. Fluid Mech*, 286:201-227 (1995).

19. R. BAI, K. KELKAR and D.D. JOSEPH, "Direct simulation of interfacial waves in a high viscosity ratio and axisymmetric core annular flow," Supercomp. Inst. Res. Rep. #UMSI 95/107, University of Minnesota (1995).

HOMOGENEOUS AND NON-LOCAL HETEROGENEOUS TRANSPORT PHENOMENA WITH VAT APPLICATION ANALYSIS

I.Catton and V.S.Travkin

University of California, Los Angeles
Mechanical and Aerospace Engineering Department
Los Angeles, Ca 90095-1597

ABSTRACT

Some fundamental questions about the mathematical description of transport phenomena in heterogeneous media are addressed to highlight the importance of the smallest scale, of using the correct equations and of choosing a consistent set of scaling parameters. Micro-pore flow is treated using a viscosity correlation that properly treats the near wall region in a capillary. Equations resulting from use of volume averaging theory (VAT) are compared with exact solutions and it shown that certain terms normally ignored must be retained. A consistent set of scaling parameters are derived and shown to yield consistent results over a wide range of different media morphologies.

1. INTRODUCTION

There are many disagreements about the applicability of models based on conventional diffusivity type models of transport phenomena in porous media to problems with the following features: multi-scaled media, media with non-linear physical characteristics, polydisperse morphologies, materials with phase anisotropy, media with non-constant or field dependent phase properties, transient problems, and many others. The most practical way has been to seek a solution by doing numerical experiments over the more or less the exact morphology of interest. This leads to heavy use of large computers to solve large algebraic statements. As in each experiment, the treatment and analysis of the results of such "Direct Numerical Modeling" (DNM) is an unappealing and difficult problem.

Mathematical simulation of physical processes in a highly non-homogeneous media, in general, calls for obtaining averaged characteristics of the medium and, consequently, the averaged equations. The averaging of processes in a randomly organized media can be performed in many different ways. If a physical model has several interdependent structurally organized levels of processes underway, it is expedient to employ one of the hierarchical methods of simulation (see, for example, Kheifets and Neimark [1], Gushman [2] among others). The hierarchical principle of simulation consists of successively studying the processes at a number of structural levels.

One first deals with the smallest scale element, for example a small smooth capillary or globular media. Next, various types of capillary wall morphology are incorporated. This is followed by studies of a range of diameters, first smooth then rough, and then networking. Regular variations of the parameters are treated first, followed by random. This is done at each level. This approach is underway for capillary morphologies as well as granular morphologies. The process leads one to find ways to deal with the large number of closure expressions that result from the averaging used to obtain the original set of equations. Although of a common form, the resulting usable form depends on the media morphology and the local boundary conditions at the each level of the hierarchy. A particular closure expression will be different for energy, mass or momentum transfer between the fluid and the solid matrix.

Three separate topics have been chosen to demonstrate the need for care at every level of the model development process. First, flow in capillaries is treated and it is found that the viscosity is different near the wall than in the bulk fluid. One can postulate why but here we will rely on data and show that there is an impact. It is not large when considering ground water flow, but may well be important in the field of MEMS. The second topic deals with the equations resulting from the use of volume averaging theory (VAT). The equations have strange additional terms that are not usually seen. One needs to ask whether or not these new terms are small enough to ignore. In what follows, it will be shown that they are not. In fact, they are of the same order of magnitude as the one term that is normally kept. The third topic is scaling. There are many analysis and experimental results in the literature. Many use different parameters to scale their data for analysis or in developing an empirical correlation. Many different equations appear in the literature. Based on a simplified VAT model, a consistent set of scaling parameters is developed.

2. FINE PORE NONLINEAR RESISTANCE

The Darcy flow assumption breaks down when the very fine passages found in a porous medium at the smallest scale must be dealt with. Physical phenomena at this scale, less than a micrometer, are often neglected when the scale of the problem is meters or tens of meters. It should be emphasized that in fine pores, the structure of liquids is different from that of the bulk liquid. Indeed, it has been shown by the many convincing experiments of Churaev et al. [3], Derijagin et al. [4], Bondarenko [5,6], and Low [7] that polar liquid (for example, water) boundary layers are characterized by elevated viscosity near boundaries. The modified structure of the liquid affects the filtration process and leads to inapplicability of the Darcy law even at very low Reynolds numbers. Calculations of the flow rates must take into account the dependence of viscosity on distance from the pore wall.

To amplify, we start with the following equation governing the stationary flow of a viscous fluid in a pipe,

$$\frac{1}{r}\frac{d}{dr}\left(r\mu(r)\frac{dV}{dr}\right) = \nabla P,$$

with $\mu(r)$ being the local viscosity near the wall given by Low [7] for a water in the form

$$\mu = \mu_p / (1 - a \exp [-b(R-r)])$$

where μ_p is the bulk viscosity of the fluid far from a wall and the parameters a and b characterize the viscosity on the wall and the corresponding effective thickness of the boundary layer. Low used data from his measurements of water flow velocity in capillaries with radii ranging from $4.5.10^{-6}$ to 10^{-4} cm to determine the Newton viscosity of water close to a solid hydrophobic surface. The water data yielded $a = 0.47$ and $b = 6.35\times10^5$ [cm^{-1}]. Using these results, the mean capillary velocity is found to be

$$V/V_p = 1 - 8a\,[1/2bR - 3/2(bR)^2 + 3/(bR)^3 - 3(1-e^{-bR})/(bR)^4],$$

where $V_p = R^2|\nabla P|/8\mu_p$ is the mean velocity in a capillary when $\mu = \mu_p = \text{const}$. Results for water, using the a and b found by Low are shown on Fig. 1 along with the step-like layered viscosity function near the pore wall.

Overall pressure loss models in porous media with the presence of very fine pores need to take into account this phenomenon when polar liquids transport considered. That means that at least two scales of description have to be combined in the model. That VAT based hierarchical modeling naturally treats such problems was demonstrated by Travkin et al. [8], Travkin and Catton [9].

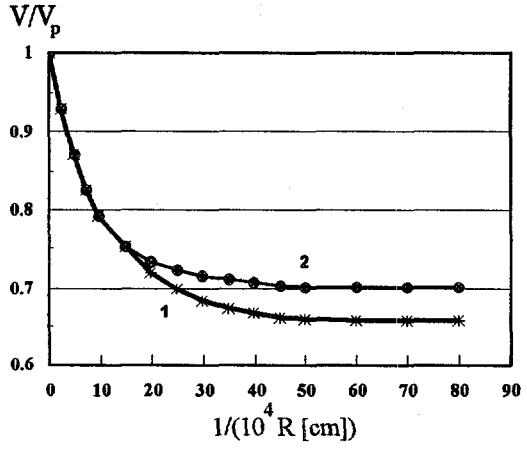

Figure 1. Nondimensional Velocity Against Inverse Radius of Pore for Exponential (1) and Discrete (2) Distribution of Viscosity

3. THEORETICAL VERIFICATION OF VAT BASED MODEL EQUATIONS

Many forms of the energy equation are used in the analysis of transport phenomena in porous media. The primary difference between such equations and those resulting from a more rigorous development based on VAT are certain additional terms. The best way to evaluate the need for these additional more complex terms is to obtain an exact mathematical solution and compare the results with calculations using the VAT equations. This will clearly display the need for using the more complex VAT mathematical statements.

Consider a two-phase heterogeneous medium consisting of an isotropic continuous (solid or fluid) matrix and an isotropic discontinuous phase (spherical particles or pores). The volume fraction of matrix, or f-phase, is $m_f = \Delta\Omega_f / \Delta\Omega$, the volume fraction of filler, or s-phase, is $m_s = 1 - m_f = \Delta\Omega_s / \Delta\Omega$, where $\Delta\Omega = \Delta\Omega_f + \Delta\Omega_s$ is the volume of representative elementary volume (REV). The constant properties (phase conductivities, λ_f and λ_s), stationary (time-independent) heat conduction differential equations for T_s and T_f, the local phase temperatures,

$$-\nabla\cdot\mathbf{q}_f = \lambda_f\nabla^2 T_f = 0 \quad \text{and} \quad -\nabla\cdot\mathbf{q}_s = \lambda_s\nabla^2 T_s = 0,$$

with the interfacial conditions representing perfect thermal contact

$$T_s = T_f \quad \text{and} \quad \mathbf{ds}_1\cdot\mathbf{q}_f = \mathbf{ds}_1\cdot\mathbf{q}_s \quad on\ S_\omega\ ,$$

describe the problem of interest. Here $\mathbf{q}_f = -\lambda_f\nabla T_f$ and $\mathbf{q}_s = -\lambda_s\nabla T_s$ are the local heat flux vectors, S_ω is the interfacial surface and $\mathbf{ds}_1$ is the unit vector outward to the s-phase. No internal heat sources are present inside the composite sample so that the temperature field is determined by the boundary conditions at the external surface of the sample. After correct formulation of these conditions, the problem is completely stated and has a unique solution.

Two ways to realize a solution to this problem are compared below (Travkin and Kushch [10]). The first is the conventional way to replace the actual composite by an equivalent homogeneous medium with an effective thermal conductivity coefficient, $\lambda = \lambda_{eff}(m_s, \lambda_f, \lambda_s)$, assuming you know what it is. To obtain the exact effective thermal coefficient was determined using DNM based on the mathematical theory of globular morphology multiphase fields developed by Kushch [11,12,13]. Averaging the heat flux $\langle\mathbf{q}\rangle$ and temperature $\langle T\rangle$ over the REV yields $\langle\mathbf{q}\rangle = \lambda_{eff}\nabla\langle T\rangle$, and for the stationary case there results

$$\nabla \cdot \left(\lambda_{eff} \nabla \langle T \rangle \right) = 0. \tag{1}$$

The boundary conditions for this equation are formulated in the same manner as for a homogeneous medium. The second way is to solve the problem using the VAT two equation, three term integro-differential equations (see, for example, Travkin and Catton [8, 9]). The solid phase equation to be solved is

$$\frac{\partial}{\partial z}\left(m_s \frac{\partial}{\partial z}\{T_s\}_s \right) + \frac{\partial}{\partial z}\left[\frac{1}{\Delta\Omega} \int_{\partial S_w} \hat{T}_s \vec{ds}_1 \right] + \left[\frac{1}{\Delta\Omega} \int_{\partial S_w} \frac{\partial T_s}{\partial x_i} \vec{ds}_1 \right] = 0, \tag{2}$$

where $\{T\}_s$ is the intrinsic phase temperature averaged over particles, and the second and third terms on the right hand side are the so called morpho-diffusive terms, MD_2 and MD_3 respectively. There is a corresponding equation for the "fluid" (matrix) phase. To evaluate and compare solutions to these equations with the DNM results one needs to know the local solution characteristics, the averaged characteristics over the both phases in each cell and in this case, the additional morpho-diffusive terms.

An infinite homogeneous isotropic medium containing a three-dimensional (3D) array of spherical particles is chosen for analysis. The particles are arranged so that their centers lie at the nodes of a simple cubic lattice with period a. The temperature field in this heterogeneous medium is caused by a constant heat flux $\mathbf{Q}_z$ prescribed at the sample boundaries, which, due to the absence of heat sources, leads to $\langle \mathbf{q} \rangle = \mathbf{Q}_z$. When all the particles have the same radii, the result is the triple periodic structure used widely, beginning from Rayleigh's [14] work, to evaluate the effective conductivity of particle reinforced composites (Fig. 2).

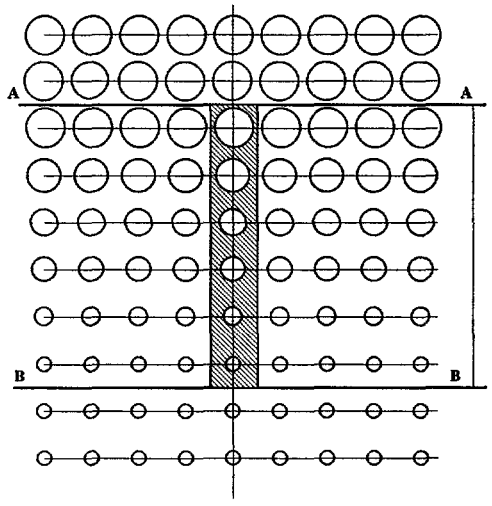

Figure 2. Model of Two-Phase Medium With Variable Volume Fraction of Disperse Phase.

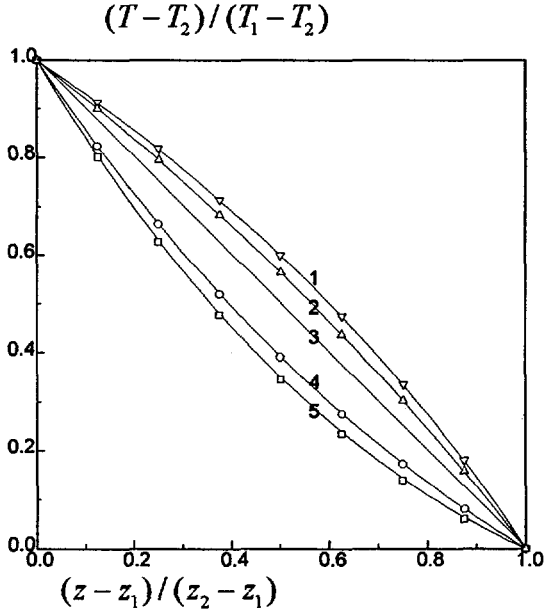

Figure 3. Comparison of VAT Three Term Equation Particle Temperature, Symbols, With the Exact Analytical Based on the Effective Conductance Coefficient Obtained by Exact DNM, Solid Lines.

The model composite medium consists of the three regions shown in Fig. 2. The half-space lying above the A-A plane has a volume content of the disperse phase $m_S = m_A$ and for half-space below the B-B plane $m_S = m_B$. To define the problem, let $m_A > m_B$. The third part is the composite layer between the plane boundaries A-A and B-B containing N double periodic lattices of spheres (screens). For the one-dimensional case, equation (1) becomes

$$\frac{\partial}{\partial z}\left(\lambda_{eff}\frac{\partial}{\partial z}T\right)=0,\ (z_1\le z\le z_2)\,,\ m_s=m_s(z)\,, \tag{3}$$

where $\lambda_{eff}(m_s)$ is the effective conductivity coefficient calculated for the perfect lattice structure composite with $\nabla m_s=0$.

The normalized solution of the both models (VAT and DNM) for the case of linearly changing porosity $m_s=m_s^{(1)}+z(m_s^{(2)}-m_s^{(1)})$, where $m_s(z_1)=m_s^{(1)}$, $m_s(z_2)=m_s^{(2)}$, $z_1=0$, $z_2=1$ are presented in Fig. 3.

Lines 1-5 represent solutions of the one-term equation with effective conductivity coefficients of $\lambda_{eff}=0$, 0.2, 1, 10, and 10000, respectively whereas the points (circles, triangles, etc.) represent the solutions of the VAT equations with accurate DNM closure of the micro model VAT integro-differential terms MD_2 and MD_3 for the composite with varying volume content of disperse phase. Here the number of screens is 9 corresponding to relatively small particle phase concentration gradient. The coincidence of the results of the exact calculation of two equation three term energy transport VAT model with the exact DNM of the one-temperature effective coefficient model for heterogeneous media with non-constant spatial morphology clearly demonstrates the need for using all the terms in the VAT equations. The need for the morpho-diffusive terms in the energy equation are further demonstrated by noting that their magnitudes are all of the same order.

4. SCALING IN EXPERIMENTS AND DATA ANALYSIS

Ergun [15] suggested two types of friction factors. One of them, the so-called kinetic energy friction factor, f_{ker}, is similar to the Fanning friction factor, f_f. When written with the same assumptions,

$$f_f=\frac{f_{ker}}{3}=\frac{d_h}{2\,\varrho_f\,\widetilde{\overline{u}}^2}\left(\frac{\Delta P}{L}\right),$$

where d_h is the hydraulic diameter and $\widetilde{\overline{u}}$ the intrinsic averaged velocity. The problem is what to choose for the hydraulic diameter for a given porous media that properly represents its morphology. Bird et al. [16] used the ratio of the "volume available for flow" to the "cross section available for flow" in their derivation of a hydraulic radius r_{hb}. This led them to

$$r_{hb}=\frac{\langle m\rangle\, d_p}{6(1-\langle m\rangle)},$$

where $\langle m\rangle$ is the porosity. A basis for a consistant hydraulic diameter for any systems is

$$d_h=\frac{4\,\langle m\rangle}{S_w}=\frac{4\,\langle m\rangle}{a_v(1-\langle m\rangle)}=\frac{2\,\langle m\rangle}{3(1-\langle m\rangle)}d_p=4r_{hb},$$

where a_v is the "particle specific surface area" which is equal to the total particle surface area divided by the volume of the particles and specific surface $S_w=a_v(1-\langle m\rangle)$. This expression is justified when an equal or mean particle diameter is $d_p=6/a_v$, which is exact for spherical particles and often used as substitute for granular media particles. The value of hydraulic radius given by Bird et al. [16] r_{hb} was chosen by Chhabra [17] and used in his determination of a specific friction factor for capillary models. The expression for friction factor given by Chhabra is

$$f_{cb}=\frac{d_p}{\langle m\rangle^2\,\varrho_f\,\widetilde{\overline{u}}^2}\frac{\Delta p}{L}.$$

This friction factor, the friction factor, f_b, given by Bird et al. [16] for a packed bed, see equation (6.4-1), the Fanning friction factor, f_f, and to Ergun's kinetic energy friction factor, f_{ker}, related by the following

$$f_{cb}=2f_b=\left(\frac{1-\langle m\rangle}{\langle m\rangle^3}\right)f_{ker}=3\left(\frac{1-\langle m\rangle}{\langle m\rangle^3}\right)f_f\,.$$

These models all use different length scales. It is not clear from evaluation of experimental data which is the most appropriate. To address this, the momentum equation for turbulent flow of an incompressible fluid in a porous

media based on a K-theory (Primak et al. [18], Travkin and Catton [19]) will be used to develop a consistant set of morphological properties and a characteristic length.

The one dimensional form of the momentum equation is

$$-\frac{d\widetilde{\overline{p}}}{dx} = \left(c_f + c_{dp}\frac{S_{wp}}{S_w}\right)\left(\frac{S_w}{\langle m\rangle}\right)\frac{\rho_f\,\widetilde{\overline{u}}^2}{2} = c_d\left(\frac{S_w}{\langle m\rangle}\right)\frac{\rho_f\,\widetilde{\overline{u}}^2}{2},$$

where c_f is the friction factor and c_{dp} the form drag, S_{wp} the cross flow form specific surface. The drag terms are combined into a single total drag coefficient

$$c_d = \left(c_f + c_{dp}\frac{S_{wp}}{S_w}\right),$$

to model the bulk flow resistence terms in the general simplifed VAT momentum equation. The drag resistance can be evaluated for a homogeneous porous media from measurements of pressure drop,

$$-\frac{d\widetilde{\overline{p}}}{dx} = f_f\left(\frac{S_w}{\langle m\rangle}\right)\frac{\rho_f\,\widetilde{\overline{u}}^2}{2}.$$

It was shown by Travkin and Catton [8, 19] that a good approximation for such media is

$$c_d \cong f_f,$$

where a bulk value of pressure loss coefficient f_f can be obtained from experimental correlations. There are few reasons that these quantities are not identical. One of them results because the media inflow and outflow pressure losses are usually incorporated into the correlations for f_f . A second reason is the loss of geometric characteristics represented by the ratio of S_{wp}/S_w. Some details of a media made up of regular globular morphologies can be described in terms of S_w, $\langle m\rangle$, d_p. For a spherical particle medium

$$S_w = \frac{6(1-\langle m\rangle)}{d_p},\quad d_h = \frac{2}{3}\frac{\langle m\rangle}{(1-\langle m\rangle)}d_p.$$

This leads to a relationship for d_h that takes the form

$$d_h = \frac{4\langle m\rangle}{S_w}.$$

This form is consistant with two major morphologies, both capillary and globular, and incorporates two properties of the media, both void fraction and specific surface area. It has a solid theoretical basis for at least for two types of canonical porous media morphology (straight capillary parallel pore morphology - SPPM and one diameter sphere globular morphology) and was arrived at with different theoretical reasonings by others in previous years like Kays and London [20]. There are a number of analysis and experimental studies of different porous media morphology leading to the use of a porous media Reynolds number with this scale. Although various porous media pressure resistance models are described by others (see, Bird et al. [16], Fand et al. [21], and Chhabra [17]), the above description for d_h allows the transformation and comparison of correlation equations and experimental results obtained for diverse morphology media and the use of various scaling. Also it allows experimentally determined characteristics of the media to be related to the closure relationship derived from the VAT analysis. It was shown by Travkin and Catton [8, 19] that a straight equal diameter tube morphology model yields the morphology functions $S_w/ < m >$ and d_h is obtained from the above experession. A c_d for this morphology was found from its corresponding skin friction coefficient expressed by the Darcy pressure loss coefficient by Travkin and Catton [19] $c_d = \widetilde{c}_d \cong f_D/4$.

With this, any experimental correlation can be reformulated for use in the simplified VAT bulk 1D momentum equation,

$$\frac{\Delta P}{L} = f_f\left(\frac{S_w}{\langle m\rangle}\right)\frac{\rho_f\,\widetilde{\overline{u}}^2}{2}.$$

where f_f is an experimentally determined function of $Re_{por} = \widetilde{\overline{u}}d_h/\nu$. With this expression, Fanning friction factor correlations can be easily compared and analyzed after reformulating corresponding expressions in terms of Re_{por} as shown in Fig. 4. The correlations presented in Fig. 4 are for experiments carried out by Gortyshov et al. [22, 23], and Beavers and Sparrow [24] among others. Gortyshov et al. used the Reynolds-Forchheimer momentum equation and a Darcy friction factor. Beavers and Sparrow used a friction factor approach but based their length scale on the measured permeability.

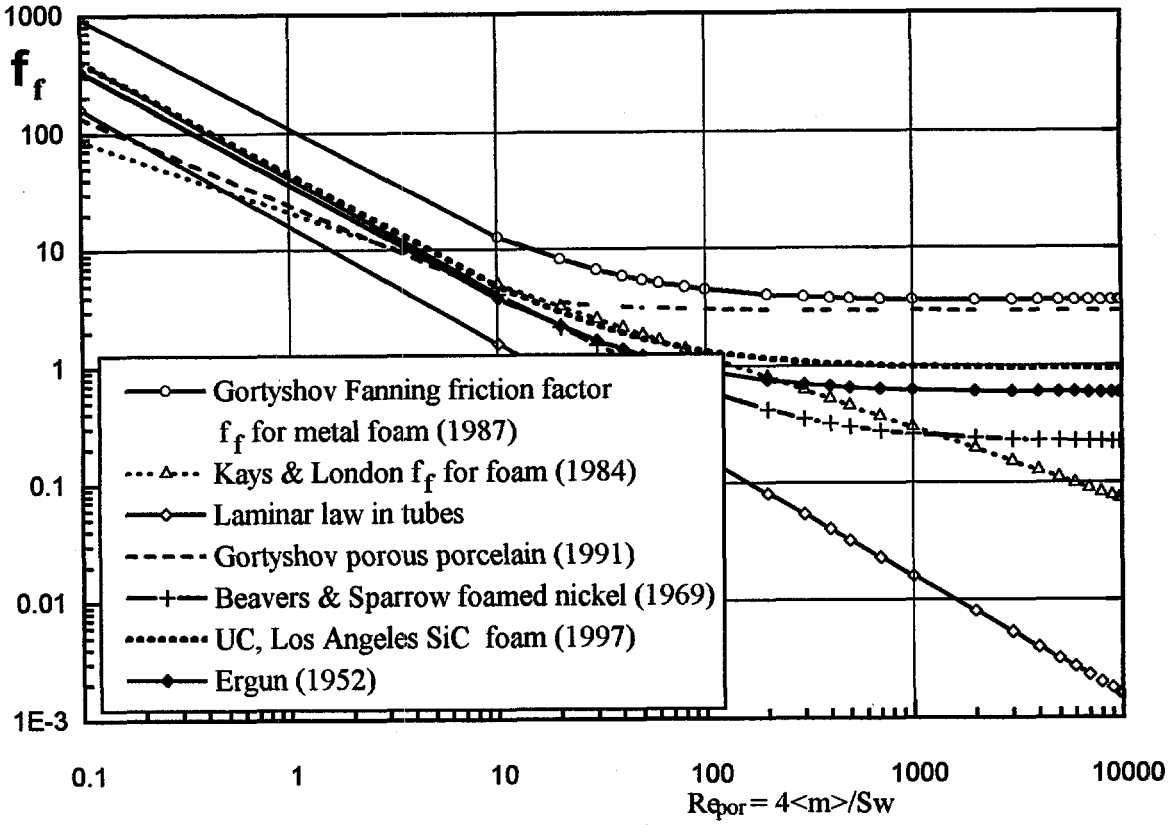

Figure 4. Comparison of Porous Media Pressure Loss Models Using Fanning Friction Factor f_f

5. CONCLUSIONS

Several conclusions are reached as a result of this work. First, one cannot neglect the small scale when dealing with a large problem. When the media includes fine pores, a hierarchical approach is needed that includes at least two levels. Calculations of the flow rates in porous media with a large diversity of morphological elements, e.g. capillaries, must take into account the dependence of viscosity on distance from the pore wall. Care must be taken when the problem statement is formulated that the equations contain all the necessary closure terms resulting from the averaging process. It was shown by comparison of a DNM solution with a VAT based solution that several terms usually ignored are of the same order as those usually kept. There are many terms that appear as a result of flow that are ignored and what their importance is yet to be determined. Analysis of many different experimental and analytical results combined with use of the VAT equations led to the conclusion that pore Reynolds number based on a hydraulic diameter that is a function of void fraction and media specific surface area make up a consistent, although not necessarily complete, set of parameters for correlation of friction factors.

6. ACKNOWLEDGMENT

The authors wish to acknowledge the help and collaboration of M.Pesenson and V.I.Kushch. This work was sponsored by the U.S. Department of Energy, Office of Basic Energy Sciences under the Grant DE-FG03-89ER14033 A002.

7. REFERENCES

1. L.I.Kheifets and A.V.Neimark, *Multiphase Processes in Porous Media*, Nadra, Moscow (1982).
2. J.H.Cushman, "Hierarchial Problems: Some Conceptual Difficulties in the Development of Transport Equations," *Inter. Seminar on Porous Media,* Dubrovnik, (1991).
3. N.Churaev, V.Sobolev, and Z.Zorin, "Thin Liquid Films and Boundary Layers," in *Special Discussion of the Faraday Society*, Academic Press, London, **1**, 213 (1970).
4. B.V.Derijagin, N.Churaev, and V.Muller, *Surface Forces,* Consultant Bureau, NY (1987).
5. N.F. Bondarenko, "On the Nature of Fluid Filtration Anomaly," *DAN SSSR*, **177**, 383 (1967).
6. N.F. Bondarenko, 1968, "Intermolecular Hydrogen Bonds Influence on the Character of Fluid Flow in the Capillaries," *Zh. Fiz. Khim.*, **42**, 225 (1968).
7. P.F.Low, "Viscosity of Interlayer Water in Montmorillonite," *Soil Sci. Amer. Journ.*, **40**, 500 (1976).
8. V.S.Travkin and I.Catton, "Turbulent Transport of Momentum, Heat and Mass in a Two Level Highly Porous Media," *Heat Transfer 1994, Proc. Tenth Intern. Heat Transfer Conf.*, Bighton, **5**, 399 (1994).
9. V.S.Travkin, L.Gratton, and I.Catton, "Modeling Technique for Closure of Transport Equations in Nonregular Globular and Capillary Porous Medium Morphology," *Procs. A.S.M.E./J.S.M.E. Thermal Engineering Joint Conference*, Hawaii, **3**, 319 (1995).
10. V.S.Travkin and V.I.Kushch, "Averaging Theorem Theoretical Closure and Verification," (to be submitted to the *J. Appl. Phys.*) (1997).
11. V.I.Kushch, "Heat Conduction in a Regular Composite With Transversely Isotropic Matrix," *Doklady AN Ukr. SSR*, No.1, 23 (1991), (in Russian).
12. V.I.Kushch, "Thermal Conductivity of Composite Material Reinforced by Periodically Distributed Spheroidal Particles," *Engng.-Phys. Journal*, **66**, 497 (1994), (in Russian).
13. V.I.Kushch, "Elastic Equilibrium of a Medium Containing Finite Number of Aligned Spheroidal Inclusions," *Int. J. Solids Structures*, **33**, 1175 (1996).
14. R.S.Rayleigh, "On the Influence of Obstacles Arranged in Rectangular Order Upon the Properties of a Medium," *Phil. Mag.*, **34**, 481 (1892).
15. S.Ergun,(1952), "Fluid Flow Through Packed Columns," *Chemical Engineering Progress*, **48**, 89 (1952).
16. R.B.Bird, W.E.Stewart, and E.N.Lightfoot, *Transport Phenomena*, Wiley, New York (1960).
17. R.P.Chhabra, *Bubbles, Drops, and Particles in Non-Newtonian Fluids*, CRC Press, Boca Raton (1993).
18. A.V.Primak, A.N.Shcherban, and V.S.Travkin, "Turbulent Transfer in Urban Agglomerations on the Basis of Experimental Statistical Models of Roughness Layer Morphological Properties," *Trans. World Meteor. Organization Conf. on Air Pollution Model. & Application*, Geneva, **2**, 259 (1986).
19. V.S.Travkin and I.Catton, "A Two-Temperature Model for Turbulent Flow and Heat Transfer in a Porous Layer," *J. Fluids Eng.*, **117**, 181 (1995).
20. W.M.Kays and A.L.London, *Compact Heat Exchangers*, 3rd ed., McGraw-Hill (1984).
21. R.M.Fand, B.Y.K.Kim, A.C.C. Lam, and R.T.Phan, "Resistance to the Flow of Fluids Through Simple and Complex Porous Media Whose Matrices are Composed of Randomly Packed Spheres," *J. Fluids Eng.*, **109**, 268 (1987).
22. Yu.F.Gortyshov, G.B.Murav'ev, and I.N.Nadyrov, "Experimental Study of Flow and Heat Exchange in Highly Porous Structures ," *Engng.-Phys. Journal*, **53**, 357 (1987), (in Russian).
23. Yu.F. Gortyshov, I.N.Nadyrov, S.R.Ashikhmin, and A.P.Kunevich, "Heat Transfer in the Flow of a Single-Phase and Boiling Coolant in a Channel with a Porous Insert, " *Engng.-Phys. Journal*, **60**, 252 (1991), (in Russian).
24. G.S.Beavers and E.M.Sparrow, "Non-Darcy Flow Through Fibrous Porous Media," J. Applied Mechanics, **36**, 711 (1969).

INTERFACIAL AREA, VELOCITY AND VOID FRACTION IN TWO-PHASE SLUG FLOW

Gunol Kojasoy

Department of Mechanical Engineering
University of Wisconsin-Milwaukee
Milwaukee, WI 53201

Jovica R. Riznic

Atomic Energy Control Board
Safety Evaluation Division
Ottawa, Canada K1 P5S9

ABSTRACT

The internal flow structure of air-water plug/slug flow in a 50.3 mm dia transparent pipeline has been experimentally investigated by using a four-sensor resistivity probe. Liquid and gas volumetric superficial velocities ranged from 0.55 to 2.20 m/s and 0.27 to 2.20 m/s, respectively, and area-averaged void fractions ranged from about 10 to 70%. The local distributions of void fractions, interfacial area concentration and interface velocity were measured. Contributions from small spherical bubbles and large elongated slug bubbles toward the total void fraction and interfacial area concentration were differentiated. It was observed that the small bubble void contribution to the overall void fraction was small indicating that the large slug bubble void fraction was a dominant factor in determining the total void fraction. However, the small bubble interfacial area contribution was significant in the lower and upper portions of the pipe cross sections.

1. INTRODUCTION

The intermittent plug/slug two-phase flow-pattern exists over a wide range of gas and liquid flow rates in a horizontal two-phase flow configuration. This flow-pattern is described as a gas slug in the form of a large elongated gas bubble in the upper part of the pipe followed by a liquid slug occupying the entire cross section. Depending on the flow rates of the gas and liquid, small bubbles may break off the large gas slug bubbles and either reside in the liquid slug and/or in the liquid underneath the gas slug or coalesce with front of the oncoming gas slugs. In order to advance the study of such a two-phase flow structure, it is essential to experimentally obtain detailed local values of fundamental parameters characterizing the internal structure of this flow-pattern.

The void fraction and interfacial area are two fundamental geometric parameters characterizing the internal structure of two-phase flow. The void fraction represents the volumetric fraction of gas phase or the probability density of the gas to exist at a given time and point and is a required parameter for hydrodynamic and thermal calculations in various industrial processes. On the other hand, the interfacial area describes the

available interfacial area for the interfacial transport of mass, momentum and energy in steady and transient two-phase flows and is a required parameter for two-fluid formulation of a two-phase flow field. However, little information is currently available on these parameters, and it is limited to vertical two-phase flow configurations. Particularly, there exists very little knowledge on the local interfacial area concentration in spite of its importance in multi-dimensional two-fluid model analysis, Boure [1] and Ishii and Kocamustafaogullari [2]. Accurate information about these parameters describing the internal structure of the plug/slug flow-pattern and generalized relationships among them are necessary to understand transport phenomena associated with this flow-pattern.

At present, several methods are available to measure interfacial area concentration in gas-liquid two-phase flows. Measurement techniques can be broadly classified into two categories: (a) chemical absorption methods, and (b) physical methods. Chemical absorption methods provide a global measurements of interfacial area concentration, and thus, do not provide the local information of interest in closure models. Briefly, this method involves measurement of a liquid film controlled gas absorption accompanied by rapid depletion of the solute through reaction in the liquid film. The physical methods involves techniques such as photography, light attenuation, ultrasonic attenuation and various intrusive probe techniques, i.e., resistivity or impedance probes, and fiber-optic probes, etc. Detailed review of all these methods have been provided by Landau et al. [3], Veteau [4], Ishii and Mishima [5], Chang et al. [6,7] and Wang and Kocamustafaogullari [8]. However, all these methods are limited to dispersed two-phase flow patterns, i.e., bubbly and droplet two-phase flows, and with the exception of Revankar and Ishii [9], no established local measurements of the interfacial area concentration exists for flow patterns other than bubbly and droplet flows. Recently, Revankar and Ishii [9] reported a theoretical formulation for the local measurements of interfacial area concentration in cap bubbly flow configuration by using four-sensor resistivity probe. According to the authors knowledge there have been no experimental data or fundamental studies available on the local distribution of interfacial area concentration in horizontal plug/slug two-phase flow-pattern.

In view of this brief discussion, it is evident that much experimental work is still necessary to attain a thorough physical understanding of the internal structure of an intermittent horizontal two-phase slug flow-pattern. In this context, an experimental investigation has been underway at the University of Wisconsin–Milwaukee to investigate the internal structure of this flow-pattern. In these experiments

- the double-sensor resistivity probe method was developed to measure local void fractions, interfacial area concentration, interfacial velocity, local bubble chord-length, size and frequency distributions of bubbles in a horizontal bubbly two-phase flow [10, 11].
- the four-sensor resistivity probe method was developed to measure the local void fraction and interfacial area concentration in a horizontal slug flow [12], and
- the hot-film anemometry technique was used to measure the time-averaged local void fractions due to small and large slug bubbles, as well as, the local axial velocity and turbulence in the liquid phase of an air-water intermittent flow in a horizontal channel [13, 14, 15].

In the present work, the local void fraction and interfacial area concentration in a horizontal plug/slug two-phase flow were studied experimentally by using four-sensor resistivity probe method. Local void fraction, interfacial area concentration, interface velocity have been measured, and the results are documented and discussed here. Furthermore, the dependence of these local parameters on the other flow variables are also presented. Besides the four-sensor resistivity probe method, the hot-film anemometer technique for liquid velocity measurements and two-sensor resistivity method for small bubble interfacial area concentration measurements were also used to supplement the results.

2. FOUR-SENSOR RESISTIVITY PROBE METHOD

2.1 Theoretical Foundation

The theoretical foundation for the local measurement of interfacial area concentration in bubbly and cap bubbly flow using four-sensor electrical resistivity probe was recently provided by Revankar and Ishii [9]. By starting the defining equation of the time-averaged local interfacial area concentration a_i at (x_o, y_o, z_o, t) as

$$a_i\ (x_o, y_o, z_o) = \frac{1}{\Omega} \sum_j \left(|\nabla f_j| / | \frac{\partial f_j}{\partial t} | \right) \tag{1}$$

they showed that the local time-averaged interfacial area concentration can be measured by three interfacial velocity components and the known geometric configuration of the four sensor probe. When the front and three rear sensors of the four-sensor probe are arranged such that they make an orthogonal system with the front sensor located at the apex and the three rear sensors at the rear plane perpendicular to the flow direction, the above relation is simplified to

$$a_i = \frac{1}{\Omega} \sum_j \left[\left(\frac{1}{v_{s1j}} \right)^2 + \left(\frac{1}{v_{s2j}} \right)^2 + \left(\frac{1}{v_{s3j}} \right)^2 \right]^{1/2}$$

In these equations, f_j (x, y, z, t) function represents jth interface in three-dimensional space, Ω is the total sampling time, the subscript j identifies the jth interface and v_{skj} (k = 1,2,3) is the passing velocity components in the three orthogonal directions with respect to rear sensor k.

Schematic of the four-sensor probe arrangement is shown on Figure 1. By considering the jth interface passing the front and any rear sensor k, with the time interval, Δt_{kj} , the passing velocity component in the k'th direction, v_{skj}, is given by

$$v_{skj} = \Delta s_{kj} / \Delta t_{kj}, \quad k = 1, 2, 3 \tag{3}$$

where Δs_{kj} is the spacing between the front and the k'th rear sensor tips. Referring to Figure 1, it is evident that combination of each rear sensor and front sensor constitutes a double-sensor to measure the interfacial velocity component in the respective orthogonal direction. The front sensor is designed to be the common sensor. Thus there are three double-sensor probes enabling the measurement of interfacial velocity components in three orthogonal directions. According to Eq. (2), measurement of the three velocity components v_{s1j} , v_{s2j} and v_{s3j} will be sufficient for determining the local time-averaged interfacial area concentration.

The time-averaged local void fraction, α, at any location, r can be obtained by either front or one of the rear sensors. Due to the finite size of the probe, only the front sensor was used for the void fraction measurements. The time-averaged void fraction at any location r is then determined as follows:

$$\alpha(r) = \frac{1}{\Omega} \left[\sum_{j=1}^{N_{lb}} \left(t_{0fj} - t_{0rj} \right) + \sum_{i=1}^{N_{sb}} \left(t_{0fi} - t_{0ri} \right) \right] \tag{4}$$

where the subscript 0 identifies the front sensor, whereas j and i identify large elongated bubbles, and small spherical bubbles respectively. t_{orj} is the time the front sensor tip enters into the large j'th bubble, and t_{ofj} is the time the front sensor enters in to the liquid phase. t_{ori} and t_{ofi} denote corresponding times for the small spherical bubbles. N_{lb}, and N_{sb}, respectively, are the number of large and small bubbles passing the front sensor tip in

the total sampling time of Ω. The first term appearing in Eq. (4) gives the large bubble void fraction, whereas the second term denotes the small bubble void fraction contribution to the overall void fraction in a slug flow.

2.2 Measurement Principle

In principle, the electrical resistivity probe consists of the instantaneous measurement of local electrical resistivity in the two-phase mixture by means of a sensor electrode. In an air-water flow the air can be considered as electrically insulating, whereas water is electrically conducting. When the sensor is in contact with the liquid, the circuit is closed. On the other hand, when it is in contact with a bubble, the circuit is open. Since the circuit is open or closed depending on whether the sensor is in contact with gas or liquid, the voltage drop across a sensor fluctuates between a V_{min} and V_{max}.

In the case of four-sensor probe method, each sensor and the return electrodes are connected to their own measuring circuits and, therefore, each sensor is used independently as a phase identifying device. Furthermore, from the timing of the shift in the voltage between V_{min} and V_{max}, the time when the gas-liquid interface passes the sensor can be recorded. Therefore, two pieces of parallel and independent information related to the phase identification and the transit time of the gas-liquid interface is obtained.

A schematic diagram indicating a typical time history record of signals from a four-sensor electrical resistivity probe in a slug flow is illustrated in Figure 2. As seen from the figure, the signals, even for the large slug bubbles, deviate from the ideal two-state square-wave signals. This deviation is largely due to the finite size of the sensor causing flow disruption and the possible deformation of the interface before the sensor enters from one phase to the other. The trailing edges are generally steeper than the leading edges. This difference is probably due to the wetting of the sensor by the residual liquid when the sensor enters into the gas phase. When the sensor tips encounter small gas bubbles in the liquid, the residence time in a small bubble is too small for the probe to react to changes fast enough because of drying period of wet sensor tips. As a result, signals for small bubbles do not vary between V_{min} and V_{max} as observed in the case of large bubbles.

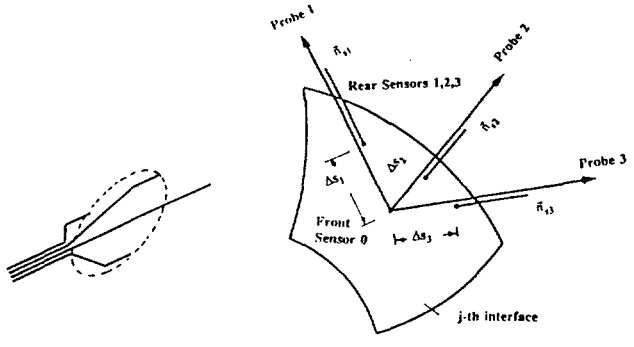

Figure 1. Schematic of four-sensor probe arrangement.

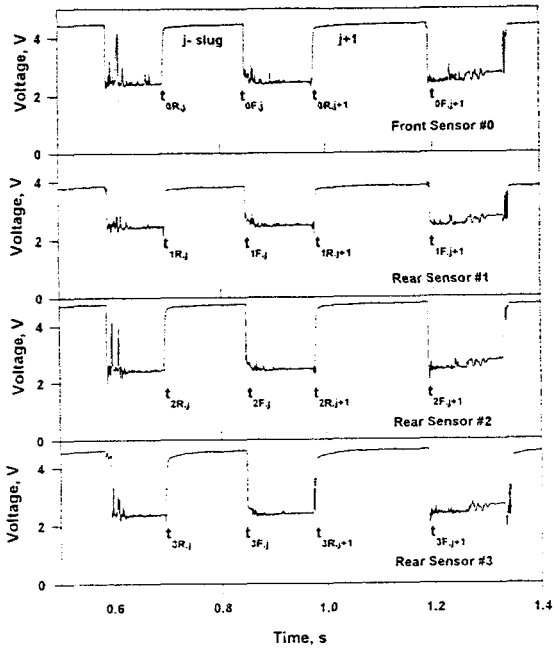

Figure 2. Typical output of four-sensor probe in a slug flow (j_f=2.20 m/s, j_g=1.1 m/s).

2.3 Four-Sensor Probe Design and Signal Processing

A typical four-sensor resistivity probe is shown in Figure 3. It consists of four identical platinum / 13% rhodium or chrome alloy wire sensors of 0.127 mm in diameter. They are completely insulated from the environment except at their exposed tips. The three rear sensor locations are positioned such that the tip of these sensors were on one plane and they were placed axisymetrically with respect to the central front sensor. Typical vertical distance between the front and rear sensor was 2 to 2.5 mm. The locations of the four sensors were arranged such that the tips of the sensors make an orthogonal coordinate system with the front sensor in the apex and the three rear sensors at the rear plane perpendicular to the flow direction. The complete assembly fits into a probe holder from which wires run to the electronic circuit. The electronic circuit uses a 5 V d.c. power supply. Variable resistors were used to enable adjustment of the maximum and minimum voltage signals.

It was found that the proper distance between the front and rear sensors was critical for analyzing the experimental data. Preliminary experiments were conducted to determine a proper distance between the front and rear sensor tips. The distance was dictated by possible bubble size and bubble interface velocity. It was found that 2 - 2.5 mm in lateral direction and 3 - 4 mm in longitudinal direction were the appropriate separation distance for the experimental conditions that were selected. It is to be noted that a very small distance results in inaccuracies in time duration measurements, since it requires very high sampling frequencies or very small bubble velocities. On the other hand, if the distance is too large, there is a strong possibility of misinterpretation of signals since multibubble contact occur between two signals originating from the same bubble.

For the case of the bubble velocity and void fraction measurements the right selection of two closely corresponding signals from each probe is important. This is so, because two sequential signals detected by the front and rear sensors do not always correspond to the same interface, and the residence time intervals of the gas or liquid phase at the sensors are not exactly the same. The signal validation was made by judging whether the following conditions were satisfied:

(1) By assuming the forward motion of the bubbles, the front sensor signal rises or falls before the rear sensor signals do. Therefore, referring to Figure 2, the following conditions should be satisfied

$$t_{kfj} > t_{krj},\ j=1,...N,\ k=0,1,2,3 \quad \text{and} \quad t_{0rj} < t_{krj},\ t_{0fj} > t_{krj},\ j=1,...N,\ k=2,3,4 \qquad \textbf{(5)}$$

where the second indices *f* and *r*, respectively denote the times of the fall and rise in each sensor, N is the number of bubbles passing through a given sensor in the total sampling time Ω.

(2) The residence time of a bubble for the front and rear sensors should be comparable to ensure that both the front and rear sensors detect the same bubble. Hence, the following condition should be also satisfied:

$$t_{0fj} - t_{0rj} \simeq t_{kfj} - t_{krj},\ j=1,...N,\ k = 1, 2, 3 \qquad \textbf{(6)}$$

(3) A passing interface should be properly identified. When there are different sized bubbles as in the slug flow the large slug bubbles and small bubbles should be identified separately. For this the bubble residence time on the front sensor was used to distinguish the elongated, large slug bubbles from the small spherical bubbles. The following condition on the bubble residence time was used to discriminate large and small bubbles:

$$c_1 \le t_{0fj} - t_{0rj} \le c_2$$

where c_1 and c_2 are time constants determined by the calibration process where the slug bubble size is estimated with flow visualization.

3. EXPERIMENTAL SETUP AND PROCEDURE

The experimental flow loop consists of a horizontal line of 50.3 mm ID Pyrex glass tubings with pressure tabs installed between them. The entire flow loop is about 15.4 m in length and is entirely transparent to facilitate flow visualization, high-speed photography and cinematography. Details of the flow loop are given elsewhere [10,11].

The air and distilled water are used as coupling fluids. The air to the test section is supplied from the university central air system. It is regulated through 0.95 m^3 capacity high-pressure storage tank, and metered by a series of turbine flowmeters. The water is pumped from 1.9 m^3 capacity storage tank by a stainless steel centrifugal pump end regulated by a transistor inverter. The flow rate is measured by a series of paddlewheel flow meters assembled in a parallel configuration. The air enters the mixing chamber from a vertical leg and is injected into the water flow through a cylindrical porous media of 100 μm porosity to achieve a uniform mixing. The two-phase mixture from the test section is directed to an air-water separator, where the air is vented to the atmosphere, and the water is returned to the water storage tank.

A Vernier, with graduations to an accuracy of 0.01 mm was used to traverse the probe in a direction perpendicular to the axis of the tube. The probe was traced through the vertical axis of the pipe, stopping at 17 positions to take measurements. The local, instantaneous interface velocity, void fraction and interfacial area concentration were measured at each location. When the experimental studies were intended to investigate the flow development and local interfacial parameters over the cross sectional plane of the pipe, the test section was affixed to the flow channel by rotary seals. The seal provided a water tight joint, yet allowed the test section to rotate freely.

The data from the probe was collected by the data acquisition system and stored in a PC. Due to the limitations of the computer, the sampling rate was set up to a maximum value of 10 kHz which allowed a statistically meaningful sampling time. At this sampling rate the measurement error of the velocity would be less than 5% for the sensor separation distance of 2 mm. Once the data were taken and stored in the memory of the computer, a FORTRAN program was used to process the data, separating the phases and calculating the interfacial velocity components.

4. EXPERIMENTAL RESULTS AND DISCUSSION

4.1 Local Void Fraction

Experimental studies were performed on plug/slug flow patterns, and data were acquired at the axial location of L/D=253 from the mixing chamber which represents a region of semi-fully developed two-phase flow. Four different liquid flow rates in combination with five different gas injection rates were studied. The gas volumetric fluxes were j_g=0.27, 0.55, 1.10, 1.65, and 2.20 m/s.

Equation (4) is used to calculate the local time-averaged void fraction. Typical slug bubble and total void fraction distributions are illustrated on Figure 4, where the total void fraction includes the small and slug bubble contributions. It is interesting to note that the shape of the total void fraction profile is similar to that of the slug bubble void fraction profile, and that the contribution from the slug bubble to the total void fraction is much larger than the small bubble contribution. It is also interesting to note that same findings were observed by Revankar and Ishii [9] for the case of vertical two-phase cap bubble flow. It is also evident from Figure 4 that the relative effect of the small bubbles on the total void distribution is much larger at the lower side of the pipe. This may be attributed to the generation of small bubbles from unstable lower surface of slug bubbles and to the vortex motion generated in front of liquid slugs where the liquid flow field is accelerated to fill the vacuum generated by the faster moving gas slugs. Toward the top of the pipe the small bubble void

fraction contribution stays almost constant although there is a slight increase toward the top of the pipe. This region is characterized by the liquid slug where the small bubbles are homogeneously distributed. However, the small bubbles tend to migrate toward the upper wall under the dominating influence of buoyancy force. Thus, the small bubble void fraction shows a slight increase near the top wall.

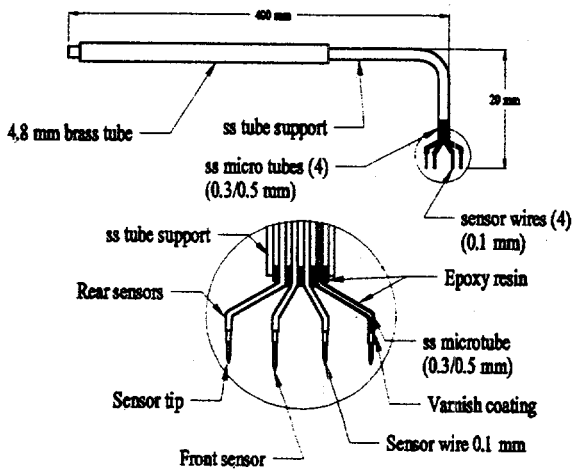

Figure 3. Four-sensor resistivity probe design.

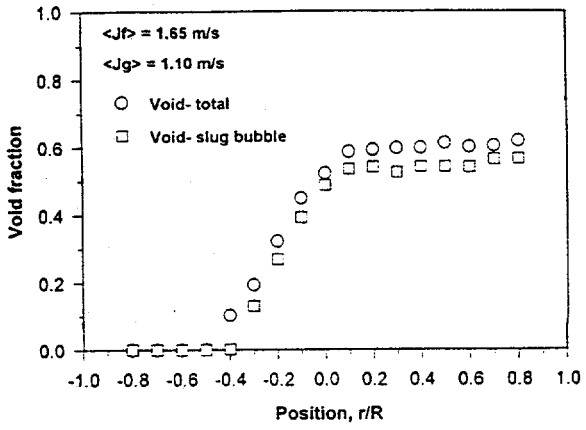

Figure 4. Local void fracation distributions obtained from the front sensor.

The effect of increasing gas flow rate on the total void fractions are, illustrated in Figure 5. It is evident from this figure that the radial profiles of the void fraction are all similar, and, the total void fractions increase with increasing gas flow rate. Comparisons of the void fraction measurement data of the resistivity probe against the hot-film anemometer measurements of References [13, 14] are shown on Figure 6. The agreement between these two data sets are reasonably good, confirming the fact that the four-sensor probe measurements can be performed with a high degree of confidence.

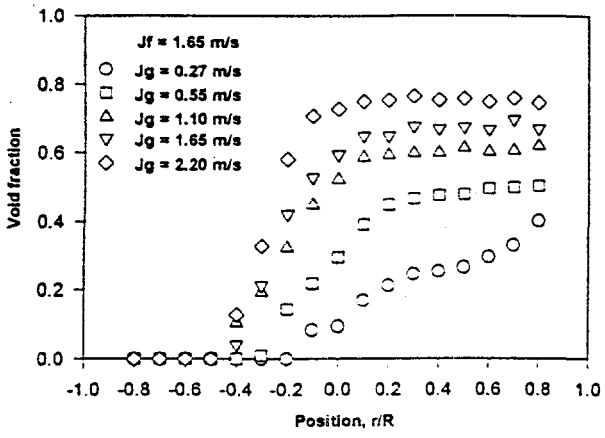

Figure 5. Influence of gas flow on the total local void fraction distributions

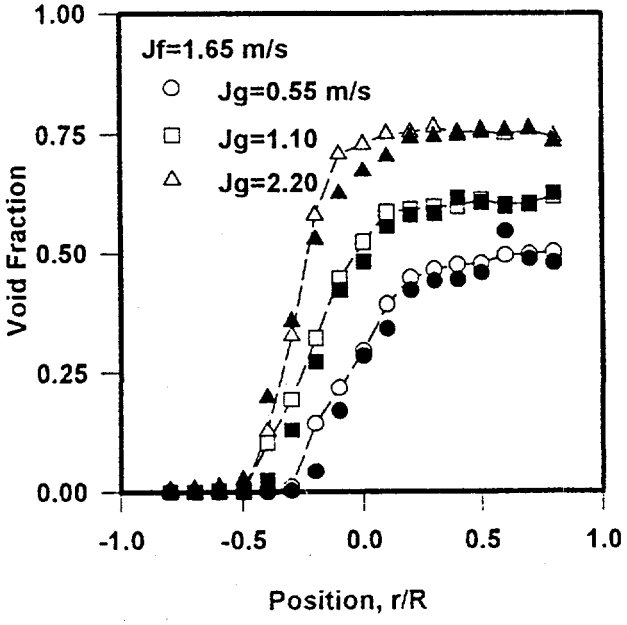

Figure 6. Total void fraction distributions (open symbols-four-sensor resistivity probes; full symbols-hot-film anemometer probe).

4.2 Local Interfacial Area Concentration

The interfacial area concentration is calculated from Eqs. (2) and (3). Figure 7 illustrates a typical interfacial area concentration profile. It is evident from this figure that the contribution from small bubbles is significant. In fact it becomes a dominating factor underneath slug bubbles and toward the top of liquid slugs. These observations are not surprising since the major generation of small bubbles occurs on the lower surface of a slug bubble where the interfacial instabilities exist. On the other hand, gravitational migration of small bubbles within the liquid slug causes an increase in bubble-population, and hence, an increase in the interfacial area concentration toward the top of liquid slugs. It is also interesting to note that interfacial area concentration for large slug bubbles goes through a maximum toward the bottom of slug bubbles. This may be attributed to the curvature effects and interfacial waviness around this location. It has been reported by Tomida et al. [16] that in the slug flow-pattern the waviness of the liquid film surrounding the long slug bubble drastically increases, suggesting an increase in interfacial area concentration.

Figure 8, demonstrate the effect of gas flow on the total interfacial area concentrations. As expected the gas flow has a significant effect on interfacial area concentrations. However, the effect of gas flow on the slug flow area contribution is confined to the bottom portion of slug bubbles. It is to be noted that interfacial area of slug bubbles toward top of the pipe cannot be measured due to finite size of the probe.

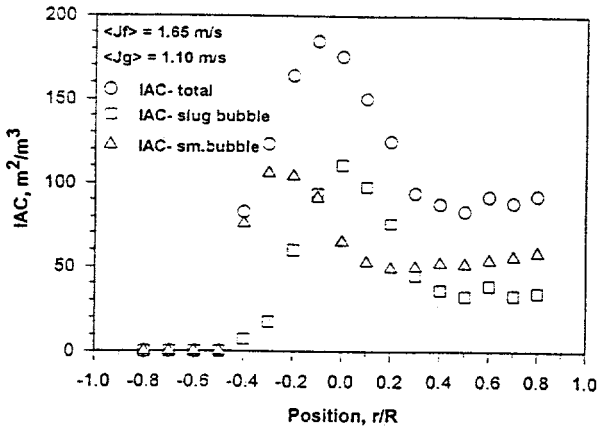

Figure 7. Local Interfacial area distributions

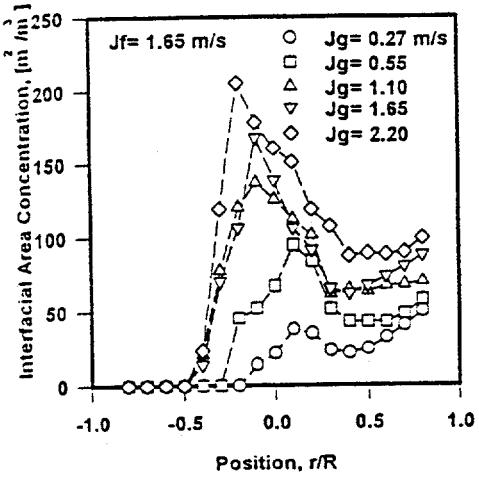

Figure 8. Influence of gas flow on the total local interfacial area concentration distributions.

4.3 Local Interfacial Velocity

The interfacial velocity components in three directions were calculated using Eq. (3). Then the axial velocity component was calculated from the resultant interface velocity, and the results are illustrated inFigure 9. The hot-film anemometer measurements of local liquid velocity [19] are also shown for the purpose of comparisons.

For the gas superficial velocity of 0.55 m/s, the interface velocity profiles were relatively flat over the whole range of investigated liquid superficial velocities. This is not surprising since $j_g \sim$ 0.55 m/s actually falls into the transition from plug to slug flow patterns. It was observed that plugs were moving smoothly with slightly higher velocity as compared to the flow of liquid slugs. As it is shown on the figure there exists a consistent peak at about r/R = 0.0~ 0.2. This was the typical case for all the flow conditions that were considered in the present study.

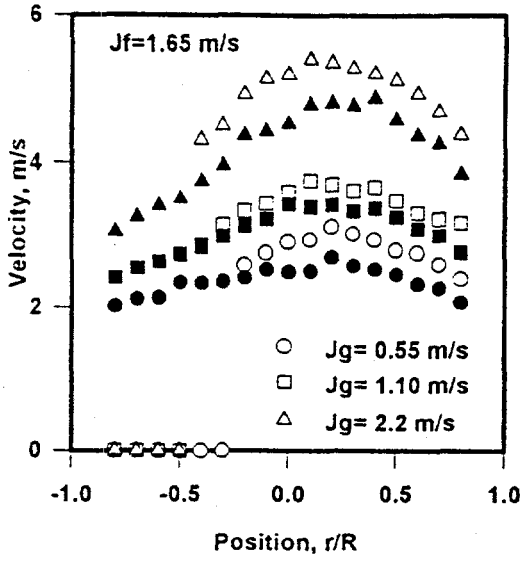

Figure 9. Local interface velocity distributions (open symbols-local interface velocity; full symbols-local liquid mean velocity by hot-film anemometry).

5. SUMMARY AND CONCLUSIONS

The internal phase distribution of air-water flow in a 50.3 mm diameter transparent pipeline has been investigated by using four-sensor resistivity probe technique. The local values of void fraction, interfacial area concentration and interface velocity distributions were measured.

The shapes of the total void fraction and void fraction due to slug bubble profiles for different gas flow rates were all similar, and higher void fractions were recorded with an increase in the gas flow rate. The local measurements obtained from the four-sensor probe compared very well with the hot-film anemometer measurements. In the region of transition from plug to slug flow patterns, with increasing gas flow rate contribution of small bubbles significantly increased.

The interfacial area concentration profiles for slugs clearly show a higher interfacial area along the bottom surface where increased interfacial waviness was reported. Experiments indicated that contribution from the increased number of small bubbles to the overall interfacial area concentration was substantial in the lower part of slug bubbles and in the upper part of liquid slugs.

ACKNOWLEDGMENT

The work reported in this paper was performed under the auspices of the U. S. Department of Energy, Office of Basic Energy Sciences. The authors gratefully acknowledge the support of the U.S. DOE/DES under the direction of Dr. O. P. Manley and Dr. R. Goulard.

REFERENCES

1. J. A. Boure, "Mathematical Modeling of Two-Phase Flow," Proceedings of CSNI Specialist Meeting, Vol. 1 (Edited by S. Banerjee and K. R. Weever), p. 85, AECL, Toronto, Ontario, (1978).

2. M. Ishii and G. Kocamustafaogullari, "Two-Phase Flow Models and Their Limitations," NATO Advanced Research Workshop on Advances in Two-Phase Flow and Heat Transfer, Spitzingsee, Germany.

3. J. Landau, J. Boyle, H. G. Gomaa, A. M. Al Tawell, "Comparison of Methods for Measuring Interfacial Areas in Gas-Liquid Dispersions," *Canadian J. of Chem Eng.*, 55, 13-28 (1977).

4. J. M. Veteau, "Contribution à l'etude des techniques de mesure de l'aire interfaciale dans les ècoulements à bulles, Thèse de Doctorat ès Sciences, Universitè Scientifique et Mèdicale et Institut National Polytechnique de Grenoble, (1981).

5. M. Ishii, K. Mishima, "Study of Two-Fluid Model and Interfacial Area, Argonne National Laboratory Report, ANL-80-111, NUREG/CR-1873, (1980).

6. J. S. Chang, B. Donevski, D. C. Groeneveld, "Examination of Correlations for Interfacial parameters in the Bubbly, Slug and Churn Flow Regimes," in *Heat Transfer Science and Technology,* B. Xuan Wang, Ed. (1988).

7. J. S. Chang, E. C. Morala, "Determination of Two-Phase Interfacial Areas by an Ultrasonic Technique," *Nuclear Engineering and Design,* 122, pp. 143-156 (1990).

8. Z. Wang, W. D. Huang, S. Srinivasmurthy, G. Kocamustafaogullari, 1990 "Interfacial Characteristic Measurements in Horizontal Bubbly Two-Phase Flow," *University of Wisconsin-Milwaukee Report*, DOE/NE/13764-4, October (1990).

9. S. T. Revankar, M. Ishii, "Theory and Measurement of Local Interfacial Area using a Four Sensor Probe in Two-Phase Flow," *Int. J. Heat and Mass Transfer,* 36, 12, 2997-3007 (1993).

10. Z. Wang and G. Kocamustafaogullari, "Interfacial Characteristic Measurements in a Horizontal Two-Phase Flow," *6th Proc. Nuclear Thermal Hydraulics*, 342-351 (1990).

11. G. Kocamustafaogullari, and Z. Wang, "An Experimental Study on Local Interfacial Parameters in a Horizontal Air-Water Bubbly Two-Phase Flow," *Int. J. Multiphase Flow,* 17, 553-572, (1991).

12. J. Riznic and G. Kojasoy, "An Experimental Study on Local Interfacial Parameters in Horizontal Slug Flow," 1997 National Heat Transfer Conference, Baltimore, Maryland, August 10-12, 1997.

13. S. Lewis, M. Herre, V. Davenport, J. R. Riznic, G. Kojasoy, "Use of Hot Film Anemometry in Horizontal Cocurrent Gas-Liquid Slug Flow," *31st ASME/AIChE/ANS/AIAA 1996 National Heat Transfer Conference,* Houston, TX, August, 3-6, ANS Proceedings, HTC-Vol. 9, 326-335, (1996).

14. S. Lewis, "Use of Hot-Film Anemometry in Horizontal Gas-Liquid Slug Flow," *MS Thesis*, University of Wisconsin-Milwaukee, May (1996).

15. S. Sharma, S. Lewis and G. Kojasoy, "Local Studies in Horizontal Gas-Liquid Slug Flow," OECD/CSNI Specialist Meeting on Advanced Instrumentation and Measurement Techniques, Sante Barbara, California, March 17-20, 1997.

16. T. Tomida, F. Yuse, O. Okezaki, "Effective Interfacial Area and Liquid-Side Mass Transfer Coefficient in the Upward Two-Phase Flow of Gas-Liquid Mixture, *Chem. Eng. J.*, 16, 81-88 (1978).